2014

IMPACT OF PHYTOPLANKTON COMMUNITY STRUCTURE AND FUNCTION ON MARINE PARTICULATE OPTICAL PROPERTIES

Malcolm Neil McFarland
University of Rhode Island, malcolmnmcfarland@gmail.com

IMPACT OF PHYTOPLANKTON COMMUNITY STRUCTURE AND FUNCTION ON MARINE PARTICULATE OPTICAL PROPERTIES

BY

MALCOLM NEIL MCFARLAND

A DISSERTATION SUBMITTED IN PARTIAL FULFILLMENT OF THE

REQUIREMENTS FOR THE DEGREE OF

DOCTOR OF PHILOSOPHY

IN

OCEANOGRAPHY

UNIVERSITY OF RHODE ISLAND

2014

DOCTOR OF PHILOSOPHY DISSERTATION

OF

MALCOLM NEIL MCFARLAND

APPROVED:

Thesis Committee:

Major Professor Jan Rines

Percy Donaghay

Brian Heikes

Carol Thornber

Nasser H. Zawia
DEAN OF THE GRADUATE SCHOOL

UNIVERSITY OF RHODE ISLAND

2014

ABSTRACT

Phytoplankton are an ecologically important and diverse group of organisms whose distribution, abundance, and population dynamics vary significantly over small spatial (cm) and temporal (minutes) scales in the coastal ocean. Our inability to observe phytoplankton community structure and function at these small scales has severely limited our understanding of the fundamental ecological and evolutionary mechanisms that drive phytoplankton growth, mortality, adaptation and speciation. The goal of this dissertation was to enhance our understanding of phytoplankton ecology by improving in situ observational techniques based on the optical properties of cells, colonies, populations, and communities. Field and laboratory studies were used to determine the effects of phytoplankton species composition, morphology, and physiology on the inherent optical properties of communities and to explore the adaptive significance of bio-optically important cellular characteristics. Initial field studies found a strong association between species composition and the relative magnitude and shape of particulate absorption (a_p), scattering (b_p), and attenuation (c_p) coefficient spectra. Subsequent field studies using scanning flow cytometry to directly measure optically important phytoplankton and non-algal particle characteristics demonstrated that the size and pigment content of large (>20 μm) phytoplankton cells and colonies vary significantly with the slope of particulate attenuation and absorption spectra, and with the ratio of particulate scattering to absorption. These relationships enabled visualization of phytoplankton community composition and mortality over small spatial and temporal scales derived from high resolution optical measurements acquired with an autonomous profiling system. Laboratory studies with diverse uni-

algal cultures showed that morphological and physiological characteristics of cells and colonies can account for ~30% of the optical variation observed in natural communities and that complex morphologies and low intracellular pigment concentrations minimize pigment self-shading that could otherwise limit bio-optical fitness. These results demonstrate that optical properties reveal detailed information about the distribution, abundance, morphology, and physiology of phytoplankton that can help explain their ecological dynamics over small spatial scales and the bio-optical function of diverse forms in the ocean.

ACKNOWLEDGMENTS

I would like to thank my advisor Dr. Jan Rines for her generous support and guidance. I also greatly appreciate the support and feedback of Dr. Percy Donaghay. Working with both Drs. Rines and Donaghay has provided me with invaluable scientific opportunities throughout my experience at the Graduate School of Oceanography. I would also like to thank the other core members of my committee, Dr. Brian Heikes and Dr. Carol Thornber, for their valuable input. I am grateful to Dr. Rebecca Robinson and Dr. Marta Gomez-Chiarri for serving as the additional members of my defense committee and providing indispensable advice. I also must acknowledge my co-author Dr. James Sullivan and colleague Dr. Michael Twardowski for their stimulating intellectual feedback and friendship. I am indebted to George Dubelaar for his extensive help with development of flow cytometric methods. I deeply appreciate the continual support and encouragement of my parents, Bruce McFarland and Kathleen Davis. Lastly, and most importantly, this dissertation would not have been possible without the understanding, companionship, and support of Eva Kane.

PREFACE

This dissertation has been formatted according to the manuscript format guidelines established by the Graduate School of the University of Rhode Island.

TABLE OF CONTENTS

LIST OF TABLES

TABLE PAGE

LIST OF FIGURES

FIGURE PAGE

MANUSCRIPT 1

MANUSCRIPT 2

MANUSCRIPT 3

INTRODUCTION

Phytoplankton are a fundamental component of ocean ecosystems that account for approximately half of global primary production and are important to global-scale biogeochemical cycling of elements such as carbon and oxygen (Longhurst et al. 1995, Field et al. 1998, Falkowski et al. 1998). The first planktonic and photosynthetic microorganisms, probably similar to extant marine cyanobacteria, appeared ~2.6 billion years ago and were responsible for the oxygenation of earth's atmosphere (Hedges et al. 2001). In the modern ocean, there are close to 25,000 described species of phytoplankton classified among eight major phylogenetic groups (Katz et al., 2004), although the number of species is likely to increase with the use of molecular genetic approaches (Amato et al. 2007). Species exhibit a wide variety of distinguishing morphological and physiological characteristics that control their distribution, population dynamics, and impact on biogeochemical processes in the pelagic environment (Smayda 2010, Smetacek et al 2004). Despite their large diversity and ecological significance, our basic understanding of phytoplankton ecology has been limited to very coarse distinctions among large taxonomic classes (e.g. diatoms, dinoflagellates, or cyanobacteria) by the difficulty of determining community structure and function in the ocean over the small spatial and temporal scales critical to their growth and mortality. Community characteristics such as the abundance of species and the processes that determine succession can vary substantially over tens of centimeters or within minutes. As a result, it is difficult to understand or predict phytoplankton community responses to environmental change at the local or global level (Falkowski & Oliver 2007).

The high diversity of phytoplankton species in a turbulent environment with little or no barriers to dispersal was described as the "paradox of the plankton" by G.E. Hutchinson in 1961. This apparent paradox stems from the principle of competitive exclusion which predicts the ultimate dominance of a single, most fit form when multiple species compete for the same resources. Of course, the ocean is not an unstructured, isotropic environment at the scales important to phytoplankton population dynamics, and all species do not compete for resources under the same environmental conditions. Consequently, the differential growth rates of forms in response to variable local conditions results in complex and heterogeneous patterns of distribution and abundance over multiple spatial and temporal scales (Longhurst 1998, Rines et al. 2010). The function of their distinctive traits is fundamental to this complex ecology (Litchman & Klausmeier 2008). Ecologists have long sought explanations for observed patterns of distribution and abundance through an understanding of the function of species traits (Gran 1912, Margalef 1978, Sournia 1982, Fogg 1991, Smayda and Reynolds 2001). Morphological traits such as the size and shape of cells can enhance nutrient acquisition rates through sinking or interaction with small scale turbulence (Smayda 1974, Margalef 1978 & 1997, Karp-Boss et al. 1996, Pahlow et al.et al. 1997, Padisak et al. 2003, Jumars et al. 2009). Size and hard cell coverings (e.g.the diatom frustule or dinoflagellate theca) can reduce grazing and defend against pathogens (Frost 1972, Smetacek 2001, Pondaven et al. 2007, Hamm & Smetacek 2007). Basic questions such as "What is this trait for?" or "Where is this trait found?" can lead to a better understanding of the ecological niches to which species are adapted and the parameters that determine community structure.

For natural phytoplankton populations, species–specific traits and their function are typically investigated by analysis of discrete samples. These analyses (e.g. identifying and counting individual species or performing bottle experiments) are often time consuming and, as a result, severely limit the resolution of observations that can be made in the ocean. Low resolution observations can lead to mischaracterization of marine ecosystem structure and function if important but small scale features are missed by sparse sample collection (Cassie 1963, Haury et al. 1978). Optical measurements provide an alternate method of determining the distribution of certain species-specific traits and their function with a high spatial resolution of ~1 cm and temporal resolution of <1 second (Cowles et al. 1998, Hanson & Donaghay 1998). Light absorption and scattering by phytoplankton cells and colonies determine, to a large extent, the particulate absorption (a_p), scattering (b_p), and attenuation (c_p) coefficient spectra measured by commercially available optical instrumentation. These instruments can be deployed on moored, profiling, and towed platforms to collect large, high resolution optical data sets that describe the spatial and temporal variation of bio-optical properties (Holliday et al. 2003, Babin et al. 2005, Stemmann & Boss 2012). The shape and magnitude of a_p, b_p, and c_p spectra are determined by particle abundance, size, shape, and complex refractive index (Morel & Bricaud 1986), characteristics that vary substantially among phytoplankton taxa and with their physiology. Measured optical properties, therefore, can serve as a proxy for these phytoplankton characteristics and can be used to map phytoplankton community types with high resolution over small scales. Through observation of ocean ecosystems, recent studies have demonstrated the importance of phytoplankton size and pigment

characteristics on the inherent optical properties of ocean waters and established the viability of optical measurements as a proxy for phytoplankton characteristics (Babin et al. 2003, Lohrenz et al. 2003, Bricaud et al., 2004, Cetinic et al. 2012, Bowers et al. 2009). Optical data could, therefore, be used to correlate phytoplankton community characteristics with environmental gradients and hydrographic processes in the ocean to obtain a deeper understanding of the selective forces that shape phytoplankton ecology and evolution.

The interaction of phytoplankton with light facilitates the discrimination of distinct communities, but is also a critical function of cells and colonies. Light is an essential and often growth limiting resource for phytoplankton in the ocean. The absorption of light energy by pigments embedded within chloroplasts drives photosynthesis which, in turn, fuels cellular metabolism and population growth. However, light absorption varies considerably among species and natural populations due to differences in cell volume, shape and pigment content. These morphological and physiological characteristics determine the amount of pigment self-shading (i.e. the "package effect"), which limits light absorption efficiency and growth as cell size or intracellular pigment concentrations increase (Duysens 1956, Das 1967, Kirk 1975, Bricaud et al. 1988, Finkel 2001). Competition for available light among bio-optically distinct species, therefore, can play an important role in structuring marine phytoplankton communities. For example, the competitive success of species with different minimum light requirements or absorption spectra can vary with light intensity (Huisman et al. 1999) and the spectral shape of the ambient light field (Stomp et al. 2004). In addition, fluctuations in available light intensity at 3-12 day

time scales have been shown to alternately favor distinct species resulting in increased diversity through disruption of competitive exclusion (Floder et al. 2002, Litchman & Klausmeier 2001, Litchman 2003). This previous work indicates absorption of light is a critical function of phytoplankton cells that varies with cellular traits and influences patterns of distribution and abundance in the ocean. Measurement of phytoplankton optical properties can provide information about the optical function of different populations and the possible strategies they employ to compete for light in the pelagic environment. Furthermore, light absorption efficiency can have a significant impact on rates of primary production and is therefore important to ecosystem models and calculations of biogeochemical fluxes (Bricaud et al. 1995, Platt & Sathyendranath 1999).

Although the broad goal of determining phytoplankton bio-optical function and ocean ecosystem structure using optical methods is promising, such methods require an understanding of the influence of specific traits on in situ particulate optical properties. While previous studies have established a basic theoretical framework with which to interpret optical measurements, there is insufficient empirical data available to adequately determine the dominant sources of optical variation over small scales in the ocean and their relationship to phytoplankton characteristics. To address this problem, this dissertation examines the variation of optical properties with community composition and the species–specific morphological and physiological characteristics of cells. The following questions are addressed using field and laboratory based approaches. First, do inherent optical properties vary with phytoplankton species composition and, if so, how? Next, how do phytoplankton size, pigment content, and

non-algal particulate material influence inherent optical properties, and can variation of these bio-optical characteristics be visualized over small scales? Finally, to what degree can species-specific morphology and physiology account for optical variation in natural environments and what is the bio-optical function and ecological significance of these characteristics? Field measurements were made over small scales critical to phytoplankton population dynamics in hydrodynamically complex coastal ocean waters using in situ optical measurements, autonomous profiling, live microscopy, and scanning flow cytometry. Laboratory studies used size fractionated optical measurements, automated photomicrographic image analysis, and scanning flow cytometry to determine the bio-optical properties of cultures with highly divergent morphologies.

Answers to the specific questions addressed in this dissertation will advance in situ bio-optical methods capable of high resolution observations that are directly related to phytoplankton cellular characteristics and functions essential to growth. With a better understanding of the influence of species and population specific traits on particulate optical properties, such methods can provide new and ecologically important information on natural phytoplankton community structure and function over small scales. The ability to infer ecologically important characteristics of phytoplankton from high resolution optical measurements can provide powerful insights into the conditions that favor certain forms over others and the processes that govern community assembly and succession. This type of detailed understanding of phytoplankton ecology has broad implications for biological processes that operate

over local (e.g. bloom dynamics) and global (e.g. biogeochemical cycles) scales throughout the world's oceans.

REFERENCES

Amato, A., W. H. C. F. Kooistra, J. H. Levialdi Ghiron, D. G. Mann, T. Proschold, and M. Montresor. 2007. Reproductive isolation among sympatric cryptic species in marine diatoms. Protist **158**: 193–207.

Babin, M., J. J. Cullen, C. S. Roesler, P. L. Donaghay, G. J. Doucette, M. Kahru, M. R. Lewis, C. A. Scholin, M. E. Sieracki, and H. M. Sosik. 2005. New approaches and technologies for observing harmful algal blooms. Oceanography **18**: 210–227.

Babin, M., D. Stramski, G. M. Ferrari, H. Claustre, A. Bricaud, G. Obolensky, and N. Hoepffner. 2003. Variations in the light absorption coefficients of phytoplankton, nonalgal particles, and dissolved organic matter in coastal waters around Europe. J. Geophys. Res. **108**, doi:10.1029/2001JC000882

Bowers, D. G., K. M. Braithwaite, W. A. M. Nimmo-Smith, and G. W. Graham. 2009. Light scattering by particles suspended in the sea: The role of particle size and density. Cont. Shelf Res. **29**: 1748–1755.

Bricaud, A., M. Babin, A. Morel, and H. Claustre. 1995. Variability in the chlorophyll-specific absorption coefficients of natural phytoplankton: Analysis and parameterization. J. Geophys. Res. **100**: 13321–13332.

Bricaud, A., A. L. Bédhomme, and A. Morel. 1988. Optical properties of diverse phytoplanktonic species: experimental results and theoretical interpretation. J. Plankton Res. **10**: 851–873.

Bricaud, A., H. Claustre, J. Ras, and K. Oubelkheir. 2004. Natural variability of phytoplanktonic absorption in oceanic waters: Influence of the size structure of algal populations. J. Geophys. Res. **109**, doi:10.1029/2004JC002419

Cassie, R. M. 1963. Microdistribution of plankton. Oceanogr. Mar. Biol. **1**.

Cetinić, I., M. J. Perry, N. T. Briggs, E. Kallin, E. A. D'Asaro, and C. M. Lee. 2012. Particulate organic carbon and inherent optical properties during 2008 North Atlantic Bloom Experiment. J. Geophys. Res. Oceans **117**.

Cowles, T. J., R. A. Desiderio, and M. E. Carr. 1998. Small-scale planktonic structure: persistence and trophic consequences. Oceanography **11**: 4–9.

Das, M., E. Rabinowitch, L. Szalay, and G. Papageorgiou. 1967. "Sieve-effect" in *Chlorella* suspensions. J. Phys. Chem. **71**: 3543–3549.

Duysens, L. N. M. 1956. The flattening of the absorption spectrum of suspensions, as compared to that of solutions. Biochim. Biophys. Acta **19**: 1–12.

Falkowski, P. G., R. T. Barber, and V. Smetacek. 1998. Biogeochemical controls and feedbacks on ocean primary production. Science **281**: 200.

Falkowski, P. G., and M. J. Oliver. 2007. Mix and match: how climate selects phytoplankton. Nat. Rev. Microbiol. **5**: 813–819.

Field, C. B., M. J. Behrenfeld, J. T. Randerson, and P. Falkowski. 1998. Primary production of the biosphere: Integrating terrestrial and oceanic components. Science **281**: 237–240.

Finkel, Z. V. 2001. Light absorption and size scaling of light-limited metabolism in marine diatoms. Limnol. Oceangr. **46**: 86–94.

Flöder, S., J. Urabe, and Z. Kawabata. 2002. The influence of fluctuating light intensities on species composition and diversity of natural phytoplankton communities. Oecologia **133**: 395–401.

Fogg, G. E. 1991. Tansley review No. 30. The phytoplanktonic ways of life. New Phytol. **118**: 191–232.

Frost, B. W. 1972. Effects of size and concentration of food particles on the feeding behavior of the marine planktonic copepod *Calanus pacificus*. Limnol. Oceanogr. **17**: 805–815.

Gran, H. H. 1912. Pelagic plant life, p. 307–386. *In* J. Murray and J. Hjort [eds.], The Depths of the Ocean. Macmillan and Co., Limited.

Hamm, C. E., and V. Smetacek. 2007. Armor: why, when, and how, p. 311–332. *In* P.G. Falkowski and A.H. Knoll [eds.], Evolution of Primary Producers in the Sea.

Hanson, A. K., and P. L. Donaghay. 1998. Micro-to fine-scale chemical gradients and layers in stratified coastal waters. Oceanography **11**: 10–17.

Haury, L. R., J. A. McGowan, and P. H. Wiebe. 1978. Patterns and processes in the time-space scales of plankton distributions, p. 277–327. *In* J.H. Steele [ed.], Spatial pattern in plankton communities. Plenum Press.

Hedges, S. B., H. Chen, S. Kumar, D. Y. Wang, A. S. Thompson, and H. Watanabe. 2001. A genomic timescale for the origin of eukaryotes. BMC Evolutionary Biology **1**: 4.

Holliday, D. V., P. L. Donaghay, C. F. Greenlaw, D. E. McGehee, M. M. McManus, J. M. Sullivan, and J. L. Miksis. 2003. Advances in defining fine- and micro-scale pattern in marine plankton. Aquat. Living Resour. **16**: 131–136.

Huisman, J., P. van Oostveen, and F. J. Weissing. 1999. Species dynamics in phytoplankton blooms: incomplete mixing and competition for light. Am. Nat. **154**: 46–68.

Hutchinson, G. E. 1961. The paradox of the plankton. Am. Nat. **95**: 137.

Jumars, P. A., J. H. Trowbridge, E. Boss, and L. Karp-Boss. 2009. Turbulence-plankton interactions: a new cartoon. Mar. Ecol. **30**: 133–150.

Karp-Boss, L., E. Boss, and P. A. Jumars. 1996. Nutrient fluxes to planktonic osmotrophs in the presence of fluid motion. Oceanogr. Mar. Biol. **34**: 71–107.

Katz, M. E., Z. V. Finkel, D. Grzebyk, A. Knoll, and P. G. Falkowski. 2004. Evolutionary trajectories and biogeochemical impacts of marine eukaryotic phytoplankton. Ann. Rev. Ecol. Evol. Syst. **35**: 523–556.

Kirk, J. T. O. 1975. A theoretical analysis of the contribution of algal cells to the attenuation of light within natural waters. I. General treatment of suspensions of pigmented cells. New Phytol. **75**: 11–20.

Litchman, E. 2003. Competition and coexistence of phytoplankton under fluctuating light: Experiments with two cyanobacteria. Aquat. Microb. Ecol. **31**: 241–248.

Litchman, E., and C. A. Klausmeier. 2001. Competition of phytoplankton under fluctuating light. Am. Nat. **157**: 170–187.

Litchman, E., and C. A. Klausmeier. 2008. Trait-based community ecology of phytoplankton. Ann. Rev. Ecol. Evol. Syst. **39**: 615–639.

Lohrenz, S. E., A. D. Weidemann, and M. Tuel. 2003. Phytoplankton spectral absorption as influenced by community size structure and pigment composition. J. Plankton Res. **25**: 35–61.

Longhurst, A. R. 1998. Ecological Geography of the Sea, Academic Press.

Longhurst, A., S. Sathyendranath, T. Platt, and C. Caverhill. 1995. An estimate of global primary production in the ocean from satellite radiometer data. J. Plankton Res. **17**: 1245–1271.

Margalef, R. 1978. Life-forms of phytoplankton as survival alternatives in an unstable environment. Oceanol. Acta **1**: 493–509.

Margalef, R. 1997. Turbulence and marine life. Sci. Mar. **61 (Supl. 1)**: 109–123.

Morel, A., and A. Bricaud. 1986. Inherent optical properties of algal cells including picoplankton: Theoretical and experimental results, p. 521–559. *In* T. Platt and W.K.W. Li [eds.], Photosynthetic Picoplankton. Department of Fisheries and Oceans.

Padisák, J., É. Soróczki-Pintér, and Z. Rezner. 2003. Sinking properties of some phytoplankton shapes and the relation of form resistance to morphological diversity of plankton – an experimental study. Hydrobiologia **500**: 243–257.

Pahlow, M., U. Riebesell, and D. A. Wolf-Gladrow. 1997. Impact of cell shape and chain formation on nutrient acquisition by marine diatoms. Limnol. Oceangr. **42**: 1660–1672.

Platt, T., and S. Sathyendranath. 1999. Spatial structure of pelagic ecosystem processes in the global ocean. Ecosystems **2**: 384–394.

Pondaven, P., Morgane Gallinari, SophieChollet, Eva Bucciarelli, Geraldine Sarthou, Sabine Schultes, and Jean Frederic. 2007. Grazing-induced changes in cell wall silicification in a marine diatom. Protist **158**: 21–28.

Rines, J. E. B., M. N. McFarland, P. L. Donaghay, and J. M. Sullivan. 2010. Thin layers and species-specific characterization of the phytoplankton community in Monterey Bay, California, USA. Cont. Shelf Res. **30**: 66–80.

Smayda, T. J. 1974. Some experiments on the sinking characteristics of two freshwater diatoms. Limnol. Oceanogr. **19**: 628–635.

Smayda, T. J. 2010. Adaptations and selection of harmful and other dinoflagellate species in upwelling systems 1. Morphology and adaptive polymorphism. Prog. Oceanogr. **85**: 53–70.

Smayda, T. J., and C. S. Reynolds. 2001. Community assembly in marine phytoplankton: Application of recent models to harmful dinoflagellate blooms. J. Plankton Res. **23**: 447 –461.

Smetacek, V. 2001. A watery arms race. Nature **411**: 745–745.

Smetacek, V., P. Assmy, and J. Henjes. 2004. The role of grazing in structuring Southern Ocean pelagic ecosystems and biogeochemical cycles. Antarct. Sci. **16**: 541–558.

Sournia, A. 1982. Form and function in marine phytoplankton. Biol. Rev. **57**: 347–394.

Stemmann, L., and E. Boss. 2012. Plankton and particle size and packaging: from determining optical properties to driving the biological pump. Annu. Rev. Mar. Sci. **4**: 263–290.

Stomp, M., J. Huisman, F. de Jongh, A. J. Veraart, D. Gerla, M. Rijkeboer, B. W. Ibelings, U. I. A. Wollenzien, and L. J. Stal. 2004. Adaptive divergence in pigment composition promotes phytoplankton biodiversity. Nature **432**: 104–107.

MANUSCRIPT 1

OPTICAL SIGNATURES OF MARINE PHYTOPLANKTON COMMUNITIES OVER SMALL SCALES

Malcolm N. McFarland, Jan Rines, Percy Donaghay, James Sullivan

Formatted for submission to the journal Limnology and Oceanography

University of Rhode Island, Graduate School of Oceanography

South Ferry Road, Narragansett, RI 02882

ABSTRACT

The shape and relative magnitude of particulate absorption (a_p), scattering (b_p), and attenuation (c_p) coefficient spectra can vary with phytoplankton pigment characteristics and suspended particle size distributions. Variation of these inherent optical properties in the ocean, therefore, conveys important information about the structure and function of pelagic ecosystems. In this study, the composition of coastal phytoplankton in Monterey Bay, CA is related to particulate scatter to absorption ratios (b_p:a_p), backscatter ratios (b_b:b), and the slopes of particulate attenuation and absorption spectra. Results show these optical parameters varied with phytoplankton species composition leading to different optical signatures associated with taxonomically distinct communities. The particulate attenuation and absorption slope parameters varied most with community composition, suggesting that size distribution and pigment content of cells are bio-optically important phytoplankton characteristics that differentiate populations over small scales in the coastal ocean. Results support the hypothesis that taxon specific morphological and physiological characteristics influence the optical properties of ocean waters in a manner consistent with optical theory. Furthermore, this study demonstrates the ability of inherent optical properties to provide ecologically important information about the structure of phytoplankton communities over small scales.

INTRODUCTION

Phytoplankton communities are composed of many species with distinct morphological and physiological characteristics. The distribution and abundance of these diverse species are important to the structure and function of marine ecosystems.

For example, species specific characteristics can affect rates of photosynthesis (Platt & Jassby 1976; Geider et al. 1986; Finkel 2001), nutrient uptake (Margalef 1978, 1997; Pahlow et al. 1997), grazing rates (Frost 1972; Verity & Smetacek 1996), sinking rates (Smayda & Boleyn 1965, 1966a, 1966b; Padisak et al. 2003) and the flux of carbon to deep ocean sediments where it can be sequestered for centuries (Smetacek et al. 2004; Smetacek et al. 2012). In hydrographically complex coastal ocean environments the composition of phytoplankton communities often varies significantly over centimeter to kilometer scales (Donaghay et al. 1992; Cowles et al. 1998; Dekshenieks et al. 2001; Rines et al. 2010). The physical and biological processes that determine species composition at these scales are not well understood, largely due to the difficulty of acquiring the number of observations necessary to resolve natural patterns of variation. In situ measurements of light scatter, absorption and attenuation provide a potential solution to this problem. In many pelagic ecosystems these optical properties are determined to a large extent by the abundance and characteristics of phytoplankton cells and colonies. In addition, optical measurements can be made with centimeter scale resolution. Modern optical instruments are capable of high data acquisition rates (> 1 Hz) and can be deployed in situ on a variety of moored, towed or vertically profiling platforms (Donaghay et al. 1992, Donaghay 2003, Holliday et al. 2003, Babin et al. 2005). Used as a proxy for phytoplankton, optical properties can facilitate the analysis of communities with very high spatial and temporal resolution. The resulting data provide a detailed picture of phytoplankton distribution and abundance that cannot be achieved with the analysis of discrete samples.

High resolution, multi-spectral measurements of the particulate absorption (a_p), attenuation (c_p), scatter (b_p), and backscatter (b_b) coefficients are of particular interest since the relative magnitude and spectral shape of these inherent optical properties (IOPs) can be influenced by cellular characteristics that vary within and among species. These coefficients are affected by the size, shape, pigment content, and refractive index of phytoplankton cells and colonies (Morel and Bricaud 1986). Intracellular pigment packaging can flatten the a_p spectrum and reduce the absorption efficiency of cells (Duysens 1956; Kirk 1994; Ciotti et al. 2002). A high ratio of photoprotective to photosynthetic carotenoids may also increase the slope of a_p spectra between 488 and 532 nm (Eisner et al. 2003 & 2005). Theoretical and empirical studies have shown that the exponential slope of the c_p spectrum is related to the shape of the particle size distribution. The c_p slope is high for size distributions dominated by very small particles and closer to zero for distributions with abundant large particles such as phytoplankton cells and colonies (Kitchen et al. 1982; Boss et al. 2001). The direction of scattered light can also be influenced by cell size and refractive index. Large cells with low refractive index will scatter most light in the forward direction, while smaller cells or cells with high refractive index will scatter a larger proportion of light in the backwards direction (Twardowski et al. 2001; Sullivan et al. 2005). Variations of these IOPs in field collected data sets, therefore, can be indicative of changes in the composition and physiological characteristics of the phytoplankton community.

Previous studies have found that a large amount of the variability of ocean water optical properties is derived from variation of the cell size distribution and pigment

packaging within phytoplankton (Babin et al. 2003; Bricaud et al. 2004). This suggests IOPs contain substantial information about the composition and characteristics of phytoplankton communities. However, previous studies have not quantified taxonomic composition, and the relationship between natural phytoplankton communities and their optical properties remains poorly understood. The ability to infer phytoplankton characteristics from in situ optical measurements, therefore, has been limited. This study tests the hypothesis that the relative abundance of morphologically and physiologically distinct taxa influences ocean water optical properties to produce unique optical signatures associated with different phytoplankton communities. To test this hypothesis discrete water samples were analyzed using manual, microscope based cell counts to determine species composition. Hierarchical cluster analysis was then used to define distinct communities based on species abundance data. For a subset of samples from each community, the size and abundance of pico- and nano-phytoplankton (2 – 20 μm in size) were also determined using image analysis of auto-fluorescent cells collected on filters. For each community we examined the relative magnitude and spectral shape of particulate attenuation, particulate absorption, and scattering coefficients; optical properties that can be influenced by the morphological and physiological characteristics of phytoplankton cells and colonies. Specifically, we measured the ratio of b_p at 555 nm to a_p at 676 nm, the spectral slope of c_p, the ratio of b_b to b at 532 nm, and the normalized slope of a_p between 488 and 532 nm for all communities. Redundancy analysis was used to assess the variation of optical properties among all samples and determine unique combinations of optical parameter values associated with different communities.

METHODS

This study was conducted in the northeast portion of Monterey Bay, CA near the 20 m isobath (Fig. 1). Data were collected between August 20th and September 2nd in 2005, and between July 17th and July 26th in 2006. Monterey Bay is a broad, open coastal system influenced primarily by three distinct water masses with different relative importance at different times of the year. During summer months recently upwelled waters are drawn into the Bay during formation of a cyclonic gyre (see Rines et al. 2010 Fig. 8), low salinity offshore waters intrude during upwelling relaxation, and tidal pulsing pumps Monterey Canyon water up from depth (Ryan et al. 2010). These different water masses can contain different environmental conditions, ecological histories and, consequently, different phytoplankton communities.

Optical data

Optical data were collected with a profiling instrument package equipped with two WET-Labs ac-9 (2005) or ac-s (2006) multi-spectral absorption and attenuation meters (25 cm path length), a Sea-Bird Electronics SBE-25 CTD, a WET-Labs ECO VSF 532 nm scattering sensor, and a WET-Labs WETStar chlorophyll fluorometer. One ac-9 meter was fitted with a 0.2 micron filter on the intake tubing to enable measurement of absorption by colored dissolved organic matter (a_g). The entire instrument package was slightly negatively buoyant and allowed to descend slowly through the water column during profiles, decoupled from ship motion (Donaghay, 1992). Profiles were conducted in duplicate to ensure that the measured water column structure was accurate.

Absorption and attenuation meters were calibrated before, during and after the study with 0.2 micron filtered, de-ionized water from a Barnstead E-Pure purification system. Optical data were corrected for the effects of temperature and salinity according to the methods of Twardowski et al. (1999) and Sullivan et al. (2006). Scattering errors in the ac-9 and ac-s meters were corrected using the proportional correction algorithm of Zaneveld et al. (1994). The unfiltered ac-9 or ac-s meter was used to measure the absorption (a_{pg}) and attenuation (c_{pg}) coefficients for particulate and dissolved water constituents. The 0.2 micron filtered ac-9 meter measured the dissolved absorption coefficient (a_g). A flow sensor in line with the filtered ac meter was used to compensate for the slower flow rate through the filter. Particulate absorption (a_p) and attenuation (c_p) were calculated by difference ($a_p = a_{pg} - a_g$, and $c_p = c_{pg} - a_g$). The particulate scattering coefficient (b_p) was calculated as the difference between the particulate absorption and attenuation coefficients ($b_p = c_p - a_p$). Backscattering coefficients (b_b) at 532 nm were calculated from the ECO VSF data according to Moore et al. (2000).

Four parameters that depend on the shape and relative magnitude of IOP spectra were computed for each sample. The ratio of scattering to absorption (b_p:a_p) was calculated from b_p measured at 555 nm and a_p measured at 676 nm. The wavelength for b_p was chosen to coincide with peak scattering and to avoid the major chlorophyll absorption wave bands. The wavelength for a_p was chosen to coincide with the red chlorophyll absorption band and to minimize the influence of non-algal particulate absorption. The slope of the attenuation coefficient (c_p) was computed by fitting an equation of the form $c_p(\lambda) = s\lambda^{-\gamma}$ where λ is the wavelength, γ is the exponential slope

of the spectrum, and s is a scale factor (Twardowski et al., 2001, Boss et al., 2001). The backscatter ratio was calculated from b_b and b, both measured at 532 nm. Finally, the negative of the a_p slope parameter was calculated according to Eisner et al. 2003 as:

$$a_p \text{ slope} = -\frac{a_p 488 - a_p 532}{a_p 676(488 - 532\ nm)}$$

Note that Eisner et al. report a_p slope as a negative value and we report this slope as a positive value to maintain consistency with conventions for c_p slope.

Discrete samples

Discrete water samples were collected with a Sea-Bird Electronics SBE-32SC sub-compact rosette bottle sampler equipped with ~1L niskin bottles (~30cm height), a Sea-Bird Electronics SBE-25 CTD, and a WET Labs WETStar chlorophyll fluorometer. As with the optical package, buoyancy was adjusted to be slightly negative and profiles were conducted with the package floating freely, decoupled from ship motion. To ensure accurate and efficient sampling over the full range of optical variation throughout the water column, an adaptive sampling strategy was employed that targeted optically distinct layers, some of which were less than a meter thick. High resolution optical profiles were conducted immediately prior to sampling (generally within 15 minutes) and depths were chosen for sampling based on in situ optical and CTD data available in real time (a_{pg}, c_{pg}, temperature, salinity, density and chlorophyll fluorescence). Sample depths were chosen to capture the full range of optical properties throughout the water column including minimum, maximum, and various intermediate values of a_{pg}, c_{pg}, and chlorophyll. During the sampling profile,

bottles were triggered manually at depths where temperature, salinity, density and chlorophyll signals matched the depths chosen previously during the optical profile. This strategy ensured that ecologically and optically important thin layers of phytoplankton were accurately sampled.

Ten sample profiles were obtained in 2005, and nine sample profiles were obtained in 2006. Between 5 and 10 depths were sampled for each profile. Live samples were examined immediately after collection using a compound microscope equipped with a digital video camera system. 250 mL sub-samples were preserved in 1% formaldehyde and 1% glacial acetic acid and stored for later analysis in the lab. Immediately prior to microscope cell counts, samples were gently homogenized by inverting the sample bottle ~50 times. 1 mL sub-samples were analyzed in a Sedgewick-Rafter chamber at 100x magnification using a Nikon Eclipse E800 light microscope equipped with phase contrast optics. Phytoplankton species greater than ~10 μm in size were identified and manually enumerated. At least 400 cells were counted for each sample. When necessary, samples with very low cell densities were gently concentrated up to 10 times their original concentration by reverse filtration with a 7 μm mesh size Nitex filter.

Small photosynthetic cyanobacteria and pico-eukaryotes between 2 and 20 μm in size are not well preserved in whole water samples and cannot be enumerated in water mounts. To determine the abundance of these small cells, 25 mL sub-samples were collected and immediately filtered through 0.2 μm pore size, 25 mm Whatman Anodisc filters. Samples were filtered to a volume of 5 mL, fixed with a 1% solution of Formaldehyde for 5 minutes, and then filtered until dry. The fixed filters were

mounted on glass slides in immersion oil, stored at -20° C, and analyzed within four weeks. Images of cells on filters were acquired with a 1600 x 1200 pixel digital color camera (Diagnostic Instruments, Spot Insight) mounted on a Nikon Eclipse E800 microscope. Cells were excited with blue light (450 - 490 nm) from a mercury arc lamp and the autofluorescence of phycoerythrin and chlorophyll was detected at wavelengths greater than 515 nm in the green and red channels of the color camera. Images collected in 2005 were acquired with a 40x objective at a resolution of 5.445 pixels μm^{-1}. Images collected in 2006 were acquired with a 20x objective at a resolution of 2.734 pixels μm^{-1} to compensate for lower cell densities by maximizing image area. To extend the dynamic range of the camera and reduce noise, four exposures at 100 ms, 800 ms, 1.5 s, and 2.5 s were captured and averaged to create each image. For each sample, 4 to 6 images were acquired from different quadrants of each filter to compensate for any uneven distribution of cells.

Color images were processed, segmented, and analyzed using MATLAB (The Mathworks, Inc.). Images were processed to reduce noise and equalize intensity by applying multiple Gaussian bandpass filters. The resulting filtered images were segmented by application of a threshold. Mean Feret diameter and mean red and green fluorescence intensity were recorded for all contiguous regions with intensities above the threshold. Regions touching the edge of the image were ignored. *Synechococcus* was discriminated from *Prochlorococcus* and photosynthetic nano-eukaryotes manually for each sample based the relative intensity of red and green fluorescence. Cell concentrations were calculated from the number of cells counted, the volume filtered (25 mL), the total filter area (283.53 mm^2), and the total filter area imaged.

Data analysis

Due to the offset in time (generally less than 15 minutes) between optical profiles and sample collection, it was necessary to align the optical and biological data sets to compensate for slight changes in water column structure caused by internal waves and other short time scale hydrographic processes. For each sample, optical data were extracted from profiles at the depth where temperature, salinity and chlorophyll fluorescence matched data from the bottle sampler package. Aligned biological and optical data sets were then compared to investigate the relationship between community composition and optical properties of samples. Statistical methods employed to assess this relationship included hierarchical cluster analysis, to identify communities based on species composition, and redundancy analysis, to explore the variation of optical properties among communities.

A distance matrix based on species abundance data was computed for all samples using the Bray-Curtis distance metric. Hierarchical cluster analysis performed on this distance matrix was used to group samples according to taxonomic composition. Cluster analysis was computed with the MATLAB statistics toolbox version 8.0 (The MathWorks, Inc. 2012). The resulting dendrogram was cut at a fixed distance to produce groups of samples representing distinct phytoplankton communities. The level at which the dendrogram was cut was determined as the smallest distance above which similarity profile tests could confirm significant structure ($p < 0.05$) for all groups (Clarke et al. 2008). Similarity profile tests were performed with the fathom toolbox (Jones 2012) in MATLAB using 10^4 iterations. To compare among communities, mean a_p, b_p, and c_p spectra were calculated for each community by

averaging the spectra for all samples in each community. Likewise, mean b_p:a_p, b_b:b, a_p slope and c_p slope were calculated for each community by averaging these parameters for all samples in each community. To examine the relationship between species composition and the optical properties of communities, redundancy analysis was performed using the Vegan package for R (Oksanen et al., 2013).

RESULTS

The species composition of samples collected over the small spatial and temporal scales in this study varied considerably within and between years. A total of 146 distinct taxa were found in 145 collected samples (72 samples in 2005 and 73 samples in 2006). 44 taxa were unique to 2005, 41 taxa were unique to 2006, and 61 taxa were found in both 2005 and 2006. The result of hierarchical cluster analysis for all samples collected in both years is shown in the dendrogram in Fig. 2. Similarity profiles supported all divisions of the dendrogram down to a distance of 0.72 ($p < 0.05$). Cutting the dendrogram at this distance (dotted line in Fig. 2) produced a total of 9 distinct phytoplankton communities. The number of samples in each community ranged from 4 to 52 (Table 1). Three of these communities were present in 2005 (communities 1, 5, & 7) and six communities were present in 2006 (communities 2, 3, 4, 6, 8, & 9). Although there was no overlap of communities between years, in some cases similarity of community composition between years was greater than within year similarity. For example, communities 3 and 9 (present in 2006) are more similar to communities 1 and 7 (present in 2005) then they are to communities 2 and 8. This suggests some degree of year to year continuity of phytoplankton populations within Monterey Bay.

The composition of each community determined by manual cell counts is shown in Fig. 3 with a selection of the most abundant taxa highlighted. Dominant taxa within the communities present during 2005 included *Pseudo-nitzschia* sp., *Alexandrium sp*., and *Akashiwo sanguinea*. Communities 1 and 7 contained a diverse array of taxa and differed predominantly in the presence of species found at relatively low concentrations. Figure 4A shows the depth distribution of communities for the duration of the 2005 field project. Community 7 was present throughout much of the water column during the early part of the field project and then at greater depths later in time. Community 1 was more prevalent towards the end of the field project. Community 5 represents samples collected within a dense thin layer of *A. sanguinea* that was migrating vertically on a diurnal cycle (Rines et al. 2010, Sullivan et al. 2010).

During 2006, dominant taxa included *Chaetoceros debilis*, *Alexandrium* sp., *Chaetoceros concavicornis*, *Pseudo-nitzschia* sp., *Chaetoceros perpusillus*, *Prorocentrum gracile*, and *Alexandrium catenella* (Fig. 3). Community 4, overwhelmingly dominated by the small colonial pennate diatom *Pseudo-nitzschia*, was present throughout the water column at the beginning of the 2006 field project (Fig. 4B). Near the surface this community was replaced by communities 2 and 8, dominated by dinoflagellates in the genera *Alexandrium* and *Prorocentrum*. Community 9, with significant populations of the small unicellular diatom *C. perpusillus*, was found at various depths during the field project. Community 6, dominated by the large colonial diatom *C. concavicornis*, was present for a short time at depth and may have been introduced with an intrusion of off shore water.

Community 3, dominated by another large colonial diatom *C. debilis*, was present only near the end of the field project. These patchy distributions of taxa over depth and time suggest a dynamic physical environment that was continuously advecting distinct communities through the study area.

The abundance of *Synechococcus*, *Prochlorococcus*, and photosynthetic nano-eukaryotes was determined for a subset of 80 samples (Fig. 5). The percentage of samples analyzed from each community ranged from 41% to 100%. Small cyanobacterial cells (1 to 5 μm) were most abundant during 2005 (communities 1, 5, & 7) with consistently high concentrations of *Synechococcus*. Community 1 had somewhat higher concentrations of cells in the 5 to 15 μm size range while communities 5 and 7 contained few of these photosynthetic nano-eukaryotes. During 2006, overall concentrations of pico and nano-phytoplankton were lower. Communities 2, 3, 6 and 9 were all similar in their composition of pico- and nano-phytoplankton. The relative abundance of larger cells in the 5 to 20 μm size range was greater for communities 4 and 8.

The relative magnitude and shape of the mean a_p, b_p, and c_p coefficient spectra varied considerably among communities (Fig. 6). Consequently, there was substantial variation in the b_p:a_p, c_p slope, b_b:b, and a_p slope parameters. The mean values and standard deviations of these optical parameters are listed for each community in Table 1. Results of the redundancy analysis (Fig. 7) show the variation of taxonomic composition and optical properties among all 145 samples from both years. A permutation test of this result was highly significant ($p = 0.005$). In the redundancy analysis biplot, symbols represent individual samples and symbol shape indicates

community membership as determined by the previous cluster analysis. Samples with similar community composition are closer together. Vectors indicate the direction of increase in value for each optical parameter. The length of a vector indicates the importance of a particular optical parameter in explaining the observed variation. The plotted result best represents the variation of the c_p and a_p slope parameters since these vectors are longest. The b_p:a_p vector is shorter and therefore explains less of the variation shown in the biplot. Vectors representing the b_p:a_p and b_b:b parameters point in similar directions indicating that these parameters are correlated. Vectors representing the c_p slope and a_p slope parameters are perpendicular indicating these parameters are not correlated.

The distribution of samples relative to the vectors shows how optical properties varied among the 9 communities. Comparison of the communities at greatest distance from the origin most clearly demonstrates the relationship between composition and optics. For example, community 4, dominated by the colony forming pennate diatom *Pseudo-nitzschia* sp. (Fig. 3), was found to have a high b_p:a_p ratio, a high b_b:b ratio, a high a_p slope, and the highest c_p slopes (Fig. 7, Table 1). This community also had relatively low concentrations of pico-phytoplankton but relatively high concentrations of nano-phytoplankton (Fig. 5). In contrast, community 5, dominated by *A. sanguinea* (Fig. 3), had low a_p slopes, intermediate b_p:a_p values, low b_b:b ratios, and moderate to high c_p slopes (Fig. 7, Table 1). *Synechococcus* were abundant in community 5 but nano-phytoplankton were not (Fig. 5). Community 6 contained substantial numbers of *Chaetoceros concavicornis* and low concentrations of pico- and nano-phytoplankton (Figs. 2 & 4). It had low c_p slopes with intermediate values of other optical

parameters. Community 8 had high concentrations of dinoflagellates in the genus *Alexandrium* (Fig. 3), low concentrations of pico-phytoplankton, and high concentrations of nano-phytoplankton (Fig. 5). This community had the lowest c_p slopes, the lowest b_p:a_p values, and intermediate values of b_b:b and a_p slope (Fig. 7, Table 1). Community 9 had the highest a_p slope values, the highest b_b:b values, high b_p:a_p values, and intermediate c_p slope values. This community was dominated by the diatoms *C. perpusillus* and *Pseudo-nitzschia sp*. (Fig. 3) and it had low concentrations of pico- and nano-phytoplankton (Fig. 5).

DISCUSSION

Analysis of phytoplankton community composition in Monterey Bay revealed a highly structured and dynamic ecosystem that supports a large number of diverse phytoplankton (Fig. 3). The fine-scale distribution of species and their general ecology during this study are discussed in Rines et al. (2010). Taxa were not evenly distributed throughout the bay but organized into communities with distinct spatial and temporal distributions (Fig. 4). Community composition varied considerably over the smallest spatial (meters) and temporal (days) scales that were resolved by our adaptive sampling methodology. Results clearly show that the spectral shape and relative magnitude of IOPs varied with phytoplankton composition (Fig. 7) leading to different optical signatures associated with taxonomically distinct communities. The c_p slope and a_p slope parameters varied most with community composition, suggesting that size distribution and pigment content of cells are bio-optically important phytoplankton characteristics that differentiate populations in the coastal ocean. These results support the hypothesis that taxon specific morphological and physiological

characteristics influence the optical properties of ocean waters and suggest that IOPs can provide detailed information about the structure of phytoplankton communities over small scales.

The optical variation among communities found in this study is generally in agreement with previous theoretical and empirical research that has examined the relationship between particle characteristics and the optical properties of particle suspensions. Previous studies that examined the relationship between c_p slope and the particle size distribution have shown that large c_p slopes are associated with abundant small particles and smaller c_p slopes are associated with abundant larger particles (Kitchen et al. 1982, Boss et al. 2001, Sullivan et al. 2005). In this study, communities with high concentrations of the pico-phytoplankton *Synechococcus* (1, 5 and 7) and communities dominated by small celled diatoms such as *Pseudo-nitzschia* sp. and *C. perpusillis* (4 and 9) had moderate to high c_p slopes (Fig. 7, Table 1). In contrast, communities dominated by larger cells such as *C. concavicornis*, *C. debilis*, or *Alexandrium* spp. with lower concentrations of pico-phytoplankton (communities 6, 3 and 8) had lower c_p slopes (Fig. 7, Table 1). This suggests c_p slope, on average, is a good indicator of the size distribution of phytoplankton cells, a characteristic that varies with community structure and function (Platt & Jassby 1976; Geider et al. 1986; Finkel 2001).

The a_p slope parameter is affected by the ratio of photoprotective to photosynthetic carotenoids (PPC:PSC), the package effect, and the relative abundance of non-algal particles. A high a_p slope is associated with a large PPC:PSC ratio typical of high light adapted cells (Eisner et al. 2003 & 2005). The a_p slopes measured for

communities in this study corresponded to moderate to high PPC:PSC ratios ranging from ~.5 – 1 (Eisner et al. 2003) suggesting phytoplankton were adapted to high light levels. Package effects, on the other hand, will decrease the slope of the a_p spectrum resulting in an a_p slope parameter closer to zero (Duysens 1956, Kirk 1975, Ciotti et al. 2002). Non-algal particles may also increase a_p slopes due to their high absorption at short wavelengths and exponentially decreasing absorption at longer wavelengths (Kishino et al. 1984, Roesler 1989). We found community 5, dominated by *A. sanguinea*, to have the lowest a_p slopes (Fig. 7, Table 1). This result may be due to strong packaging and is consistent with microscope observations of high intracellular pigment concentrations within live cells (Rines et al. 2010). Community 1 also had a relatively high a_p slope which may reflect low PPC:PSC ratios. Communities 4, 6 and 9 had the lowest a_p slopes (Fig. 7, Table 1). These communities were all dominated by diatoms of various size and had relatively low concentrations of pico-phytoplankton (Figs. 3 & 5). These low a_p slopes therefore may indicate high PPC:PSC ratios for these communities.

Previous studies have shown that b_b and b_b:b can vary among particle populations with different size distributions, carbon content, and refractive indexes (Vaillancourt et al. 2004, Sullivan et al. 2005). The range of mean b_b:b values in this study is relatively small compared to the range of values obtained from diverse locations (Sullivan et al. 2005) and there was substantial variation within communities. In our data the b_b:b parameter was highest for communities 4 and 9 dominated by small micro-phytoplankton sized cells (Figs. 3 & 7, Table 1). This is consistent with expectations for communities dominated by small cells. However, this parameter was

lowest for community 1 despite high concentrations of pico- and nano-phytoplankton (Figs. 5 & 7, Table 1). These cells may have been too small, or their refractive index may have been too low to contribute significantly to the measured scatter. Non-algal particles not measured in this study may also have influenced b_b:b since they have been shown to contribute significantly to backscatter (Green et al. 2003). It is possible both the c_p slope and b_b:b parameters responded not only to overall cell size, but also to the morphological features of individual cells. *Pseudo-nitzschia* cells, for example, have widths of ~3 to 7 µm, but they also have numerous striations along the valve face with sizes at or near the wavelengths of visible light (~500 nm to 1 µm). Also, *C. perpusillus* and *C. debilis* have 4 siliceous setae per cell that are ~1 µm or less in width, although these species form larger cells and colonies (Rines et al. 2010 Fig. 1F & Fig. 5H). It is possible that small morphological features of cells such as striations and setae behave optically as abundant small particles.

In laboratory based studies, Stramski & Reynolds (1993) have shown b_p:a_p ratios are related to the ratio of intracellular carbon to chlorophyll. Photoadaptation, which can affect intracellular pigment content, may also be important to b_p:a_p ratios for natural communities (Sosik et al. 2001). Physiological differences among taxa, therefore, are likely to have contributed to variation of this parameter among communities in Monterey Bay. We found the b_p:a_p parameter to be highest for communities 4, 5, 7, and 9 (Table 1) although this result is poorly represented by the redundancy analysis (Fig. 7). In the case of communities 4, 7 and 9, this parameter was likely high due to the weak absorption of *Pseudo-nitzschia* sp. and *C. perpusillis* cells which had very low amounts of chlorophyll and appeared physiologically

stressed (see Rines et al. 2010, Figs. 1C, 1D, 5A, & 5H). In the case of community 5, the relatively high b_p:a_p ratio may be attributable to a strong package effect for *A. sanguinea* that reduced a_p at 676 nm relative to total scatter. Microscopy of live *A. sanguinea* showed high intracellular chlorophyll concentrations for these relatively large (~40 μm) cells. *A. sanguinea* may be able to reach high cell concentrations in spite of this high package effect and reduced absorption efficiency due to its motility. Cells can vertically migrate to surface waters where high light levels may minimize any reduction in fitness associated with package effects. The b_p:a_p parameter was lowest for communities 1 and 8 (Table 1). Both of these communities have somewhat higher concentrations of photosynthetic nano-eukaryotes and dinoflagellates such as *Alexandrium* spp. or *A. sanguinea* (Figs. 3 & 5) that may have had different physiological characteristics.

Although we found that variation of mean optical properties among phytoplankton communities was related to phytoplankton morphological and physiological characteristics in agreement with our current understanding of ocean optics, there was substantial variation within communities for all optical parameters. Much of this within community variation may be due to non-algal particles that were not measured in this study. Some of the variation among communities may also be attributable to co-varying non-algal particles (e.g. bacteria, cell debris, exopolymers, and suspended sediments). These particles would likely increase b_p:a_p, b_b:b, c_p slope and a_p slope. However, Monterey Bay receives very little freshwater run-off during summer months and there was little evidence of significant re-suspension of sediments in our optical profiles and samples. Furthermore, a_p values in the blue portion of the

spectrum for all communities are higher at 440 nm than at 400 nm (Fig. 6), characteristic of absorption by photosynthetic pigments and not by non-algal particulate material (Kishino et al. 1984, Roesler 1989). It seems likely, therefore, that non-algal particles made only small contributions to measured values of a_p. Also, it is important to note that the relative abundance of taxa as depicted in Fig. 3 does not take into account the projected area of cells and therefore may underestimate the contribution of large, rare taxa to the measured optical properties. Despite some methodological limitations, our data show a compelling pattern of correlation between phytoplankton community characteristics and optical properties that is in agreement with our basic understanding of the optical properties of suspended particles in ocean waters. Future work should employ methods to quantify the abundance of non-algal particles and take into account the effect of a particle size.

The results presented here build upon previous studies to show that the optical properties of phytoplankton communities can provide valuable biological information on the morphological and physiological characteristics of cells. We found evidence that cell size and intracellular pigment content can influence the shape and relative magnitude absorption, attenuation, and scattering coefficient spectra. Consequently, the measurement of optical properties can facilitate the analysis of these phytoplankton community characteristics in the ocean with very high spatial and temporal resolution. Mapping distribution patterns of phytoplankton traits over smaller scales than has traditionally been possible could greatly enhance our understanding of the processes that determine species succession, community assembly and ecosystem change.

Acknowledgements

We are grateful for the help of Jason Graff during data collection. We thank ONR for their commitment to our research program. This work was supported by ONR grants N000140410275 (JR) and N000140410276 (PD and JS).

REFERENCES

Babin, M., J. J. Cullen, C. S. Roesler, P. L. Donaghay, G. J. Doucette, M. Kahru, M. R. Lewis, C. A. Scholin, M. E. Sieracki, and H. M. Sosik. 2005. New approaches and technologies for observing harmful algal blooms. Oceanography **18**: 210–227.

Babin, M., D. Stramski, G. M. Ferrari, H. Claustre, A. Bricaud, G. Obolensky, and N. Hoepffner. 2003. Variations in the light absorption coefficients of phytoplankton, nonalgal particles, and dissolved organic matter in coastal waters around Europe. J. Geophys. Res. **108**, doi:10.1029/2001JC000882

Boss, E., M. S. Twardowski, and S. Herring. 2001. Shape of the particulate beam attenuation spectrum and its inversion to obtain the shape of the particulate size distribution. Appl. Opt. **40**: 4885–4893.

Bricaud, A., H. Claustre, J. Ras, and K. Oubelkheir. 2004. Natural variability of phytoplanktonic absorption in oceanic waters: Influence of the size structure of algal populations. J. Geophys. Res. **109**, doi:10.1029/2004JC002419

Ciotti, A. M., M. R. Lewis, and J. J. Cullen. 2002. Assessment of the relationships between dominant cell size in natural phytoplankton communities and the spectral shape of the absorption coefficient. Limnol. Oceanogr. **47**: 404–417.

Clarke, K. R., P. J. Somerfield, and R. N. Gorley. 2008. Testing of null hypotheses in exploratory community analyses: similarity profiles and biota-environment linkage. J. Exp. Mar. Biol. Ecol. **366**: 56–69.

Cowles, T. J., R. A. Desiderio, and M. E. Carr. 1998. Small-scale planktonic structure: persistence and trophic consequences. Oceanography **11**: 4–9.

Dekshenieks, M. M., P. L. Donaghay, J. M. Sullivan, J. E. B. Rines, T. R. Osborn, and M. S. Twardowski. 2001. Temporal and spatial occurrence of thin phytoplankton layers in relation to physical processes. Mar. Ecol. Prog. Ser. **223**: 61–71.

Donaghay, P. L. 2003. Profiling systems for understanding the dynamics and impacts of thin layers of harmful algae in stratified coastal waters. 44–53.

Donaghay, P. L., H. M. Rines, and J. M. Sieburth. 1992. Simultaneous sampling of fine scale biological, chemical, and physical structure in stratified waters. Arch. Hydrobiol. **36**: 97–108.

Duysens, L. N. M. 1956. The flattening of the absorption spectrum of suspensions, as compared to that of solutions. Biochim. Biophys. Acta **19**: 1–12.

Eisner, L. B., and T. J. Cowles. 2005. Spatial variations in phytoplankton pigment ratios, optical properties, and environmental gradients in Oregon coast surface waters. J. Geophys. Res. **110**, doi:10.1029/2004JC002614

Eisner, L. B., M. S. Twardowski, T. J. Cowles, and M. J. Perry. 2003. Resolving phytoplankton photoprotective: photosynthetic carotenoid ratios on fine scales using in situ spectral absorption measurements. Limnol. Oceanogr. **48**: 632–646.

Finkel, Z. V. 2001. Light absorption and size scaling of light-limited metabolism in marine diatoms. Limnol. Oceanogr. **46**: 86–94.

Geider, R. J., T. Platt, and J. A. Raven. 1986. Size dependence of growth and photosynthesis in diatoms: a synthesis. Mar. Ecol. Prog. Ser. **30**: 93–104.

Holliday, D. V., P. L. Donaghay, C. F. Greenlaw, D. E. McGehee, M. M. McManus, J. M. Sullivan, and J. L. Miksis. 2003. Advances in defining fine- and micro-scale pattern in marine plankton. Aquat. Living Resour. **16**: 131–136.

Jones, D. L. 2012. The Fathom Toolbox for MATLAB: multivariate ecological and oceanographic data analysis, College of Marine Science, University of South Florida.

Kirk, J. T. O. 1994. Light and Photosynthesis in Aquatic Ecosystems, 2nd ed. Cambridge University Press.

Kitchen, J. C., J. R. V. Zaneveld, and H. Pak. 1982. Effect of particle size distribution and chlorophyll content on beam attenuation spectra. Appl. Opt. **21**: 3913–3918.

Margalef, R. 1978. Life-forms of phytoplankton as survival alternatives in an unstable environment. Oceanol. Acta **1**: 493–509.

Margalef, R. 1997. Turbulence and marine life. Sci. Mar. **61 (Supl. 1)**: 109–123.

Moore, C., M. S. Twardowski, and J. R. V. Zanaveld. 2000. The ECO VSF - A multi-angle scattering sensor for determination of the volume scattering function in the backward direction.

Morel, A., and A. Bricaud. 1986. Inherent optical properties of algal cells including picoplankton: Theoretical and experimental results, p. 521–559. *In* T. Platt and W.K.W. Li [eds.], Photosynthetic Picoplankton. Department of Fisheries and Oceans.

Padisák, J., É. Soróczki-Pintér, and Z. Rezner. 2003. Sinking properties of some phytoplankton shapes and the relation of form resistance to morphological diversity of plankton – an experimental study. Hydrobiologia **500**: 243–257.

Pahlow, M., U. Riebesell, and D. A. Wolf-Gladrow. 1997. Impact of cell shape and chain formation on nutrient acquisition by marine diatoms. Limnol. Oceanogr. **42**: 1660–1672.

Platt, T., and A. D. Jassby. 1976. The Relationship Between Photosynthesis and Light for Natural Assemblages of Coastal Marine Phytoplankton. J. Phycol. **12**: 421–430.

R Core Team. 2013. R: a language and environment for statistical computing, R Foundation for Statistical Computing.

Rines, J. E. B., M. N. McFarland, P. L. Donaghay, and J. M. Sullivan. 2010. Thin layers and species-specific characterization of the phytoplankton community in Monterey Bay, California, USA. Cont. Shelf Res. **30**: 66–80.

Ryan, J. P., M. A. McManus, and J. M. Sullivan. 2010. Interacting physical, chemical and biological forcing of phytoplankton thin-layer variability in Monterey Bay, California. Cont. Shelf Res. **30**: 7–16.

Smayda, T. J., and B. J. Boleyn. 1965. Experimental observations on the flotation of marine diatoms. I. *Thalassiosira cf. nana*, *Thalassiosira rotula* and *Nitzschia seriata*. Limnol. Oceanogr. **10**: 499–509.

Smayda, T. J., and B. J. Boleyn. 1966a. Experimental observations on the flotation of marine diatoms. II. *Skeletonema costatum* and *Rhizosolenia setigera*. Limnol. Oceanogr. **11**: 18–34.

Smayda, T. J., and B. J. Boleyn. 1966b. Experimental observations on the flotation of marine diatoms. III. *Bacteriastrum hyalinum* and *Chaetoceros lauderi*. Limnol. Oceanogr. **11**: 35–43.

Smetacek, V., P. Assmy, and J. Henjes. 2004. The role of grazing in structuring Southern Ocean pelagic ecosystems and biogeochemical cycles. Antarct. Sci. **16**: 541–558.

Smetacek, V., C. Klaas, V. H. Strass, P. Assmy, M. Montresor, B. Cisewski, N. Savoye, A. Webb, F. d' Ovidio, J. M. Arrieta, U. Bathmann, R. Bellerby, G. M. Berg, P. Croot, S. Gonzalez, J. Henjes, G. J. Herndl, L. J. Hoffmann, H. Leach, M. Losch, M. M. Mills, C. Neill, I. Peeken, R. Röttgers, O. Sachs, E. Sauter, M. M. Schmidt, J. Schwarz, A. Terbrüggen, and D. Wolf-Gladrow. 2012. Deep carbon export from a Southern Ocean iron-fertilized diatom bloom. Nature **487**: 313–319.

Sosik, H. M., R. E. Green, W. S. Pegau, and C. S. Roesler. 2001. Temporal and vertical variability in optical properties of New England shelf waters during late summer and spring. J. Geophys. Res. **106**: 9455–9472.

Stramski, D., and R. A. Reynolds. 1993. Diel variations in the optical properties of a marine diatom. Limnol. Oceanogr. **38**: 1347–1364.

Sullivan, J. M., P. L. Donaghay, and J. E. B. Rines. 2010. Coastal thin layer dynamics: Consequences to biology and optics. Cont. Shelf Res. **30**: 50–65.

Sullivan, J. M., M. S. Twardowski, P. L. Donaghay, and S. A. Freeman. 2005. Use of optical scattering to discriminate particle types in coastal waters. Appl. Opt. **44**: 1667–1680.

Sullivan, J. M., M. S. Twardowski, J. R. V. Zaneveld, C. M. Moore, A. H. Barnard, P. L. Donaghay, and B. Rhoades. 2006. Hyperspectral temperature and salt dependencies of absorption by water and heavy water in the 400-750 nm spectral range. Appl. Opt. **45**: 5294–5309.

The MathWorks, Inc. 2012. MATLAB, The MathWorks, Inc.

Twardowski, M. S., E. Boss, J. B. Macdonald, W. S. Pegau, A. H. Barnard, and J. R. V. Zaneveld. 2001. A model for estimating bulk refractive index from the optical backscattering ratio and the implications for understanding particle composition in case I and case II waters. J. Geophys. Res. **106**: 14129–14142.

Twardowski, M. S., J. M. Sullivan, P. L. Donaghay, and J. R. V. Zaneveld. 1999. Microscale quantification of the absorption by dissolved and particulate material in coastal waters with an ac-9. J. Atmos. Ocean Tech. **16**: 691–707.

Vaillancourt, R. D., C. W. Brown, R. R. L. Guillard, and W. M. Balch. 2004. Light backscattering properties of marine phytoplankton: relationships to cell size, chemical composition and taxonomy. J. Plankton Res. **26**: 191–212.

Zaneveld, J. R. V., J. C. Kitchen, and C. C. Moore. 1994. Scattering error correction of reflecting-tube absorption meters. Proceedings of the Ocean Optics XII. 44–55.

TABLES

Table 1. Mean and standard deviations (s.d.) of b_p:a_p, c_p slope, b_b:b, and a_p slope for samples in each community and for all samples. The magnitude of the standard deviation indicates the range of values within each community. Also shown is the number of samples (N) for each community.

com-		b_p:a_p		c_p slope		b_b:b		a_p slope	
munity	N	mean	s.d.	mean	s.d.	mean	s.d.	mean	s.d.
1	52	7.59	3.82	0.36	0.16	0.0108	0.0023	0.0134	0.0018
2	4	9.69	2.78	0.38	0.15	0.0171	0.0013	0.0175	0.0011
3	8	9.18	5.49	0.25	0.19	0.0127	0.0028	0.0179	0.0020
4	13	11.26	4.31	0.61	0.09	0.0194	0.0017	0.0206	0.0023
5	5	11.06	8.93	0.54	0.28	0.0126	0.0014	0.0107	0.0016
6	17	9.11	2.67	0.27	0.13	0.0123	0.0040	0.0192	0.0017
7	15	14.28	5.38	0.57	0.13	0.0131	0.0031	0.0169	0.0033
8	19	6.43	1.25	0.09	0.16	0.0142	0.0035	0.0175	0.0020
9	12	12.17	8.36	0.37	0.18	0.0201	0.0041	0.0215	0.0046
all	145	9.28	5.06	0.36	0.22	0.0136	0.0043	0.0166	0.0038

FIGURES

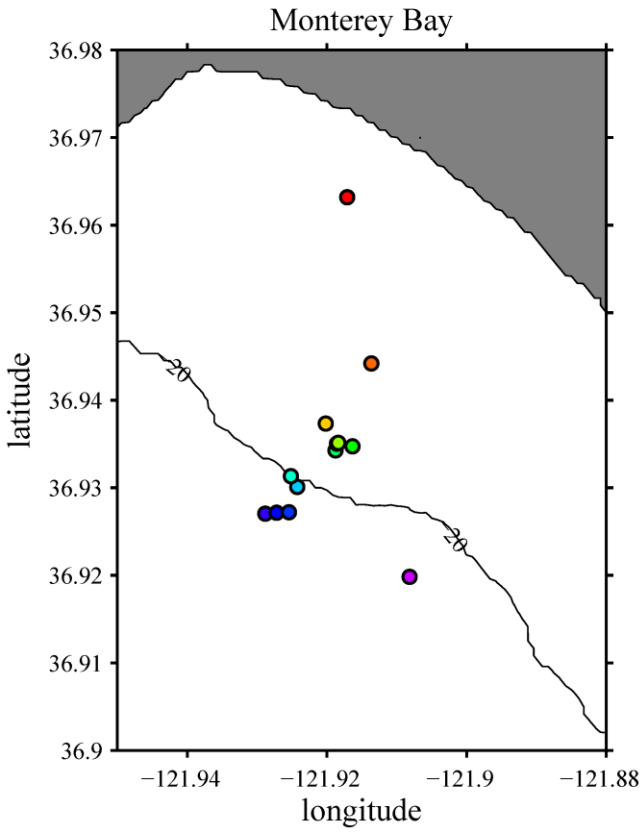

Figure 1. Map of the northeast corner of Monterey Bay showing locations of high resolution optical profiles and water sample collection. Colors for each location correspond to samples plotted according to time and depth in figure 4.

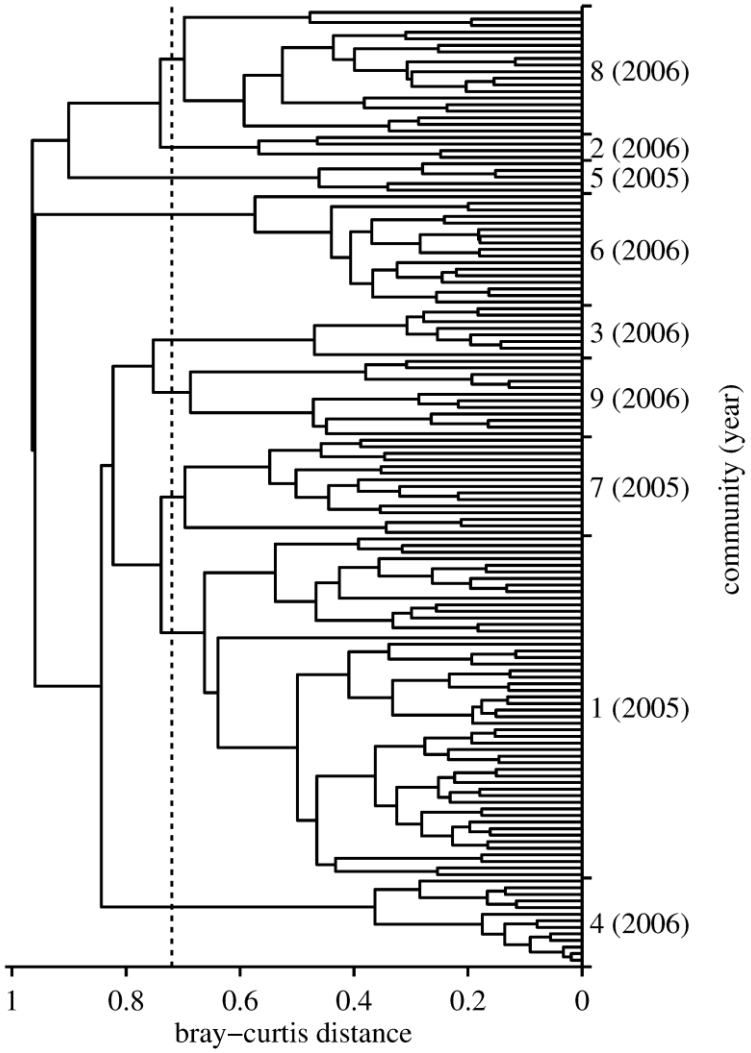

Figure 2. Dendrogram showing results of hierarchical cluster analysis based on phytoplankton species abundance determined for all 145 samples from both years. Dotted line indicates distance (0.72, similarity profiles $p < 0.05$) at which the dendrogram was cut to produce 9 distinct communities.

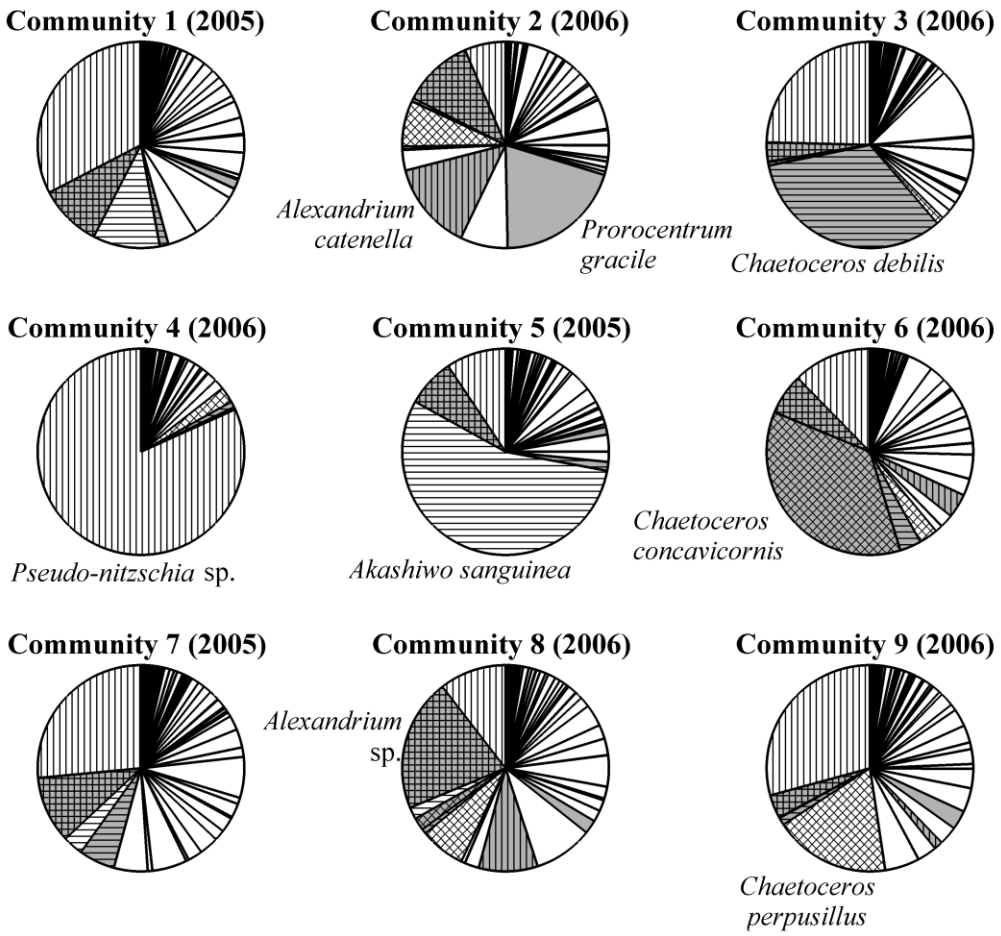

Figure 3. Relative taxonomic composition for each community with most abundant taxa labelled. Hatched patterns represent the same species in all charts. Pie charts represent the relative cell concentration (cells mL^{-1}) of species averaged among samples grouped into communities according to cluster analysis.

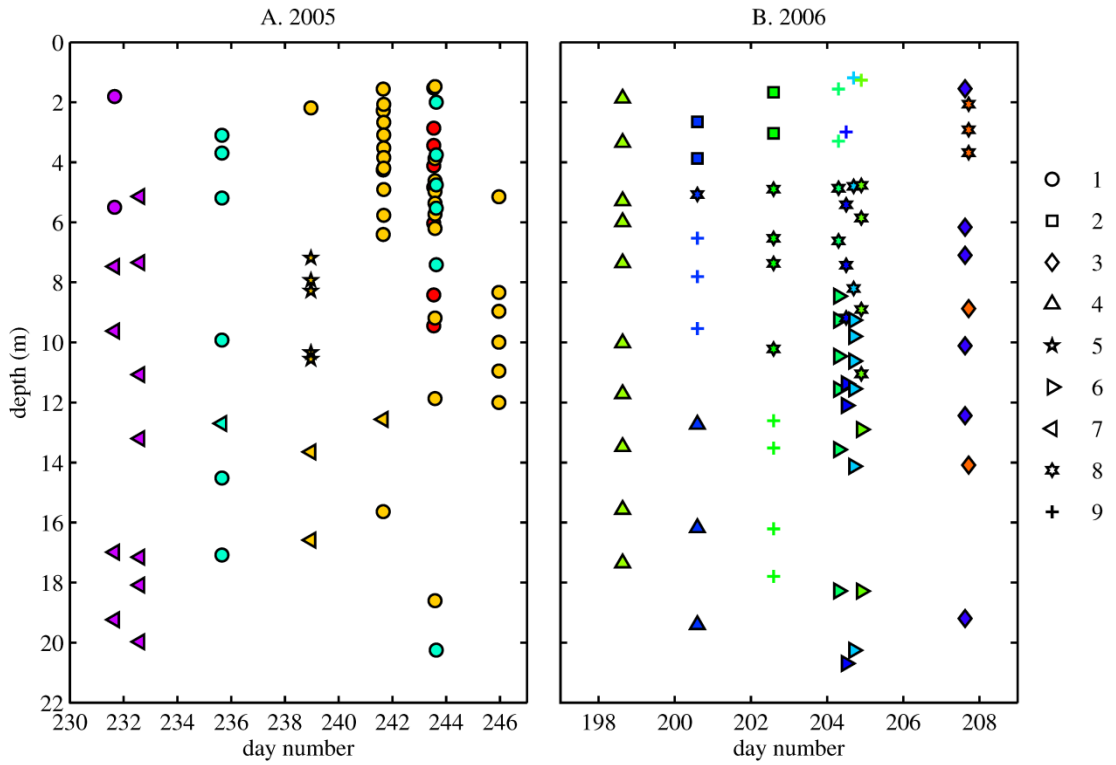

Figure 4. Distribution of samples over time, depth, and location for 2005 (A) and 2006 (B) showing variation of community composition over small scales. Symbol shapes indicate community membership as determined by cluster analysis. Color indicates profile location as in figure 1.

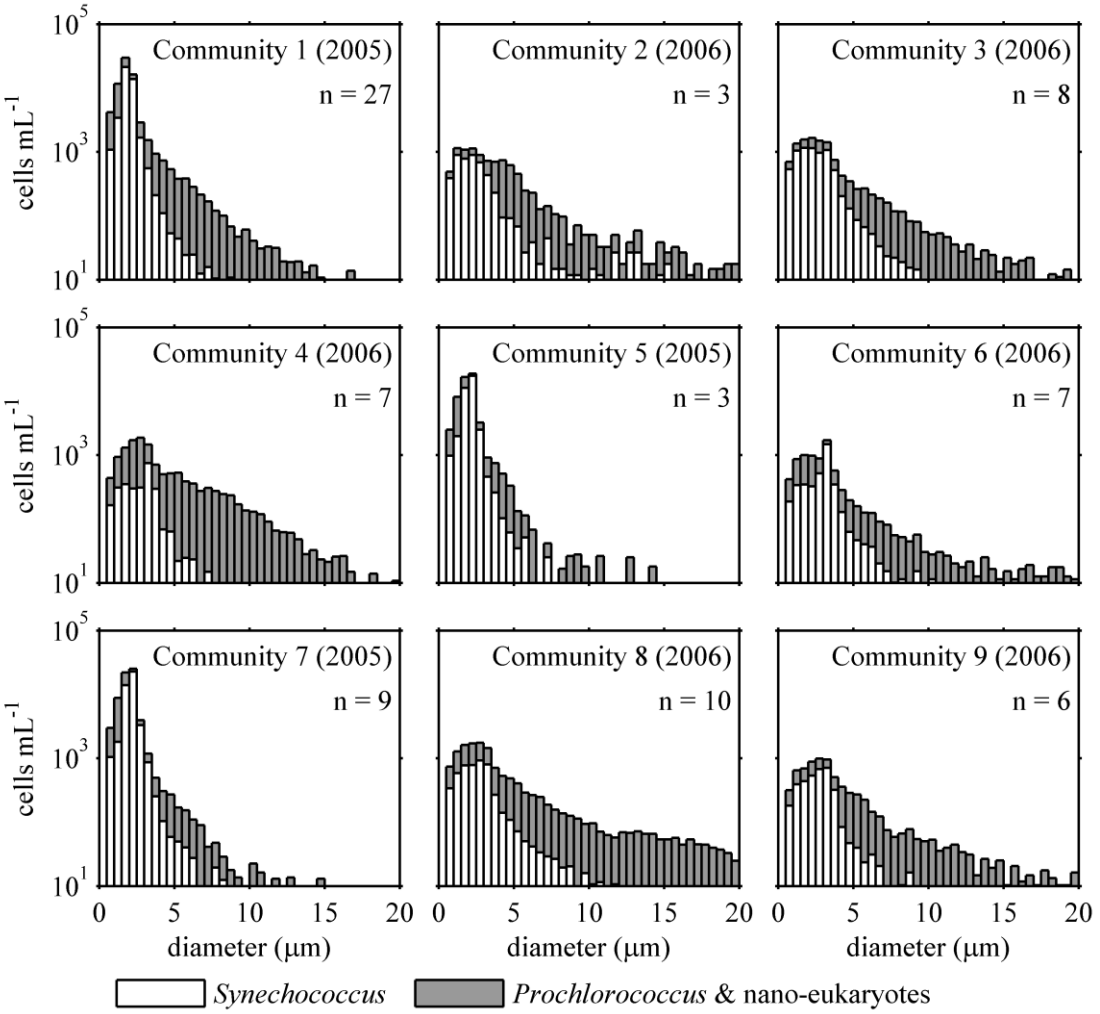

Figure 5. Size and abundance of pico- and nano-phytoplankton determined by image analysis for a sub-set of n samples from each community. Stacked histograms show cell concentrations (cells mL^{-1}) in 0.5 μm mean diameter size bins between 0.5 and 20 μm.

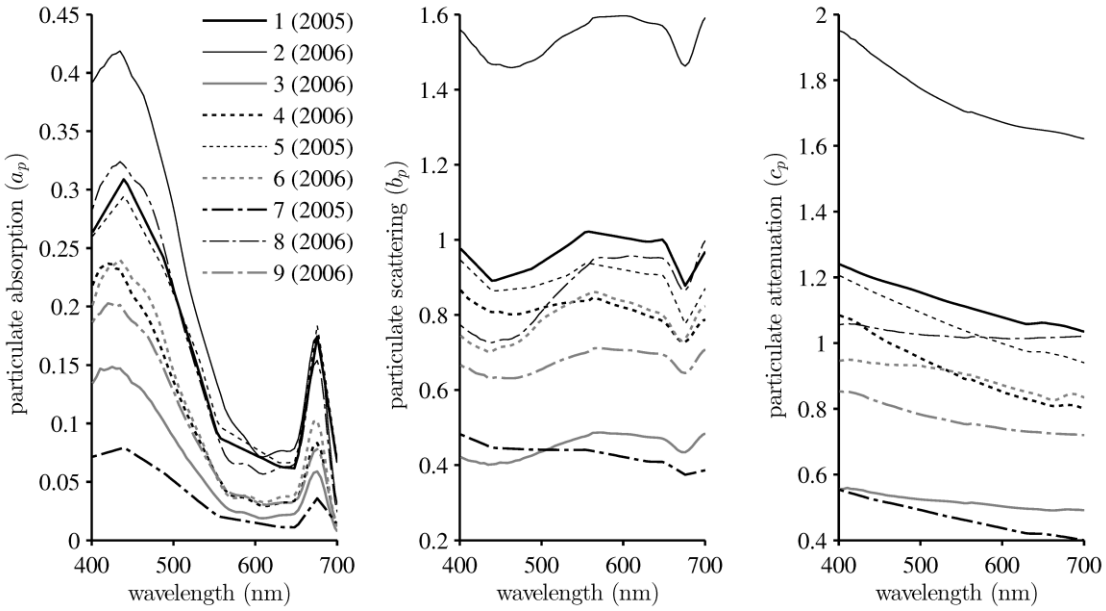

Figure 6. Mean a_p, b_p and c_p spectra calculated for all samples in each community.

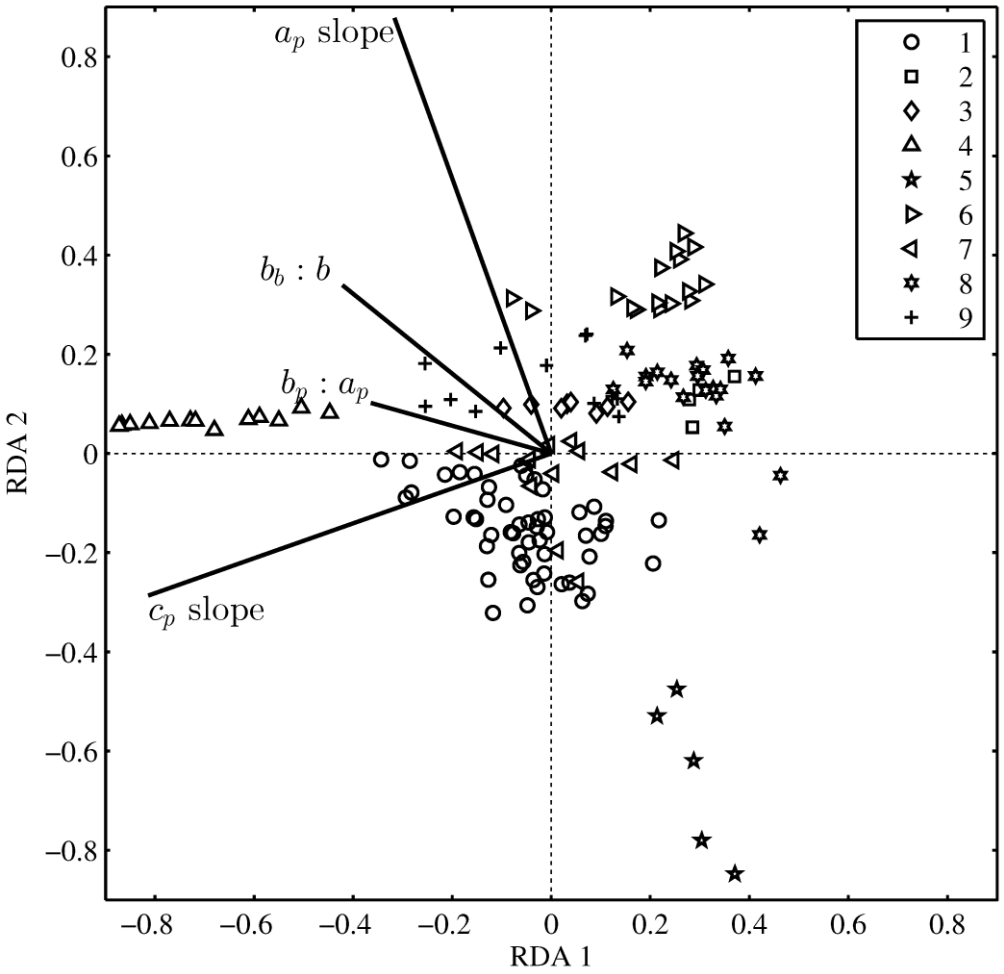

Figure 7. Results of the redundancy analysis for all samples based on community composition and optical parameters. Symbols indicate community membership of samples as determined by cluster analysis. Vectors indicate direction of increase for optical parameters.

MANUSCRIPT 2

VARIATION OF MARINE PHYTOPLANKTON COMMUNITY SIZE STRUCTURE AND PHYSIOLOGY OVER SMALL SCALES DETERMINED WITH IN SITU OPTICAL MEASUREMENTS

Malcolm N. McFarland, Jan Rines, Percy Donaghay, James Sullivan

Formatted for submission to the journal Marine Ecology Progress Series

University of Rhode Island, Graduate School of Oceanography

South Ferry Road, Narragansett, RI 02882

ABSTRACT

Small scale layers and patches of phytoplankton are ubiquitous/widespread features in the coastal ocean that are fundamental to population dynamics and community structure in pelagic ecosystems. To better understand biological processes at small scales, we developed methods to assess phytoplankton community composition and physiological characteristics based on high resolution, in situ optical measurements. Scanning flow cytometry was used to determine the effects of abundance, size, and pigment content of phytoplankton cells and non-algal particles on the spectral shape and relative magnitude of particulate absorption, scatter, and backscatter. We found the slope of particulate attenuation varied with phytoplankton size and morphology, the slope of particulate absorption and the ratio of scatter to absorption varied primarily with cellular pigment content, and the backscatter ratio varied primarily with the relative abundance of non-algal particles. The ability of these relationships to predict particle and phytoplankton characteristics over small spatial and temporal scales was tested with two independent high resolution optical data sets collected from an in situ autonomous profiling system. Comparison of high resolution optical data with flow cytometric sample analyses agreed with the previously determined relationships. High resolution data revealed small scale variations in community size structure and physiology that would be difficult to visualize with discrete samples or measures of total chlorophyll concentration.

INTRODUCTION

It is well established that marine phytoplankton communities can vary considerably over very small spatial (decimeter) and temporal (minutes) scales (Cassie 1963; Haury et al. 1978; Derenbach et al. 1979; Bjørnsen and Nielsen 1991; Donaghay et al. 1992; Cowles et al. 1998; Rines et al. 2010). In the ocean, this small scale structure is often observed as horizontal patches or thin vertical layers that can contain a large proportion of chlorophyll biomass and can persist over time and space scales of critical importance to phytoplankton growth, mortality and life history (Dekshieneks et al. 2001; McManus et al. 2003; Sullivan et al. 2010b). Variations in distribution and abundance over small scales, therefore, are fundamental to the ecology of planktonic organisms and to the function of marine pelagic ecosystems. This heterogeneous distribution of organisms is a result of their interactions with physical, chemical and biological ecosystem components. Thin layers, for example, can be generated by a variety of mechanisms including shear, lateral intrusions, active migration, buoyancy, differential growth rates, and gyrotactic trapping (Durham and Stocker 2012). The physical, chemical and biological processes that occur within and around small scale structures can be important to the establishment of harmful algal blooms (Donaghay and Osborn 1997; Smayda and Reynolds 2001; Rines 2002), trophic interactions (Nielsen et al. 1990; Menden-Deuer 2008; Benoit-Bird et al. 2009; Greer et al. 2013), biochemical cycling (Sieburth and Donaghay 1993; Hanson and Donaghay 1998), sexual reproduction (Peperzak 2006), and community assembly, succession and diversity (Smayda and Reynolds 2001; Reynolds 2006).

Technological developments over the past several decades have enabled the analysis of natural phytoplankton communities with increasing resolution over decreasing spatial and temporal scales. High resolution methods targeting phytoplankton typically use in situ optical measurements of absorption, attenuation, scattering or fluorescence to detect and map small scale structure (Derenbach et al. 1979, Cowles & Desiderio 1993, Twardowski et al. 1999). Modern optical instrumentation can routinely collect data at high rates (> 1 Hz) and can be deployed on a variety of profiling, towed, moored, or autonomous platforms (Babin et al. 2005, Holliday et al. 2009, Sullivan et al. 2010a). While these data are often used to infer total phytoplankton biomass, a better understanding of ecological processes over small scales could be obtained from optical parameters that respond to variation of phytoplankton characteristics such as cell size, shape, or physiology (Stemmann & Boss 2012).

Theoretical and empirical studies have shown the shape and relative magnitude of particulate absorption (a_p), scattering (b_p), and attenuation (c_p) coefficient spectra are determined by particle size, morphology, and complex refractive index (Morel & Bricaud 1986, Sathyendranath et al. 1987). These particle characteristics can vary significantly among phytoplankton taxa and with their physiology (Bricaud et al. 1983, Spinrad & Yentsch 1987, Ackleson et al. 1988, Stramski & Reynolds 1993). Intracellular pigment packaging can flatten and decrease the slope of the a_p spectrum while reducing the absorption efficiency of cells (Duysens 1956; Kirk 1975; Ciotti et al. 2002). The slope of a_p spectra between 488 and 532 nm may also increase as the ratio of photoprotective to photosynthetic carotenoids increases (Eisner et al. 2003).

The ratio of scattering to absorption (b_p:a_p) can vary among particle types and with intracellular carbon and pigment concentrations (Stramski & Morel 1990, Sosik et al. 2001). The proportion of light scattered in the backward direction (b_b:b) is low for large particles and particles with low refractive index. Smaller particles or those with high refractive index have a higher b_b:b (Twardowski et al. 2001; Sullivan et al. 2005). The exponential slope of the c_p spectrum is high for suspensions dominated by very small particles such as picoplankton or suspended sediments, and closer to zero for suspensions with abundant large particles such as diatom or dinoflagellate cells (Kitchen et al. 1982; Boss et al. 2001). Because of their dependence on particle characteristics, these optical parameters convey ecologically important information about the composition and physiology of phytoplankton populations in the ocean.

Previous work in multiple different pelagic ecosystems suggests that particle characteristics are important to the bulk inherent optical properties (IOPs) of ocean waters that can be measured in situ with high resolution (Babin et al. 2003, Eisner & Cowles 2005, Bricaud et al. 2004, Sullivan et al. 2005). However, few field studies have directly measured individual phytoplankton and non-algal particle characteristics to determine their influence on bio-optical parameters and test the predictive capabilities of optical data. Iturriaga and Siegel (1989) used microspectrophotometric measurements of individual particles to show substantial variation in the absorption characteristics of different phytoplankton and non-algal particles. However, their methods were limited to approximately 50 particles for each water sample. In a study conducted in New England continental shelf waters, Green et al. (2003) used flow cytometry to show that bulk IOPs were highly dependent on the abundance, size and

complex refractive index of different plankton and particle groups. While focusing primarily on larger scales, Green et al. documented significant variation in phytoplankton optical cross sections and complex refractive indexes between spring and summer communities and with depth. A previous study in Monterey Bay, CA found that variation of phytoplankton community taxonomic composition and characteristics over small scales, determined with microscope based observations and cell counts, were associated with changes in the relative magnitude and spectral shape of a_p, b_p, and c_p coefficient spectra (McFarland et al. in prep.). This study, however, clearly demonstrated the need for quantitative measurements of cell size, pigment content, and non-algal particles.

In the present study, conducted in the coastal fjord of East Sound, WA, we determined the influence of natural phytoplankton and non-algal particle characteristics on particulate IOPs, and tested the ability of in situ optical measurements to predict phytoplankton community characteristics over small spatial and temporal scales. The b_p:a_p, a_p slope, c_p slope, and b_b:b parameters were used to determine the extent to which particulate optical properties vary with phytoplankton composition, morphology and physiological characteristics. We used a CytoSense (CytoBuoy b.v.) scanning flow cytometer to directly measure abundance, size, and fluorescence of phytoplankton cells and non-algal particles in discrete seawater samples. The relationships between these particle characteristics and corresponding measurements of the b_p:a_p, a_p slope, c_p slope, and b_b:b parameters were determined with a redundancy analysis. Based on these relationships, we used an independent, high resolution optical data set collected with an autonomous profiler to predict

phytoplankton and non-algal particle characteristics over small scales. Finally, these predictions were tested by comparison with the particulate composition of discrete samples determined with flow cytometry. The methods employed in this study enabled visualization of phytoplankton community characteristics with high resolution and can be used to better understand the ecological dynamics of phytoplankton populations and the processes that determine the abundance of different taxa over small scales.

METHODS

High resolution optical profiles and samples were collected in East Sound, Washington between May 14th and May 26th in 2009 and between May 8th and May 20th in 2010. East Sound is a small fjord located in the northwest corner of Washington State at 48.7 degrees north latitude. It is approximately 13 km in length, 2 km wide, oriented in a north-northwest direction and open at the southern end. The sound is 30 - 40 m deep on average with narrow topographical constraints and a partial shallow sill at the southern mouth. Currents and mixing are primarily driven by wind and tides. When mixing is not intense, East Sound often develops complex layered structure. Multiple distinct water masses can be stacked on top of each other with significant differences in phytoplankton community composition (Dekshieneks et al. 2001, Rines et al. 2002, McManus et al. 2003). This layered water column structure makes East Sound an excellent system in which to capture large amounts of biological and optical variation over small scales.

Ship based optical profiles

Optical data for comparison with discrete samples was collected from multiple locations throughout the sound with a ship based profiling instrument package.

Instruments included a 0.2 μm filtered WET Labs ac-9 absorption and attenuation meter, an unfiltered WET Labs ac-9 (2009) or ac-s (2010) absorption and attenuation meter, a SeaBird Electronics SBE-25 CTD, a WET Labs WETStar chlorophyll fluorometer, and a WET Labs ECO VSF 532 nm scatter sensor. During 2010 the profiler also included a WET Labs CDOM fluorometer. The buoyancy of the optical instrument package was adjusted to be slightly negative and, during data collection, was allowed to descend freely through the water column decoupled from ship motion (Donaghay 1992). Profiles were conducted in duplicate to ensure accuracy of measurements and stability of the local water column structure.

Absorption and attenuation meters were calibrated before, during and after each field project with 0.2 μm filtered de-ionized water from a Barnstead E-pure water purification system. Optical data were corrected for the effects of temperature and salinity according to the methods of Twardowski et al. (1999) and Sullivan et al. (2006). Scattering errors in the ac-9 and ac-s meters were corrected using the proportional correction algorithm of Zaneveld et al. (1994). Particulate absorption (a_p) and attenuation (c_p) coefficients were calculated by subtracting dissolved absorption (a_g) measured with the 0.2 μm filtered ac-9 from total absorption (a_{pg}) and attenuation (c_{pg}) measured with the unfiltered ac-9 or ac-s meters. A flow sensor in line with the filtered ac meter was used to compensate for the slower flow rate through the filter. To match the higher spectral resolution of the ac-s meter used during 2010, the dissolved absorption spectrum was interpolated by fitting to measured values, an equation of the form $a_g(\lambda) = s\lambda^{-\gamma}$ where λ is the wavelength, γ is the exponential slope, and s is a scale factor. The particulate scattering coefficient (b_p) was calculated as the difference

between the particulate absorption and attenuation coefficients ($b_p = c_p - a_p$). Backscattering coefficients (b_b) at 532 nm were calculated from the ECO VSF data according to Sullivan et al. (2013).

Adaptive sampling

Optical profiles were conducted immediately prior to water sample collection and target sample depths were selected based on total phytoplankton biomass inferred from optical data available in real time. Depths were selected to capture the maximum amount of variation of biomass throughout the water column in the most efficient manner possible. At each profiling station samples were generally collected from two or three depths where total absorption and chlorophyll fluorescence exhibited minimum and maximum values. This adaptive sampling procedure ensured that thin layers of phytoplankton were accurately sampled and the full range of phytoplankton biomass and optical variation throughout the water column were captured at each station. Samples were collected with a ~2 L, hand deployed, Ruttner type water sampler (KC Denmark) on a graduated line. Phytoplankton cells and colonies in collected samples were immediately viewed and recorded on deck with a compound microscope equipped with a video camera. Sub-samples for microscopy were gently concentrated with a 20 μm Nitex mesh. Sub-samples (~20 mL) were also acquired for immediate flow cytometric analysis. In addition, 250 mL of each sample was preserved with 1% formalin and 1% glacial acetic acid for later analysis in the lab.

Scanning flow cytometry

A CytoSense scanning flow cytometer (CytoBuoy b.v., http://www.cytobuoy.com) was used to measure the size, concentration, light scatter

and chlorophyll fluorescence of phytoplankton cells and non-algal particles in collected samples. This instrument has a wide flow path that can accommodate particles up to 800 µm in width. The CytoSense records a scan (0.5 µm resolution) of the light scattered and fluoresced by particles as they pass individually through the incident laser beam at a fixed speed (Fig. 1). Descriptive particle parameters such as total light scatter, total fluorescence and length are computed for each particle from scan data. Particles that are elongate in shape tend to align lengthwise along the axis of flow and length measurements therefore represent maximum particle dimensions rather than spherical equivalent diameters (Fig. 1A & B). For each sample, the volume of fluid analyzed is recorded and used to calculate particle concentrations. Sample volumes generally ranged from several hundred microliters to several milliliters depending on particle concentration. The CytoSense flow cytometer used in this study was equipped with a 488 nm blue laser and detectors for forward scatter, side scatter, and fluorescence at green (515 – 565 nm), yellow (565 – 595 nm), orange (595 – 664 nm), and red (>664 nm) wavelengths. Detector gain settings and trigger levels were adjusted using natural samples and phytoplankton cultures to ensure adequate signal strength and detection of cells as small as 2 µm (e.g. *Synechococcus*), and to avoid saturation by large dinoflagellates or colonial diatoms (e.g. *Chaetoceros*) that are common in East Sound. Gain settings and trigger levels were kept consistent for all samples within each year to ensure comparable results. Alignment and performance of detectors was checked daily by running a broad spectrum fluorescent, 2.5 µm diameter bead standard (Molecular Probes, AlignFlow beads).

The standard algorithm in the CytoBuoy CytoClus analysis software (version 3.0) calculates particle length from scan width at half maximum with a correction for particles smaller than the focused beam height. This algorithm was found to be inaccurate for large particles such as pennate diatoms or *Chaetoceros* spp. colonies that had low signal intensity near the ends of scans. We developed a modified algorithm to calculate length according to scan width at a fraction of scan height that was dependent on the log of total integrated forward scatter. The algorithm used a generalized logistic function of the form:

$$f = .594 + \frac{.01 - .594}{(1 + .001e^{-2.92(s-3.415)})^{1000}}$$

where *f* is the fraction of scan height at which to determine length and *s* is the base 10 log of the integrated forward scatter scan. The parameters for this logistic function were determined by unconstrained nonlinear optimization using the fminsearch function in Matlab (The Mathworks Inc.). The procedure found parameter values that minimized the length measurement error of six bead size standards (Duke Scientific polymer microspheres) with diameters of 2.7, 9.7, 14.6, 20, 30.1, and 69.9 µm. Length measurements were then recalculated based on this optimized algorithm for scan data from all collected samples.

The accuracy of CytoSense concentration measurements was tested by comparison with manual microscope based cell counts of a sub-set of samples collected during 2009 and two uni-algal phytoplankton cultures. Field samples contained an abundant population of the large pennate diatom *Haslea* sp. which was easily identified in the microscope and in CytoSense data due to its consistent size and shape. A culture of this taxon, isolated from East Sound in 2011, and a culture of the

dinoflagellate *Akashiwo sanguinea*, isolated from Grays Harbor, WA were also used to test CytoSense cell concentration measurements. Manual microscope based cell counts of preserved field samples and cultures were conducted in the lab on a Nikon Eclipse E800 compound microscope using a 10X objective and phase contrast illumination. Cells were counted in a 0.1 mL Palmer-Maloney or 1mL Sedgewick-Rafter chamber depending on concentration.

The accuracy of CytoSense length measurements were tested for four uni-algal cell cultures by comparison with automated image analysis using a FlowCAM imaging particle analyzer. Selected species varied in size from approximately 10 µm to nearly 1 mm and included *Teleaulax amphioxeia* (Cryptomonadacea), *Akashiwo sanguinea* (Dinophyceae), *Chaetoceros socialis* (Bacillariophyceae), and *Chaetoceros eibenii* (Bacillariophyceae). Cultures were isolated from Narragansett Bay RI, East Sound (*C. eibeneii*), or Grays Harbor WA (*A. sanguinea*) and grown in L1 sea water medium (Guillard & Hargraves 1993) with a 12:12 light:dark cycle at 15°C. To promote proper morphology of large colonial diatoms and prevent settling, cells were grown in 10 L tanks equipped with stir bars to simulate moderate levels of natural turbulence. Measurements from six replicate tanks for each species were acquired while cells were in exponential growth phase.

Particle length, forward scatter, side scatter, chlorophyll fluorescence, and phycoerythrin fluorescence were used to classify particles into separate types. Classification was performed by manually defining parameter value ranges (gates) for different particle types on scatter plots of length vs. maximum red fluorescence, maximum forward scatter vs. maximum side scatter, and maximum red vs. maximum

yellow fluorescence. Identifiable particle types included non-algal particles (without chlorophyll fluorescence), picoplankton sized (~1-2 μm) *Synechococcus*, nanoplankton sized (2-20 μm) photosynthetic eukaryotes, microplankton sized (>20 μm) diatoms and dinoflagellates, nano- and microplankton sized cells with phycoerythrin (e.g. cryptomonads and *Dinophysis* sp.), and nano- and microplankton sized dead algal cells. Dead cells were distinguished from live cells and non-algal particles by having very low, residual chlorophyll fluorescence but with length and scatter characteristics similar to live cells.

Data analysis

For comparison with flow cytometry data, optical data were extracted from ship based profiles collected at the same location, depth and time as samples. For each sample, four optical parameters that describe the shape and relative magnitude of a_p, c_p, and b_p spectra were calculated. These included the ratio of b_p at 555 nm to a_p at 676 nm (b_p:a_p), the spectral slope of the a_p coefficient between 488 and 532 nm, the spectral slope of c_p, and the ratio of b_b to b at 532 nm (b_b:b). Wavelengths for b_p:a_p were chosen to coincide with the peak scattering signal and the long wavelength chlorophyll absorption peak to minimize the influence of absorption by non-algal particles. The negative a_p slope was calculated according to Eisner et al. (2003 & 2005) as

$$a_p \text{ slope} = -\frac{a_p 488 - a_p 532}{a_p 676(488 - 532 \text{ nm})}$$

Note that Eisner et al. report a_p slope as a negative value and we report this slope as a positive value to maintain consistency with conventions for c_p slope. The slope of c_p

was determined between 412 and 650 nm by fitting an equation of the form $c_p(\lambda) = s\lambda^{-\gamma}$ where λ is the wavelength, γ is the exponential slope of the spectrum, and *s* is a scale factor (Twardowski et al. 2001, Boss et al. 2001). The backscatter ratio (b_b:b) at 532 nm was calculated from b_b measured with the ECO VSF and b_p measured with the ac-9 or ac-s, both at 532 nm.

A percent scatter distribution based on scanning flow cytometry data was used to characterize the particulate composition of samples. We used scatter, rather than particle concentration, to account for differences in particle cross sectional area that determine their impact on bulk absorption, scattering and attenuation coefficients (Bricaud and Morel 1986). For every sample, flow cytometry data for each of the six particle types was binned according to length into 50 logarithmically sized bins between 1 μm and 2 mm. This resulted in 300 categories of particles (50 sizes of each type) for which the percentage of total particle scatter was calculated. For each particle, scatter was calculated as the sum of the integrated forward scatter and side scatter scan data. Percent total scatter was calculated as the sum of scatter for all particles of a given type in a size bin normalized by the sum of total scatter for all particles in the sample.

A combination of hierarchical cluster analysis and redundancy analysis was used to determine the relationship between the particulate composition of samples and their corresponding optical properties. These analyses were conducted separately for each year due to differences in gain settings for the flow cytometer that may have affected particle detection and classification. The percentage of particle scatter by all 300 categories was used to cluster samples into four groups in each year. Hierarchical

cluster analyses (complete linkage method) were based on a Bray-Curtis distance matrix and computed with the Matlab statistics toolbox version 8.0. Dendrograms were subdivided at a fixed distance above which similarity profile tests could confirm significant structure ($p < 0.01$) for all groups (Clarke et al. 2008). This resulted in four clusters of samples in each year. Means for each cluster were determined by averaging percent scatter distributions and optical parameters among all samples in each community. Similarity profile tests were performed with the Fathom toolbox for Matlab (Jones 2012) using 10^4 iterations. Redundancy analysis was performed with the Vegan package for the R statistical computing environment (Oksanen et al. 2013). Redundancy analyses were based on the same 300 categories of percent scatter data used for cluster analyses and measurements of the four optical parameters b_p:a_p, a_p slope, c_p slope, and b_b:b corresponding to each sample.

High resolution autonomous profiles

High spatial and temporal resolution optical data were collected with an Ocean Response Coastal Analysis System (ORCAS) autonomous vertical profiler (Donaghay 2003, Babin et al. 2005, Sullivan et al. 2005, Sullivan et al. 2010) moored in the upper sound from May 20th through May 26th in 2009 and from May 11th through May 15th in 2010. This system is equipped with a programmable submersible winch anchored to the sea floor, floats to provide positive buoyancy, batteries, a data logger, and a radio system to transmit collected data to a receiving station. The instrument payload included a WET Labs ac-9 absorption and attenuation meter, a Sea-Bird SBE49 CTD, a WET Labs WETstar chlorophyll fluorometer, a WET Labs ECO VSF three angle back scatter sensor (532 nm), and a WET Labs CDOM fluorometer. The system

collected profiles at an ascent rate of ~3 cm s^{-1} resulting in data with a vertical spatial resolution of ~1 cm. Profiles were conducted hourly in 2010 and every 2 hours in 2009. The ac-9 meter was calibrated before and after deployment and corrections for temperature, salinity and backscatter errors were applied to data as with the ship based profiling system. Profiles were smoothed with a 10 point running mean after outliers greater than 3 standard deviations from the running mean were removed. Chlorophyll concentrations were calculated from absorption spectra according to the methods of Sullivan et al. (2005) using a chlorophyll specific absorption coefficient of 0.014 m^2 mg^{-1} typical for East Sound. Absorption based chlorophyll concentrations were used to avoid the effects of fluorescence quenching by photo-inhibition that can happen in near surface waters.

Since the ORCAS profiler could not be equipped with a filtered ac meter, a_g was determined from measurements of CDOM fluorescence. A model of a_g based on CDOM fluorescence and depth was developed from a_g and CDOM fluorescence measurements acquired with the ship based profiling package during 2010. The value of a_g at 412 nm was found to be linearly related to CDOM fluorescence according to:

$$a_g\,(412\,nm) = 0.0135\,F + 0.1806$$

where F is CDOM fluorescence. The exponential slope (s) of the a_g spectrum was found to vary with depth according to:

$$s = \ 0.0008e^{(-0.2334d)} + 0.016$$

where d is depth. These relationships determined the parameters used to calculate a_g spectra according to:

$$a_g(\lambda) = a_g(412\,nm)e^{(-s(\lambda-412))}$$

where λ is wavelength and s is the spectral slope. Modeled a_g spectra were then subtracted from total attenuation spectra to determine a_p spectra, c_p spectra and c_p slope.

To test the association between optical parameters and particle characteristics, b_p:a_p, a_p slope, c_p slope, and b_b:b derived from high resolution data were compared to samples collected from three points during the time series from each year. Samples were analyzed with flow cytometry to determine particle composition and characteristics as described above.

RESULTS

CytoSense validation

Particle concentrations determined by flow cytometry and manual microscope counts were linearly related (Fig. 2A). A model II least squares linear fit to the log converted data had an r^2 value of 0.97 indicating consistent precision over a wide range of cell densities. Cell concentrations determined with the flow cytometer were generally slightly lower than cell concentrations determined manually for all samples, a result that appears exaggerated at lower cell densities on the log:log plot. Cell length measurements determined with the CytoSense flow cytometer were similar to measurements of cell length determined by automated image analysis with a FlowCAM particle analyzer (Fig. 2B). Cytosense length measurements are slightly higher than FlowCAM measurements for the smallest cells (*T. amphioxeia*) and slightly lower than FlowCAM measurements for the larger *C. socialis*.

Ship based optical profiles and sample analyses

A total of 55 samples in 2009 and 61 samples in 2010 were acquired and analyzed. Microscopy of live samples collected during 2009 revealed a phytoplankton community dominated by an abundant population of a pennate diatom in the genus *Haslea* (Fig. 1A & B, see also Rines et al. in prep.). During 2010, live microscopy revealed a phytoplankton community still dominated by diatoms but with a greater diversity of species including multiple *Chaetoceros* (especially *C. socialis*, Fig. 1C) and a number of other colony forming centric and pennate diatoms such as *Dactyliosolen fragilissimus*, *Detonula pumila*, *Ditylum brightwellii*, *Eucampia zodiacus*, *Guinardia delicatula*, *Pseudo-nitzschia* spp., *Skeletonema* spp., *Rhizosolenia* spp., *Leptocylindrus danicus*, and *Thalassiosira spp*. These species represent a wide range of cell sizes, shapes, and modes of colony formation. Individual cells of these species could be as small as ~10 µm (e.g. *Skeletonema* spp.) while colonies *C. socialis* or single cells of *Rhizosolenia* spp. could be several hundred µm in size. The morphology of the siliceous frustules for many of these diatoms was quite complex with some species having long siliceous setae or interconnecting spines (e.g. *Chaetoceros* spp. and *Skeletonema* spp.) and others with patterns of pores or striations along the valve face (e.g. *Thalassiosira* spp., *Pseudo-nitzschia* spp., and *Haslea* sp.).

Approximately 1 mL of seawater and an average of 16,589 particles were analyzed per sample during 2009. Average sample volumes and number of particles analyzed were increased during 2010 to 1.7 mL of seawater and 58,681 particles per sample to account for a lower overall concentration of phytoplankton and a more diverse phytoplankton community. During 2009 particles were classified as non-algal,

eukaryotic cells containing phycoerythrin, live *Haslea* sp., dead *Haslea* sp., nanophytoplankton, or microphytoplankton. Despite initial efforts to calibrate detector gain settings and trigger levels prior to sample analyses, signal strength from picoplankton sized cells was insufficient for accurate enumeration in most samples. However, despite their high abundance, these small cells accounted for a very small proportion of total scatter or fluorescence most likely due to their small size and low refractive index. Low contributions of picophytoplankton sized cells to total scatter were also found by Green et al. (2003). During 2010, gain settings were increased and trigger levels were decreased to ensure efficient detection of *Synechococcus*. Flow cytometer data collected during 2010 were classified as non-algal, eukaryotic cells with phycoerythrin, *Synechococcus*, nanophytoplankton, microphytoplankton, and dead cells.

Cluster analyses based on the particulate composition of samples identified four distinct communities in each year (Fig. 3). Simprof analyses confirmed the significance of all clusters ($p < 0.01$) and produced cutoff distances of 0.52 and 0.49 for 2009 and 2010, respectively. The mean composition of these communities is shown in Fig. 4 as stacked histograms representing percent scatter for each particle type. In 2009 (Fig. 4A – D), community 3 was overwhelmingly dominated by live *Haslea* sp. cells (Fig. 4C). Community 2 was also dominated by live *Haslea* sp. but had a higher proportion of scatter by other particle types (Fig. 4B). Community 1 had a large proportion of scatter from dead *Haslea* sp. cells (Fig. 4A) and community 4 had a more even mixture of scatter by different particle types (Fig. 4D). During 2010 phytoplankton communities were not dominated by a single taxon but contained a far

more diverse complement of particles with a range of sizes and shapes (Fig. 4E - F). Community 5, although consisting only of 3 samples, was distinctive in composition due to a very high proportion of scatter by dead cells (Fig. 4E). Community 7 contained a high proportion of scatter by large (> 100 m) phytoplankton cells and colonies (Fig. 4G). Community 6 was dominated by non-algal particles (Fig. 4F) and community 8 had a more even mixture of scatter by all particle types (Fig. 4H).

Mean values and standard deviations of b_p:a_p, c_p slope, a_p slope, and b_b:b for each community are shown in Table 1. Results of redundancy analyses for each year (Figs. 5 & 6) show the variation of these optical parameters among communities. Permutation tests found results of both redundancy analyses to be highly significant ($p < 0.005$). In the resulting biplots (Figs. 5 & 6), symbols represent samples and symbol shape indicates community membership determined by cluster analyses as in Fig. 3. The labeled vectors extending from the origin indicate the direction of increase for each optical parameter among all samples. In both years, the a_p slope was correlated with b_p:a_p, and c_p slope was correlated with b_b:b. These correlations are most evident in the 2010 data. Vector length indicates how well the plotted result represents variation of a particular parameter. In Fig. 6, for example, the vector representing c_p slope is relatively short indicating that the variation of this parameter is not represented as well as other optical parameters in the biplot. In 2009 community 1, dominated by dead *Haslea* sp., was found to have high values of b_p:a_p and a_p slope, intermediate c_p slopes, and low values of b_b:b (Fig. 5, Table 1). Samples from community 2 spanned a range of moderate to high c_p slopes, moderate to high b_b:b, and had intermediate values of a_p slope and b_p:a_p. Community 3, dominated by live

Haslea sp. cells, had low values of c_p slope and a_p slope, low values of b_p:a_p and moderate values of b_b:b. Community 4 had high c_p and a_p slopes, high b_p:a_p, and moderate to high vales of b_b:b. During 2010, samples in community 5 had the highest values of b_p:a_p, and a_p slopes, low c_p slopes, and low b_b:b (Fig. 6, Table 1). Community 6 had high values of b_b:b, high values of c_p slope, and intermediate values of b_p:a_p and a_p slope. Community 7 had moderate to low values of c_p slope and a_p slope, low b_p:a_p, and intermediate values of b_b:b. Community 8 spanned a range of intermediate values of all optical parameters.

Comparison of community composition (Fig. 3) with results of redundancy analyses (Figs. 5 & 6) and mean community optical parameters (Table 1) shows the influence of particle types on particulate IOPs. During 2009 c_p slopes decreased with the relative amount of scatter by live or dead *Haslea* sp. cells. Also during 2009, the lowest a_p slopes were associated with live *Haslea* sp. cells (community 3) and the highest a_p slopes were associated with dead *Haslea* sp. cells (community 1). Conversely, high b_p:a_p was associated with dead *Haslea* sp. cells (community 1), and low b_p:a_p was associated with live *Haslea* sp. cells (community 3). However, the b_p:a_p parameter may also have been affected by non-algal particles since the highest mean values were associated with community 4 (Table 1). High values of b_b:b were associated with non-algal particles and low b_b:b was associated with dead *Haslea* sp. cells. Lower b_b:b for community 1 compared to community 2 may be attributed to dead *Haslea* sp. cells since these communities are otherwise similar. Higher b_b:b for community 2 compared to community 3 is likely due to non-algal particles since these communities are otherwise similar. During 2010 high c_p slopes were associated with

scatter from small non-algal particles (community 6) and c_p slopes decreased in association with scatter by large (> 100 μm) phytoplankton cells and colonies (communities 7 & 8). However, the lowest mean c_p slopes were associated with the high scatter from dead cells in community 5 (Table 1). As in 2009, high b_p:a_p and high a_p slopes were associated with dead cells (community 5) while low b_p:a_p and a_p slopes were associated with large, healthy phytoplankton (community 7). Also similar to 2009, low values of b_b:b were associated with dead cells and high values of b_b:b were associated with scatter from non-algal particles.

Results from both years support three general conclusions for East Sound waters. First, communities dominated by large phytoplankton cells and colonies are generally associated with low c_p slope values. This is consistent with previous studies that show c_p slope is a function of the slope of the particle size distribution (Kitchen et al. 1982; Boss et al. 2001). However, the low c_p slope values associated with dead cells during 2010 represent a deviation from this general trend within the context of this study. Second, communities dominated by non-algal particles tend to have higher b_b:b, communities dominated by live phytoplankton cells have low b_b:b, and communities dominated by dead cells have the lowest b_b:b values. Third, communities with abundant concentrations of dead phytoplankton are associated with high b_p:a_p ratios and high a_p slopes.

High resolution autonomous profiles

High resolution optical data collected with an ORCAS autonomous profiling system was used to infer phytoplankton community characteristics over small scales based on results of discrete sample analyses (Figs. 7 & 8). During both years the

ORCAS profiler captured a transition from high chlorophyll, bloom conditions to waters with low chlorophyll concentrations. In 2009, chlorophyll concentrations were highest below the pycnocline at the start of the high resolution time series and decreased over time (Fig. 7A). The b_p:a_p ratio was highest near the surface at the beginning of the time series (Fig. 7B). Low b_p:a_p values were found below the pycnocline through the beginning and middle of the time series. The lowest b_p:a_p values were found associated with the pycnocline between 5 and 10 m depth during the middle of the time series. The b_p:a_p parameter was of intermediate value and uniform throughout the water column at the end of the time series. The a_p slope parameter was highest in near surface waters at the beginning of the time series and decreased with depth below the pycnocline (Fig. 7C). This parameter was lowest throughout the water column near the end of the time series (Fig. 7C). The c_p slope parameter was lowest below the pycnocline and of intermediate value in surface waters at the beginning of the time series (Fig. 7D).Values of c_p slope were high throughout the water column at the end of the time series. The b_b:b data collected by the autonomous profiler during 2009 was of poor quality and is not shown.

High resolution optical data collected in 2010 showed high chlorophyll concentrations in surface waters near the beginning of the time series that decreased over time to form a subsurface maximum between 5 and 10 m depth (Fig. 8A). The b_p:a_p ratio was initially low where chlorophyll concentrations were high, and increased in near surface waters at the end of the time series (Fig. 8B). Elevated b_p:a_p values in thin layers were associated with the pycnocline between 15 and 20 m on May 12th and between 10 and 15 m on May 13th. The a_p slope parameter was lowest at depth at the

start of the time series, moderately high where chlorophyll concentrations were highest, and generally increased for most of the water column over time with some lower values remaining in layers between 10 and 20 meters (Fig. 8C). The c_p slope parameter was lowest near the surface throughout the time series (Fig. 8D) with strong gradients located along the pycnocline. The b_b:b ratio was consistently higher at depth throughout the time series (Fig. 8E).

Based on results of the redundancy analyses, c_p slope values suggest that waters below the pycnocline near the beginning of the time series in 2009 were dominated by large *Haslea* sp. cells. Low b_p:a_p and a_p slopes suggest a low proportion of dead cells in this high chlorophyll region. In surface waters, moderate c_p slopes, high b_p:a_p, and high a_p slopes suggest abundant dead *Haslea* sp. cells and more abundant small particles. Towards the end of the 2009 time series, high c_p slope and low a_p slope values suggest smaller average particle sizes and a smaller proportion of dead cells. Flow cytometric analyses of samples collected at three points during the time series support these optical predictions of particle composition (Fig. 7). A sample collected from high chlorophyll waters below the pycnocline on May 20th was dominated by live *Haslea* sp. (Fig. 9A) with a low proportion of scatter by dead cells (3.03%). There was a greater proportion of scatter by dead cells (10.1%) in near surface waters on May 21st where b_p:a_p and a_p slope were high (Fig. 9B). There was also considerably more scatter by small non-algal particles (< 10 μm) in these surface waters as predicted by moderate c_p slopes. The sample collected on May 25th near the end of the time series contained a higher proportion of scatter by cells in the 10 to 100 μm size range and a lower proportion of scatter (5.5%) by dead *Haslea* sp. cells (Fig. 9C).

The spatial and temporal distribution of c_p slopes in 2010 high resolution data (Fig. 8D) suggest that large particles dominated in much of the upper portion of the water column throughout the time series, especially after May 13th when chlorophyll concentrations were low. Also throughout the time series, b_b:b is higher in near bottom waters suggesting non-algal particles, possibly re-suspended sediments, are more abundant at depth. High b_p:a_p and a_p slope in near surface waters at the end of the time series suggest a high proportion of dead cells. Samples collected close to the ORCAS profiler in 2010 partially support these predictions. A near surface sample collected on May 12th from the region of high chlorophyll, low b_p:a_p, and moderate a_p slope showed scatter was dominated by large (> 100 µm) phytoplankton cells and colonies (Fig. 9D). A sample collected from ~20 m depth on May 14th showed scatter dominated by non-algal particles (Fig. 9E). A sample collected near the surface at the end of the time series showed considerable scatter from dead cells (Fig. 9F). Although c_p slope for waters dominated by phytoplankton colonies > 100 µm in size was lower than c_p slope for waters dominated by small non-algal particles, the lowest c_p slopes were associated with abundant dead cells in the 10 to 100 µm size range. Higher b_p:a_p and a_p slopes in surface waters also suggest that surface waters after May 13th are dominated by dead cells. This is contrary to the normal positive correlation between c_p slope and the relative abundance of large particles (Kitchen et al. 1982; Boss et al. 2001) but in agreement with results from previous sample analyses that showed low c_p slopes associated with dead cells (community 5, Table 1). For the large diatom colonies that were found in East Sound during the study in 2010, morphology may

play an important role in determining their scattering characteristics and the c_p slope parameter.

DISCUSSION

This study compared the phytoplankton and non-algal particle composition of ocean waters with in situ measurements of particulate IOPs over small scales. Results show a strong influence of phytoplankton morphological and physiological characteristics on the spectral shape and relative magnitude of a_p, c_p, and b_p, coefficients. Variation in phytoplankton community composition, primarily driven by the relative abundance of large diatom cells and colonies, determined c_p slope. However, it appears the complex morphology of some large colonies resulted in higher c_p slopes than would be expected based on their size as measured with the Cytosense scanning flow cytometer. Phytoplankton cell death and subsequent loss of chlorophyll increased b_p:a_p and a_p slopes. In addition, the relative abundance of non-algal particles primarily determined b_b:b. These results demonstrate the ability of optical parameters to reveal variation of phytoplankton community characteristics with high resolution over ecologically critical, small spatial and temporal scales in the ocean.

Results were similar for two very different field collected data sets. In the first year, suspended particles in East Sound were dominated by a single diatom taxon in the genus *Haslea*. It's relative abundance throughout the water column over time determined variation of the c_p slope parameter. The death of this population caused dramatic changes in b_p:a_p and a_p slope as cellular pigment content changed and the proportion of empty frustules increased. Increases in b_p:a_p are likely due to a decrease

in absorption by dead cells through loss of chlorophyll. Increases in a_p slope may be associated with a relative increase in absorption by photoprotective carotenoids, or with changes in pigment packaging as cells die. In Monterey Bay, high a_p slopes were associated with large cells with high pigment packaging (McFarland et al. in prep.) while in East Sound it seems more likely that changes in pigment ratios as cells died determined changes in a_p slope. Although the phytoplankton community contained very different taxa and was far more diverse in the second year, similar results were found. Large colonial diatoms (*C. socialis* in particular) drove changes in c_p slope. As these cells died b_p:a_p and a_p slope increased. In this case, dead and dying cells covered a range of sizes as colonies fell apart into single cells or short chains. Contrary to expectations, these smaller dead cells were associated with the highest c_p slopes. The complex morphology of these large intact diatom colonies may have resulted in lower c_p slopes than would be expected from theoretical predictions based on the assumption that particles are spheres or ellipsoids (e.g. Mie theory). Diatoms such as *C. socialis* form colonies several hundred μm in size, composed of curving intertwined chains of cells, each with multiple long thin siliceous setae (Fig. 1C). This highly non-spherical colony may scatter light similar to a population of smaller particles resulting in lower than expected c_p slopes. Disruption of this structure as cells die and possible aggregation of colony fragments may result in particle populations with c_p slopes higher than for healthy intact colonies.

In both years, optical data proved to be an effective tool for determining changes in phytoplankton community characteristics with high resolution over small spatial and temporal scales. Autonomous in situ measurements from an ORCAS profiler

enabled visualization of small scale features and important ecological processes that would have been otherwise very difficult to detect. During 2009, dead *Haslea* cells accumulated near the surface rather than sinking. This was visually confirmed by a distinctive surface slick seen throughout the sound at the termination of the bloom. Dead *Haslea* sp. cells may have been positively buoyant due to intracellular accumulation of lipids (Rines et al. in prep.). Also during 2009, the depth of the pycnocline corresponded to a minimum in b_p:a_p values and high c_p slopes (Fig. 7). This suggests that the transition region between low and high density waters contained very few dead cells or large particles. During 2010, the depth of the pycnocline at times corresponded to elevated b_p:a_p values. This suggests that dying cells were settling out of surface waters and accumulating at the interface between low and high density waters (Alldredge et al. 2002), a process that may have implications for biogeochemical cycling on a global scale. These small scale features would not have been visible by looking only at measures of total phytoplankton abundance such as chlorophyll absorption or fluorescence.

Previous work conducted in Monterey Bay showed that particulate optical properties varied among phytoplankton communities composed of taxa with very different morphological and physiological characteristics (McFarland et al. in prep.). The methods employed in the present study used direct flow cytometric measurements of these taxon specific characteristics to provide further evidence that phytoplankton morphological and physiological characteristics can be derived from in situ optical measurements to determine ecological patterns and processes in the ocean.

Currently the ecological dynamics of phytoplankton communities over small spatial and temporal scales in the ocean are poorly understood. Processes at these scales, however, are critical to the ecology of individual species and populations. Use of optical techniques as demonstrated here, can provide the tools necessary to greatly enhance our understanding of phytoplankton ecology in the pelagic ocean environment. Results show the particulate optical properties of natural phytoplankton communities clearly vary with biologically important morphological and physiological characteristics of cells and colonies. However, the relationship between cellular characteristics and optical properties can be influenced by multiple factors, and optical data may be difficult to interpret. Simultaneous biological or chemical analyses of discrete samples, therefore, may be required to accurately determine ecological patterns and processes from in situ optical measurements.

Acknowledgements

We are grateful for the help and collaboration of George Dubelaar. We also thank ONR for their commitment to our research program. This work was supported by ONR grants N000140410275 (JR), N000140811217 (PD, JS and JR) and N000140910492 (PD, JR and JS).

REFERENCES

Ackleson SG, Spinrad RW, Yentsch CM, Brown J, Korjeff-Bellows W (1988) Phytoplankton optical properties: flow cytometric examinations of dilution-induced effects. Appl Opt 27:1262–1269

Alldredge AL, Cowles TJ, MacIntyre S, Rines JEB, Donaghay PL, Greenlaw CF, Holliday DV, Dekshenieks MM, Sullivan JM, Zaneveld JRV (2002) Occurrence and mechanisms of formation of a dramatic thin layer of marine snow in a shallow Pacific fjord. Mar Ecol Prog Ser 233:1–12

Babin M, Cullen JJ, Roesler CS, Donaghay PL, Doucette GJ, Kahru M, Lewis MR, Scholin CA, Sieracki ME, Sosik HM (2005) New approaches and technologies for observing harmful algal blooms. Oceanography 18:210–227

Babin M, Stramski D, Ferrari GM, Claustre H, Bricaud A, Obolensky G, Hoepffner N (2003) Variations in the light absorption coefficients of phytoplankton, nonalgal particles, and dissolved organic matter in coastal waters around Europe. J Geophys Res 108

Benoit-Bird KJ, Cowles TJ, Wingard CE (2009) Edge gradients provide evidence of ecological interactions in planktonic thin layers. Limnol Oceanogr 54:1382–1392

Bjørnsen PK, Nielsen TG (1991) Decimeter scale heterogeneity in the plankton during a pycnocline bloom of *Gyrodinium aureolum*. Mar Ecol Prog Ser 73:263–267

Boss E, Twardowski MS, Herring S (2001) Shape of the particulate beam attenuation spectrum and its inversion to obtain the shape of the particulate size distribution. Appl Opt 40:4885–4893

Bricaud A, Claustre H, Ras J, Oubelkheir K (2004) Natural variability of phytoplanktonic absorption in oceanic waters: Influence of the size structure of algal populations. J Geophys Res 109

Bricaud A, Morel A, Prieur L (1983) Optical efficiency factors of some phytoplankters. Limnol Oceanogr 28:816–832

Cassie RM (1963) Microdistribution of plankton. Oceanogr Mar Biol Ann Rev 1

Ciotti AM, Lewis MR, Cullen JJ (2002) Assessment of the relationships between dominant cell size in natural phytoplankton communities and the spectral shape of the absorption coefficient. Limnol Oceanogr 47:404–417

Clarke KR, Somerfield PJ, Gorley RN (2008) Testing of null hypotheses in exploratory community analyses: similarity profiles and biota-environment linkage. J Exp Mar Biol Ecol 366:56–69

Cowles TJ, Desiderio RA (1993) Resolution of biological microstructure through in situ fluorescence emission spectra. Oceanography 6:105–111

Cowles TJ, Desiderio RA, Carr ME (1998) Small-scale planktonic structure: persistence and trophic consequences. Oceanography 11:4–9

Dekshenieks MM, Donaghay PL, Sullivan JM, Rines JEB, Osborn TR, Twardowski MS (2001) Temporal and spatial occurrence of thin phytoplankton layers in relation to physical processes. Mar Ecol Prog Ser 223:61–71

Derenbach JB, Astheimer H, Hansen HP, Leach H (1979) Vertical microscale distribution of phytoplankton in relation to the thermocline. Mar Ecol Prog Ser 1:187–193

Donaghay PL (2003) Profiling systems for understanding the dynamics and impacts of thin layers of harmful algae in stratified coastal waters. In: Renvyle, County Galway, p 44–53

Donaghay PL, Osborn TR (1997) Toward a theory of biological-physical control of harmful algal bloom dynamics and impacts. Limnol Oceanogr 42:1283–1296

Donaghay PL, Rines HM, Sieburth JM (1992) Simultaneous sampling of fine scale biological, chemical, and physical structure in stratified waters. Arch Hydrobiol 36:97–108

Durham WM, Stocker R (2012) Thin phytoplankton layers: characteristics, mechanisms, and consequences. Annu Rev Mar Sci 4:177–207

Duysens LNM (1956) The flattening of the absorption spectrum of suspensions, as compared to that of solutions. Biochim Biophys Acta 19:1–12

Eisner LB, Cowles TJ (2005) Spatial variations in phytoplankton pigment ratios, optical properties, and environmental gradients in Oregon coast surface waters. J Geophys Res 110

Eisner LB, Twardowski MS, Cowles TJ, Perry MJ (2003) Resolving phytoplankton photoprotective: photosynthetic carotenoid ratios on fine scales using in situ spectral absorption measurements. Limnol Oceanogr 48:632–646

Green RE, Sosik HM, Olson RJ (2003) Contributions of phytoplankton and other particles to inherent optical properties in New England continental shelf waters. Limnol Oceanogr:2377–2391

Guillard RRL, Hargraves PE (1993) *Stichochrysis immobilis* is a diatom, not a chrysophyte. Phycologia 32:234–236

Hanson AK, Donaghay PL (1998) Micro-to fine-scale chemical gradients and layers in stratified coastal waters. Oceanography 11:10–17

Haury LR, McGowan JA, Wiebe PH (1978) Patterns and processes in the time-space scales of plankton distributions. In: Steele JH (ed) Spatial Pattern in Plankton Communities. Plenum Press, New York, p 277–327

Holliday DV, Donaghay PL, Greenlaw CF, McGehee DE, McManus MM, Sullivan JM, Miksis JL (2003) Advances in defining fine- and micro-scale pattern in marine plankton. Aquat Living Resour 16:131–136

Jones DL (2012) The Fathom Toolbox for MATLAB: multivariate ecological and oceanographic data analysis. College of Marine Science, University of South Florida, St. Petersburg, Florida, United States

Kirk JTO (1975) A theoretical analysis of the contribution of algal cells to the attenuation of light within natural waters. I. General treatment of suspensions of pigmented cells. New Phytologist 75:11–20

Kitchen JC, Zaneveld JRV, Pak H (1982) Effect of particle size distribution and chlorophyll content on beam attenuation spectra. Appl Opt 21:3913–3918

McFarland M, Rines J, Donaghay P, Sullivan J (in prep.) Optical signatures of marine phytoplankton communities over small scales.

McManus MA, Alldredge AL, Barnard AH, Boss E, Case JF, Cowles TJ, Donaghay PL, Eisner LB, Gifford DJ, Greenlaw CF, Herren CM, Holliday DV, Johnson D, MacIntyre S, McGehee DM, Osborn TR, Perry MJ, Pieper RE, Rines JEB, Smith DC, Sullivan JM, Talbot MK, Twardowski MS, Weidemann A, Zanaveld JR (2003) Characteristics, distribution and persistence of thin layers over a 48 hour period. Mar Ecol Prog Ser 261:1–19

Menden-Deuer S (2008) Spatial and temporal characteristics of plankton-rich layers in a shallow, temperate fjord. Mar Ecol Prog Ser 355:21

Morel A, Bricaud A (1986) Inherent optical properties of algal cells including picoplankton: Theoretical and experimental results. In: Platt T, Li WKW (eds) Photosynthetic Picoplankton. Department of Fisheries and Oceans, p 521–559

Nielsen TG, Kiørboe T, Bjørnsen PK (1990) Effects of a *Chrysochromulina polylepis* subsurface bloom on the planktonic community. Mar Ecol Prog Ser 62:21–35

Oksanen J, Blanchet FG, Kindt R, Legendre P, Minchin PR, O'Hara RB, Simpson GL, Solymos P, Henry M, Stevens H, Wagner H (2013) vegan: community ecology package.

Peperzak L (2006) Below the Kolmogorov scale: the non-turbulent sex life of phytoplankton. Afr J Mar Sci 28:261–264

Reynolds, Colin (2006) Ecology of Phytoplankton. Cambridge University Press

Rines JEB, Donaghay PL, Dekshenieks MM, Sullivan JM, Twardowski MS (2002) Thin layers and camouflage: hidden *Pseudo-nitzschia* spp. (Bacillariophyceae) populations in a fjord in the San Juan Islands, Washington, USA. Mar Ecol Prog Ser 225:123–137

Rines JEB, McFarland MN, Donaghay PL, Sullivan JM (2010) Thin layers and species-specific characterization of the phytoplankton community in Monterey Bay, California, USA. Cont Shelf Res 30:66–80

Sathyendranath S, Lazzara L, Prieur L (1987) Variations in the spectral values of specific absorption of phytoplankton. Limnol Oceanogr 32:403–415

Sieburth JMN, Donaghay PL (1993) Planktonic methane production and oxidation within the algal maximum of the pycnocline: seasonal fine-scale observations in an anoxic estuarine basin. Mar Ecol Prog Ser 100:3–3

Smayda TJ, Reynolds CS (2001) Community assembly in marine phytoplankton: Application of recent models to harmful dinoflagellate blooms. J Plankton Res 23:447–461

Sosik HM, Green RE, Pegau WS, Roesler CS (2001) Temporal and vertical variability in optical properties of New England shelf waters during late summer and spring. J Geophys Res 106:9455–9472

Spinrad RW, Yentsch CM (1987) Observations on the intra- and interspecific single cell optical variability of marine phytoplankton. Appl Opt 26:357–362

Stemmann L, Boss E (2012) Plankton and particle size and packaging: from determining optical properties to driving the biological pump. Annu Rev Mar Sci 4:263–290

Stramski D, Morel A (1990) Optical properties of photosynthetic picoplankton in different physiological states as affected by growth irradiance. Deep-Sea Res A 37:245–266

Stramski D, Reynolds RA (1993) Diel variations in the optical properties of a marine diatom. Limnol Oceanogr 38:1347–1364

Sullivan JM, Donaghay PL, Rines JEB (2010) Coastal thin layer dynamics: Consequences to biology and optics. Cont Shelf Res 30:50–65

Sullivan JM, Holliday D Van, McFarland M, McManus MA, Cheriton OM, Benoit-Bird KJ, Goodman L, Wang Z, Ryan JP, Stacey M (2010) Layered organization in the coastal ocean: An introduction to planktonic thin layers and the LOCO project. Cont Shelf Res 30:1

Sullivan JM, Twardowski MS, Donaghay PL, Freeman SA (2005) Use of optical scattering to discriminate particle types in coastal waters. Appl Opt 44:1667–1680

Sullivan JM, Twardowski MS, Zaneveld JRV, Moore CM, Barnard AH, Donaghay PL, Rhoades B (2006) Hyperspectral temperature and salt dependencies of absorption by water and heavy water in the 400-750 nm spectral range. Appl Opt 45:5294–5309

Twardowski MS, Boss E, Macdonald JB, Pegau WS, Barnard AH, Zaneveld JRV (2001) A model for estimating bulk refractive index from the optical backscattering ratio and the implications for understanding particle composition in case I and case II waters. J Geophys Res 106:14129–14142

Twardowski MS, Sullivan JM, Donaghay PL, Zaneveld JRV (1999) Microscale quantification of the absorption by dissolved and particulate material in coastal waters with an ac-9. J Atmos Ocean Tech 16:691–707

Zaneveld JRV, Kitchen JC, Moore CC (1994) Scattering error correction of reflecting-tube absorption meters. In: Proceedings SPIE 2258.p 44–55

TABLES

Table 1. Number of samples (N) and the mean and standard deviations (s.d.) of optical parameters for samples in each community.

	com-munity	N	b_p:a_p		c_p slope		b_b:b		a_p slope	
			mean	s.d.	mean	s.d.	mean	s.d.	mean	s.d.
2009	1	8	16.82	5.33	0.410	0.061	0.0096	0.0012	0.0218	0.0049
	2	8	10.35	1.88	0.502	0.132	0.0160	0.0023	0.0131	0.0016
	3	27	6.44	0.86	0.281	0.054	0.0112	0.0027	0.0109	0.0012
	4	12	18.78	8.78	0.637	0.202	0.0131	0.0032	0.0187	0.0062
2010	5	3	20.90	4.32	0.091	0.166	0.0070	0.0004	0.0176	0.0037
	6	16	10.31	3.49	0.417	0.155	0.0148	0.0045	0.0122	0.0021
	7	13	9.21	3.03	0.211	0.157	0.0084	0.0020	0.0120	0.0025
	8	29	10.41	4.89	0.241	0.203	0.0082	0.0024	0.0122	0.0033

FIGURES

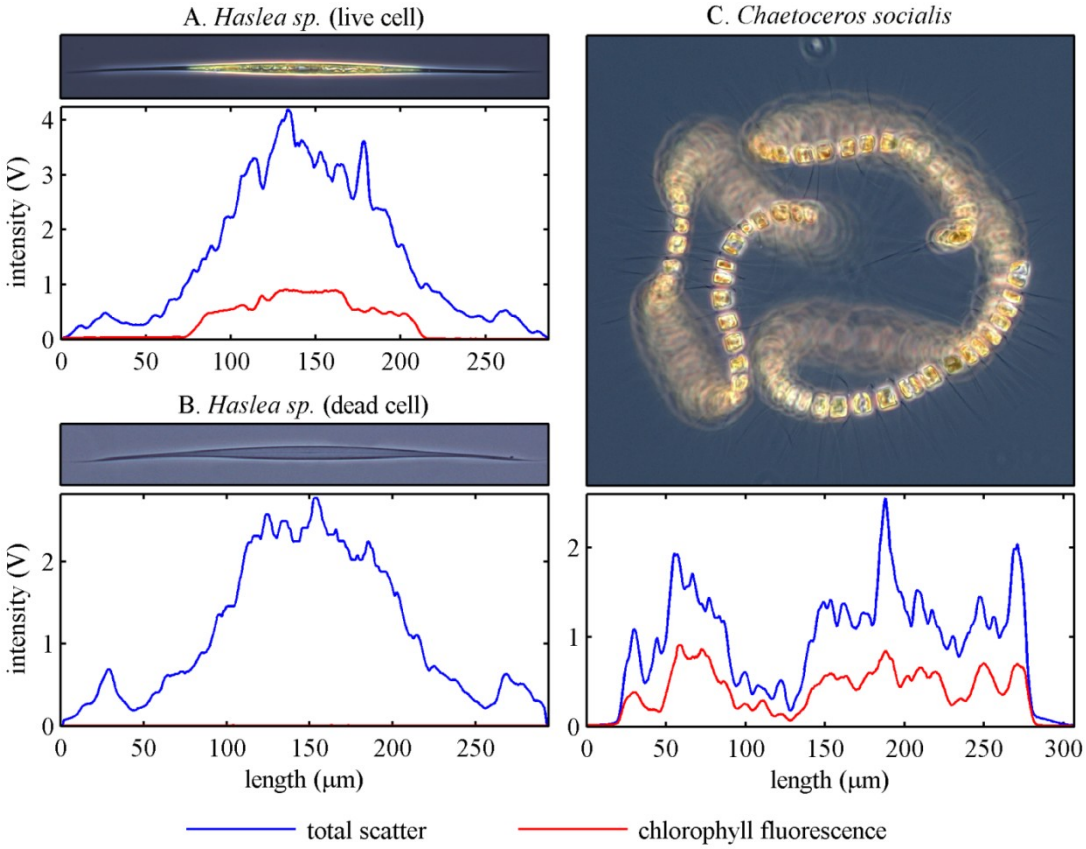

Figure 1. Examples of several phytoplankton cells and corresponding scan data from the Cytosense flow cytometer. (A) Image of live *Haslea* sp. cell above corresponding Cytosense scan. (B) Image and scan of empty *Haslea* sp. frustule. Note lack of chlorophyll fluorescence. (C) Image and corresponding scan of live *Chaetoceros socialis* colony.

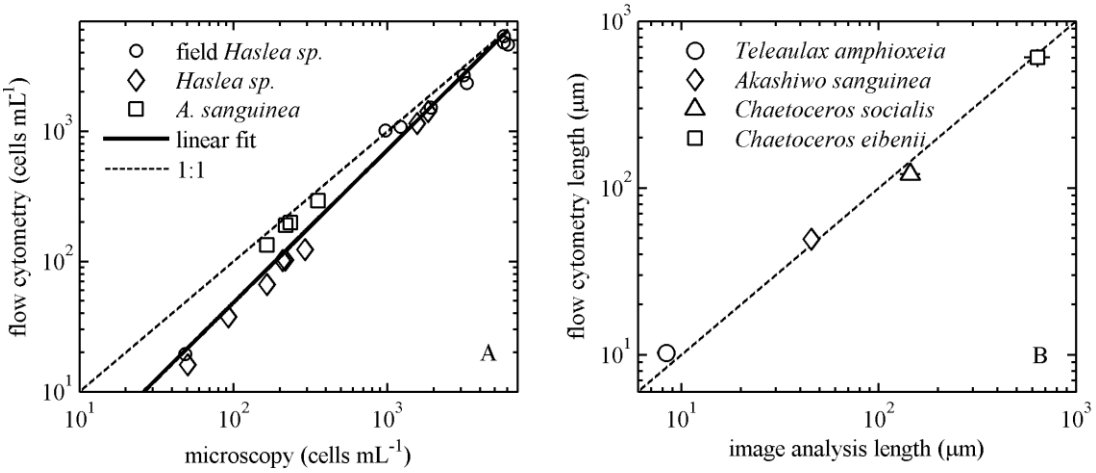

Figure 2. (A) Comparison of phytoplankton cell concentrations determined by flow cytometry and manual, microscope based cell counts. (B) Comparison of mean phytoplankton cell length measurements determined by scanning flow cytometry and automated image analysis for four different uni-algal cultures. Standard error bars are smaller than most symbols.

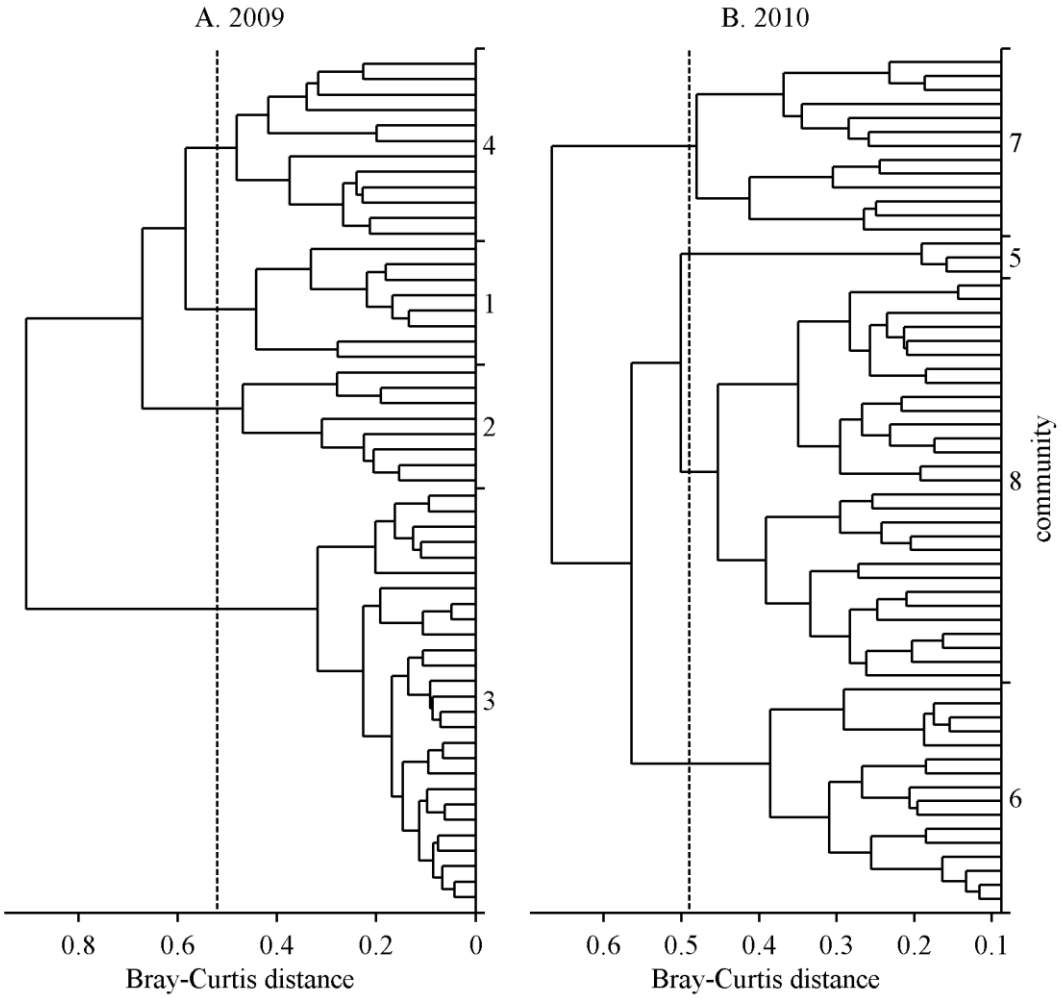

Figure 3. Dendrograms showing results of cluster analyses for 2009 (A) and 2010 (B) based on particle size-scatter distributions of samples determined with scanning flow cytometry (See Fig. 4). Dashed lines indicate cutoff levels of 0.52 (2009) and 0.49 (2010) determined with similarity profiles ($p < 0.01$).

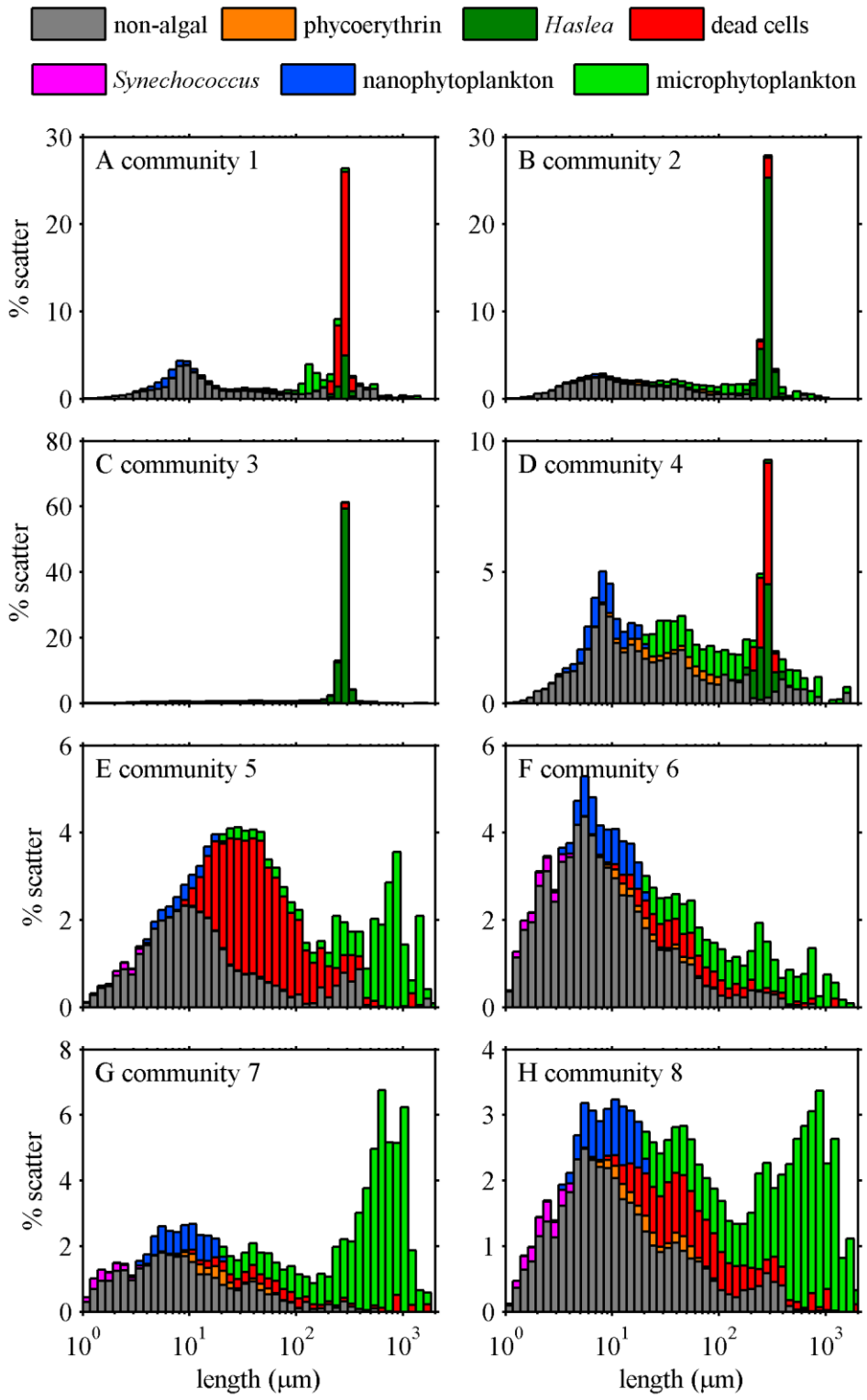

Figure 4. Mean particulate composition of communities determined with scanning flow cytometry for 2009 (A – D) and 2010 (E – H). Stacked histograms show percentage of total scatter as a function of particle type and length (μm).

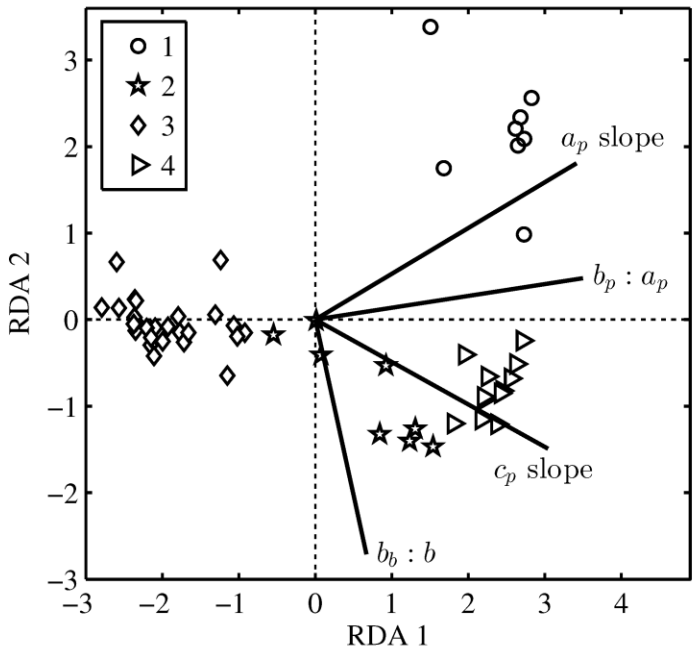

Figure 5. Biplots showing results of redundancy analysis for 2009. Symbols indicate community membership of samples as determined by hierarchical cluster analyses (Fig. 3). Vectors indicate direction of increase for optical parameter values.

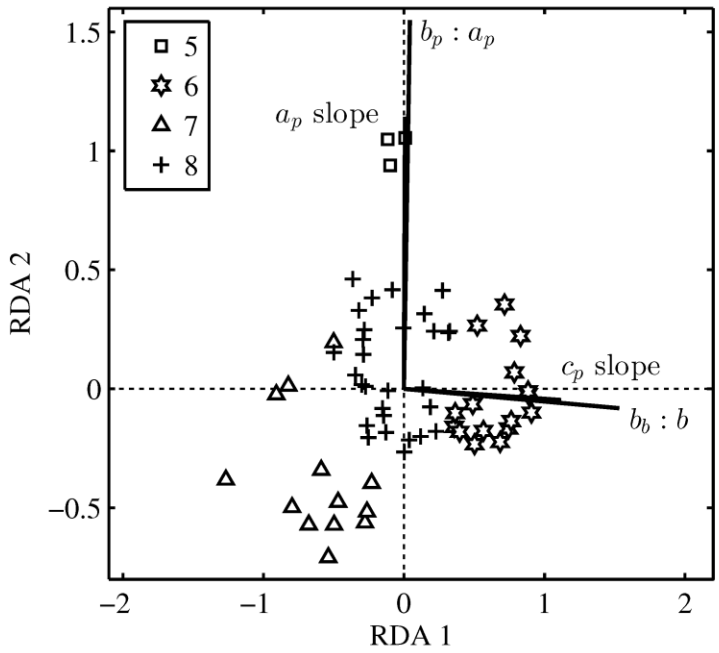

Figure 6. Biplots showing results of redundancy analysis for 2010. Symbols indicate community membership of samples as determined by hierarchical cluster analyses (Fig. 3). Vectors indicate direction of increase for optical parameter values.

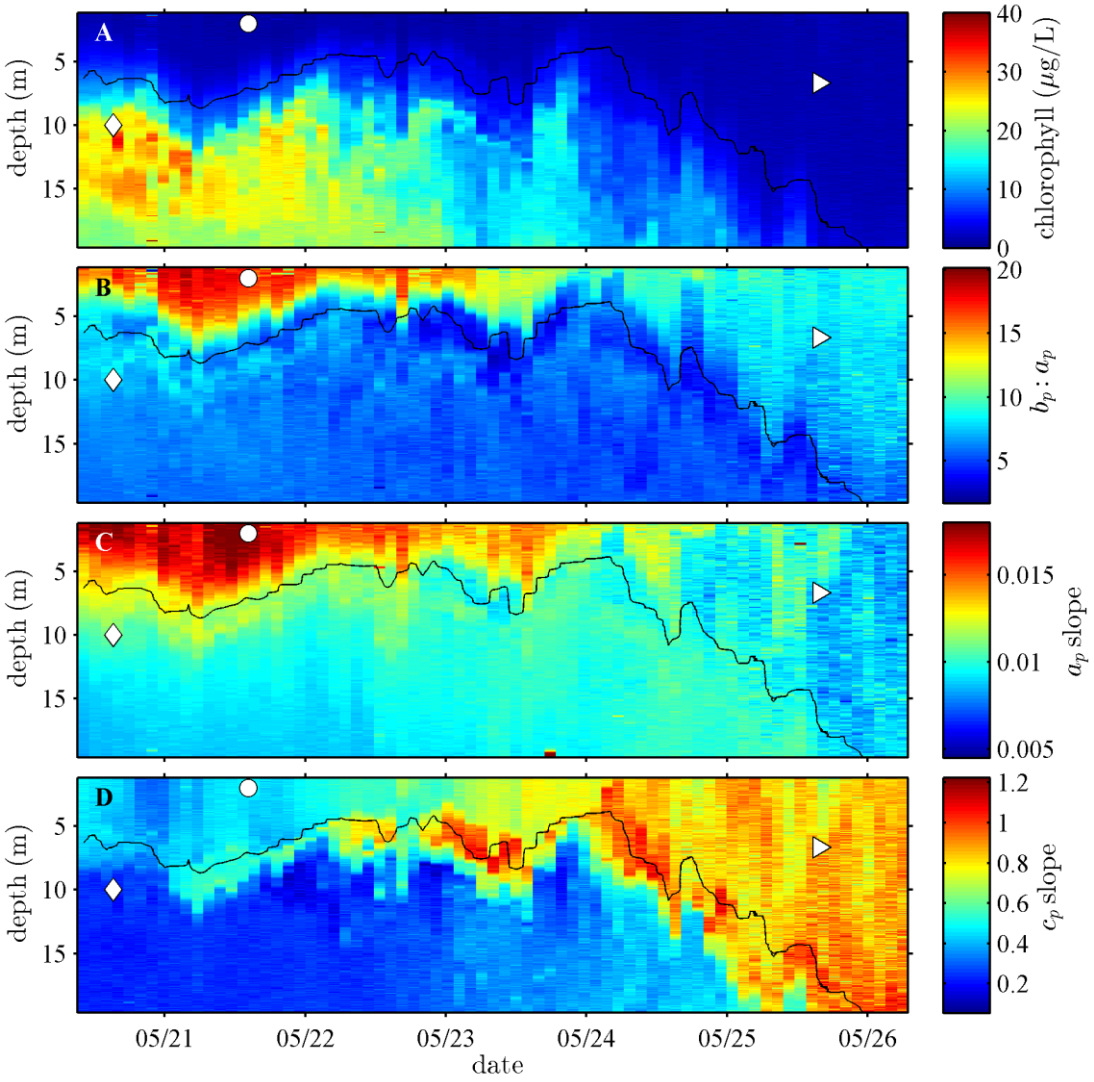

Figure 7. High resolution optical data collected during 2009 with the ORCAS autonomous profiler. Symbols indicate location of samples shown in Fig. 9A – C. Black line indicates depth of the pycnocline.

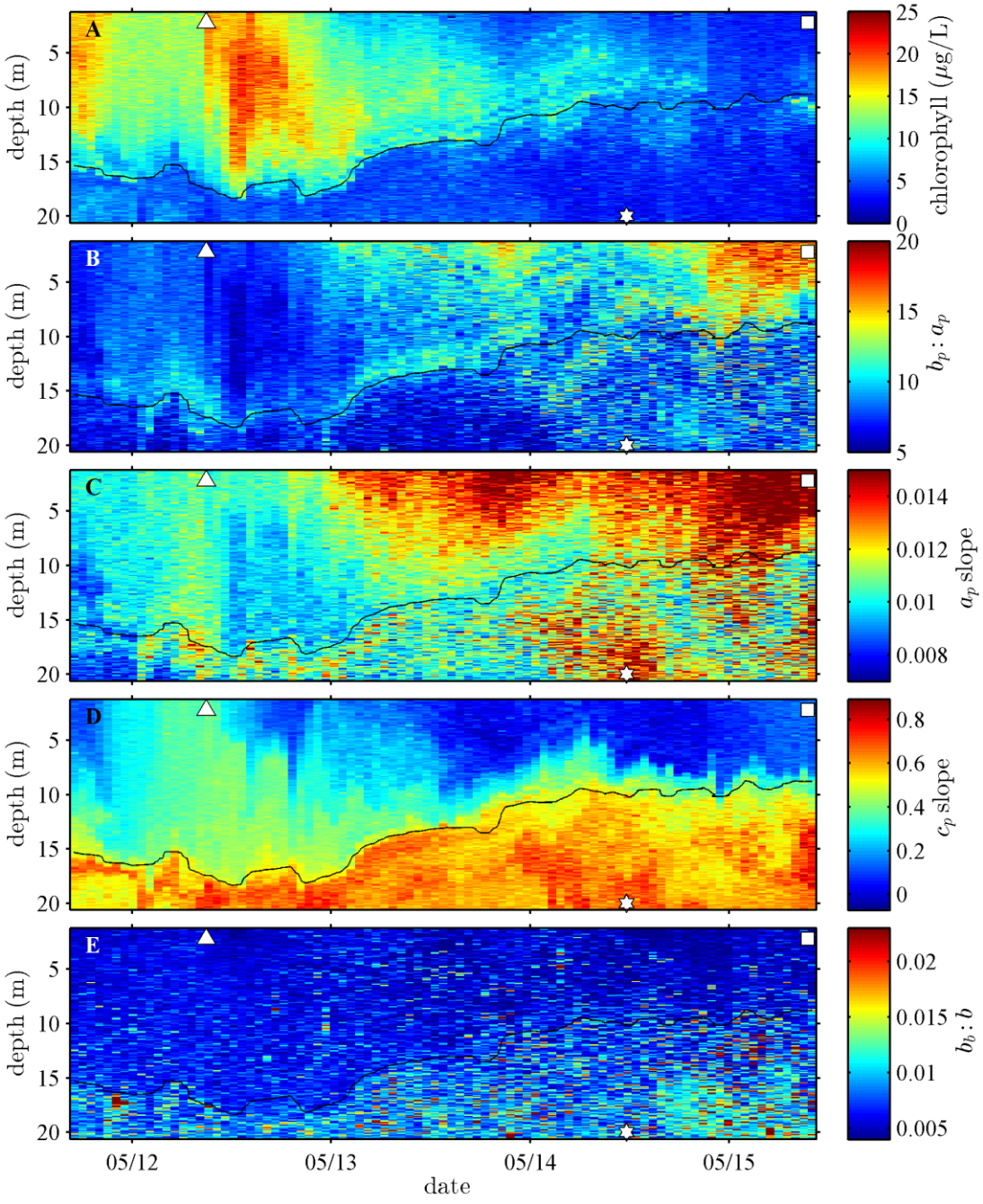

Figure 8. High resolution optical data collected during 2010 with the ORCAS autonomous profiler. Symbols indicate location of samples shown in Fig. 9D – F. Black line indicates depth of the pycnocline.

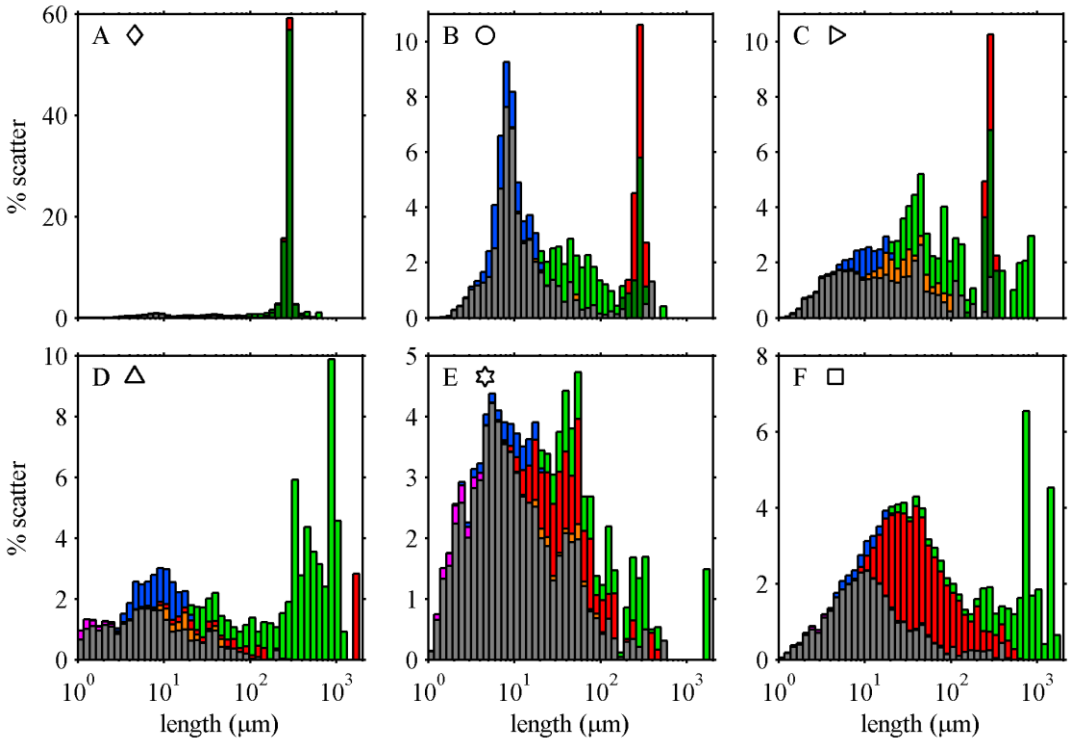

Figure 9. Composition of individual samples collected near the ORCAS autonomous profiler during 2009 (A – C) and 2010 (D – F) shown as percent scatter determined by scanning flow cytometry. Symbols correspond to sample locations in Figs. 7 & 8 and to the communities they most resemble as in Figs. 5 & 6. Colors represent particle types as in Fig. 4.

MANUSCRIPT 3

THE EFFECTS OF SIZE, SHAPE AND PIGMENT CONTENT ON LIGHT ABSORPTION AND SCATTERING FOR FIVE MARINE PHYTOPLANKTON SPECIES

Malcolm N. McFarland, Jan Rines, Percy Donaghay

Formatted for submission to the Journal of Plankton Research

University of Rhode Island, Graduate School of Oceanography

215 South Ferry Road, Narragansett, RI 02882

ABSTRACT

The optical properties of phytoplankton determine the light harvesting efficiency of cells and influence light absorption and scattering in the ocean. To improve our understanding of the effects of morphology and physiology on the optical properties of cells and colonies we measured light absorption and scattering by 5 uni-algal cultures with distinct size, shape, and pigment characteristics. Light absorption and scattering efficiency factors, the ratio of scattering and absorption coefficients, and the shape of the absorption coefficient spectra all varied among cultures during exponential growth and after senescence. Results suggest that the size and intracellular pigment content of diverse species are ecologically important traits of cells that compete for available light in the marine pelagic environment. The low intracellular pigment concentrations and complex morphology of large forms appear to minimize the negative impact on fitness caused by self-shading of pigments (i.e. package effects). Results also suggest that optical properties measured in situ may be used to infer the morphological and physiological characteristics of large phytoplankton cells and colonies to better understand natural community structure and function.

INTRODUCTION

For more than 100 years ecologists have sought to explain the function of the many diverse forms of phytoplankton found in the marine pelagic environment (Gran 1912, Sournia 1982, Fogg 1991). Acquisition of light to fuel photosynthesis is one of the critical functions of these autotrophic organisms influenced by species-specific traits (Raven 1984). Phytoplankton morphological and physiological characteristics such as size, shape, structure, and pigment content determine how cells and colonies

absorb and scatter light (Morel & Bricaud 1986, Johnsen et al. 1994, Ciotti et al. 2002). These characteristics vary considerably among the tens of thousands of described species and eight major phylogenetic groups of phytoplankton (Katz et al. 2004). Distinct taxa have different photoprotective and photosynthetic accessory pigments with characteristic absorption spectra (Hoepffner & Sathyendranath 1991). Cells and colonies of different species range in size over 4 orders of magnitude from less than 1 μm to greater than 1 mm. Taxa also exhibit a wide variety of morphologies ranging from simple spheres to complex three-dimensional structures. Despite these differences, all phytoplankton rely on the absorption of light to fuel photosynthesis and growth. Bio-optically important cellular characteristics, therefore, influence the ability of cells to compete for available light, and may determine the fitness of different forms in the marine pelagic environment where light is often a limiting resource (Huisman et al. 1999a, Huisman et al. 1999b, Finkel 2001, Litchman 2003, Litchman et al. 2004, Stomp 2007, Huisman et al. 2004).

In many ocean waters, absorption and scattering of light by phytoplankton cells and colonies determine, to a large extent, the magnitude and shape of particulate absorption (a_p) and scattering (b_p) coefficient spectra (Lorenzen 1972, Itturiaga & Siegel 1989, Stramski et al. 2001). These inherent optical properties (IOPs) are functions of phytoplankton and non-algal particle abundance, their projected area (i.e. the shadow cast on a 2 dimensional plane representing the amount of light intercepted), and the efficiency with which particles absorb or scatter the light they intercept. With modern optical and oceanographic instrumentation, a_p and b_p can be measured in situ with high resolution to reveal detailed patterns of variation over a

wide range of spatial and temporal scales (Cowles et al. 1998, Babin et al. 2005, Churnside & Donaghay 2009). Optical measurements made at very high spatial or temporal frequencies (less than 10 cm, greater than 1 Hz) can resolve small scale bio-optical variation critical to the ecological processes that determine phytoplankton community structure and function (Holliday et al. 2003, Rines et al. 2010, McFarland et al. in prep. b). IOPs, therefore, represent a valuable tool in the study of pelagic marine ecology that can be used to investigate ecosystem structure and the interactions between light and phytoplankton that affect growth rates of different species.

When measured for natural particle assemblages over various scales in the ocean, b_p and a_p exhibit substantial variability in magnitude and spectral shape (Sosik et al. 2001, Eisner & Cowles 2005, Sullivan et al. 2005, McFarland et al. in prep. a & b). Numerous field studies show that differences in cell size, accessory pigments, and intracellular pigment packaging strongly influence measurements of absorption and scattering by natural phytoplankton communities (Bricaud & Stramski 1990, Hoepffner & Sathyendranath 1992, Ciotti et al. 2002, Babin et al. 2003, Eisner et al. 2003, Lohrenz et al. 2003, Roy et al. 2008, Astoreca et al. 2012, Ferreira et al. 2013, McFarland et al. in prep. b). The effects of cell size and pigment content on light absorption and scattering are also well documented by laboratory based studies (Das 1967, Kirk 1975, Kitchen et al 1982, Morel and Bricaud 1986, Sathyendranath et al. 1987, Hoepffner & Sathyendranath 1991, Stramski & Reynolds 1993, Zhou et al. 2012). However, most theoretically based studies assume particles are spherical in shape and few empirically based studies directly measure the abundance or characteristics of large, morphologically complex phytoplankton cells and colonies

that often dominate coastal phytoplankton blooms. Consequently, the extent to which in situ optical variability can be attributed to ecologically relevant morphological and physiological differences among populations is not well known. Previous studies employing microscopy or flow cytometry to directly examine individual cells and colonies demonstrated that large phytoplankton can contribute substantially to particulate IOPs and that physiological changes affecting pigment content can have a significant impact on the relative magnitude and shape of a_p and b_p spectra (McFarland et al. in prep. a & b). With a better understanding of the optical effects of cellular morphology and physiology, in situ measurements of a_p and b_p may reveal the biological function of optically important phytoplankton characteristics and help explain ecological processes within natural phytoplankton communities.

In this study, the effects of morphological and physiological characteristics on ecologically important optical properties are analyzed for five distinct uni-algal phytoplankton cultures representing 3 taxonomic classes. We selected species that have been observed to vary with in situ measurements of a_p and b_p in the field (Rines et al. 2010, McFarland et al. in prep. a & b). The selected taxa ranged from ~10 µm long single cells with simple shapes to complex, 3-dimensional colonies greater than 700 µm in length. Cultured species included *Teleaulax amphioxeia* (Cryptophyceae), *Akashiwo sanguinea* (Dinophyceae), *Haslea* sp. (Bacillariophyceae), *Chaetoceros socialis* (Bacillariophyceae), and *Chaetoceros eibenii* (Bacillariophyceae). We measured the phytoplankton specific absorption and scattering coefficients (a_{ph} and b_{ph}) for each species by size fractionation. Automated image analysis was used to measure the concentration and projected area of phytoplankton cells or colonies and

calculate their mean absorption and scattering efficiencies (Q_a and Q_b). We also examined the slope of a_{ph} between 440 nm and 532 nm, and the ratio of b_p at 555 nm to a_p at 676 nm (b_{ph}:a_{ph}) as biologically sensitive optical parameters that can be measured with high resolution in the ocean to study natural phytoplankton community structure and ecological processes. In addition, we used scanning flow cytometry to determine the particulate composition of cultures and quantify the contribution of cells, colonies, and non-algal particles to measured optical parameters. Measurements were obtained during exponential growth and after cells had settled from suspensions to evaluate the optical effects of physiological changes associated with senescence.

METHODS

For each species, six replicate sets of optical measurements, image analysis, and flow cytometry data were obtained during exponential growth. Four sets of these measurements were obtained for each species after cultures had settled out of suspension. Comparison among species during exponential growth allowed for assessment of the effects of species-specific characteristics on optical properties. Comparison between exponential growth phase and settled cultures allowed for assessment of the effects of physiology on the optical properties of each species.

Culture isolation and growth

Uni-algal cultures were obtained from field samples collected with a 64 μm mesh size plankton net or from un-concentrated sea water samples. *T. amphioxeia* was isolated from a Narragansett Bay, RI water sample. *C. socialis* was isolated from a water sample collected from Falmouth, ME. *Haslea* sp. and *C. eibenii* were isolated from samples collected in East Sound, WA. *A. sanguinea* was isolated from a sample

collected in Grays Harbor, WA. Single cells were identified and isolated by hand using an inverted compound microscope and a drawn glass pipet. Cells were washed 4 to 5 times by transferring into clean 0.2 μm filtered sea water and then placed into glass tubes with 10 mL of L1 sea water medium (Guillard & Hargraves 1993). *A. sanguinea* and *T. amphioxeia* were grown in L1/2 strength medium without enrichment of Si. Diatoms were grown in L1/10 strength medium. All cultures were maintained at 15°C with a 12:12 light:dark cycle and transferred into fresh medium every two weeks.

For all measurements, replicate cultures were grown in 6 polycarbonate tanks (25 cm width, 10 cm depth, and 60 cm height) containing 10 L of sea water medium. Tanks were housed in a walk-in incubator maintained at 15°C (±1°C) and illuminated with cool white fluorescent lights on a 12:12 light:dark cycle. To prevent settling and enhance growth by simulating natural turbulence, cultures were continuously stirred with a horizontal 2.54 cm diameter polycarbonate rod that was raised and lowered through the tank by an electric motor at a rate of twice per minute.

Automated Image Analysis

A FlowCAM imaging particle analyzer (Fluid Imaging Technologies, Inc.) was used to determine the projected area and concentrations of cells, colonies (Fig. 1) and non-algal particles. The FlowCAM uses flow cells and objective lenses of various size and magnification to capture images of suspended particles in a known fluid sample volume. We used a 10x objective and a 100 μm width flow cell to image *T. amphioxeia* at a resolution of 0.553 μm pixel^{-1}. A 2x objective and an 800 μm width flow cell were used to image *C. eibenii* at 2.94 μm pixel^{-1}. Other cultures were imaged

at a resolution of 1.36 μm pixel^{-1} with a 4x objective and a 300 μm width flow cell. FlowCAM software (Visual Spreadsheet version 3.2) automatically segments images (i.e. divides images into subject and background regions) by applying a threshold and calculates particle area and concentrations along with other particle shape dependent parameters such as length and width. Threshold levels were set manually for each species by visually inspecting segmented images to ensure accurate detection of particle edges. Cells and colonies were discriminated from non-algal particulate material based on their Mahalanobis distance from the mean of a sub-set of manually identified images of cells or colonies for each species. This distance metric takes into account correlation among parameters within the data set (Mahalanobis, 1936). Twenty-six descriptive particle parameters calculated by Visual Spreadsheet were used to compute the Mahalanobis distance. The maximum distance allowed for classification of particles as cells or colonies was set as the maximum distance from the mean within the sub-set of manually identified images. Mean values of particle area and concentration for particles classified as as cells, colonies or non-algal particles were computed for each replicate tank. Mean area for each species was calculated as the mean of mean areas determined for each replicate tank.

Scanning Flow Cytometry

A CytoSense (CytoBuoy b.v.) scanning flow cytometer was used to determine the particulate composition of cultures and the chlorophyll fluorescence of cells and colonies (Dubelaar et al. 2004). This instrument has a large sample flow path that can accommodate particles up to 800 μm in width. The CytoSense records scans of particles as they pass individually through a focused laser beam. Particles travel at a

fixed speed and the intensity of scattered and fluoresced light is measured at a fixed interval corresponding to 0.5 μm along the length of the particle (see also McFarland et al. in prep. b). Elongate particles tend to align lengthwise in the flow and the length of scans therefore represents maximum particle dimensions. The instrument used here was equipped with a blue laser (488 nm). Detectors for forward scatter, side scatter, yellow fluorescence (565 to 595 nm) and red fluorescence (>664 nm) were used to detect populations of cells, colonies and non-algal particles. Scans were triggered by scatter and fluorescence detectors to ensure accurate detection of all optically important particles within cultures. Detector gain and trigger levels were consistent for all measurements and set to ensure accurate detection of particles as small as ~2.5 μm. Cell, colony, and non-algal particle populations were discriminated by gating based on their length and maximum chlorophyll fluorescence. The total light scattered by particles was determined by integrating forward and sideward light scatter scans for each particle. The relative percentage of light scatter was determined by dividing total light scatter for each particle type by the total light scattered by all particles in a sample. Similarly, the total chlorophyll fluorescence of cells or colonies was determined by integrating red fluorescence scans. Mean chlorophyll fluorescence was calculated for all cells or colonies analyzed in each tank. Mean chlorophyll fluorescence for each species was calculated as the mean of mean values for all replicate tanks.

Optical Measurements

The a_{ph} and b_{ph} coefficients of each culture were determined with a WET Labs ac-s hyperspectral absorption and attenuation meter used in a bench-top mode. The ac-s

measures absorption and attenuation coefficients at >80 wavelengths between 400 and 730 nm. Absorption is measured in a reflective flow tube designed to capture most scattered light. A correction is made for light scattered in the backward direction. The instrument was mounted vertically and fitted with blacked-out tubing attached to the inlet and outlet ports of each flow cell. Measurements were conducted within the walk-in incubator chamber at the ambient culture temperature (15°C) to minimize errors induced by changes in sample temperature during measurements. For each of 3 replicate sub-samples, flow cells and attached tubing were filled with approximately 200 mL of culture. Samples were gently agitated during measurements to avoid particle settling by raising and lowering the inlet tube. For each measurement, 60 seconds of data acquired at a rate of 4 Hz was recorded for each sub-sample and subsequently averaged. Mean values for each tank were calculated as the mean of these averaged sub-sample measurements.

Total absorption (a_t) and attenuation (c_t) were measured using unfiltered culture containing both particulate and dissolved components. Absorption by dissolved substances (a_g) was determined by measuring a ~600 mL sub-sample of culture filtered through a 0.2 μm pore size filter. Further size fractionation was used to partition total absorption and attenuation into non-algal and phytoplankton specific parameters. Cells or colonies of all species except *T. amphioxeia* were separated from non-algal particulate material in cultures by gentle reverse filtration through 10 (for *A. sanguinea* only) or 20 μm size Nitex mesh. Optical data were corrected for the effects of temperature and salinity according to the methods of Twardowski et al. (1999) and Sullivan et al. (2006). Particulate IOPs (a_p & c_p) were determined by subtracting a_g

from a_t and c_t. Scattering errors in a_p due to scatter in the backward direction were corrected for using the proportional algorithm of Zaneveld et al. (1994). The scattering coefficient (b_p) was computed for each tank by difference according to $b_p = c_p - a_p$. Measurements of a_p and b_p for Nitex mesh filtered samples were subtracted from particulate IOPs to obtain a_{ph} and b_{ph} of cells and colonies in each tank during exponential growth. For settled cultures, non-algal particles larger than the Nitex mesh screen size could not be physically separated from cells and colonies and were therefore included in measurements of a_p and b_p. The abundance of this large non-algal particulate material was also quantified by flow cytometry.

Data Analysis

To compare absorption and scattering spectra among species while accounting for cell or colony density and projected area, we computed the mean absorption and scattering efficiencies (Q_a and Q_b) for each replicate tank according to:

$$Q_a(\lambda) = \frac{a_{ph}(\lambda)}{N\sigma} \qquad Q_b(\lambda) = \frac{b_{ph}(\lambda)}{N\sigma}$$

Where λ represents wavelength, N represents cell or colony concentration in number m^{-3} and σ represents their mean projected area in m^2 (Morel & Bricaud 1986). N and σ for all particles larger than the Nitex mesh screen size were determined by automated image analysis with the FlowCAM. Q_a and Q_b describe the proportion of light absorbed or scattered by particles relative to their total projected area, and are functions of particle size, shape and complex refractive index. Values of Q_a can range from 0 to 1 with a value of 1 indicating all light intercepted by the particle is absorbed. Values of Q_b can be larger than 1 due to interference effects, especially for particles near visible wavelengths in size. For comparison with measured values, Q_a and Q_b

were modeled according to Mie theory using the computer code of Bohren and Huffman (1998). Q_a was modeled over a range of imaginary parts of the complex refractive index for 10 µm diameter homogeneous spheres with a real part of the refractive index equal to 1.045 (Ackleson & Spinrad 1988, Stramski & Reynolds 1993, Aas 1996, Green et al. 2003). Q_b was modeled for spheres up to 250 µm in diameter with a complex refractive index of 1.045-0.001i.

We used the mean total chlorophyll fluorescence of cells or colonies measured with the flow cytometer and normalized by total projected area to determine a relative measure of intracellular pigment concentration (C_i) for each replicate. The ratio of phytoplankton specific scattering to absorption (b_{ph}:a_{ph}) was computed for each replicate using b_{ph} at 555 nm and a_{ph} at 676 nm to minimize the impact of absorption by non-algal particles. Non-algal particulate absorption decreases exponentially with increasing wavelength (Kishino et al. 1984, Roesler et al. 1989) and should, therefore, have minimal impact on absorption measurements at the long wavelength chlorophyll absorption peak (676 nm). The b_{ph}:a_{ph} ratio is related to the carbon:chlorophyll ratio of cells (Stramski & Reynolds 1993) and is therefore indicative of changes in cellular composition. This parameter may also vary with Q_b among particles of different size and shape.

The shape of phytoplankton absorption spectra varies significantly with intracellular pigment content and cell size especially between 450 and 550 nm (Kirk 1975, Hoepffner & Sathyendranath 1991, Johnsen et al. 1994, Ciotti et al. 2002). To quantify this variation among cultures we used the negative normalized slope of a_p between 488 and 532 nm calculated for each replicate according to Eisner et al. (2003)

as:

$$a_{ph}\ \text{slope} = -\frac{a_{ph}488 - a_{ph}532}{a_{ph}\ 676(488 - 532)}$$

Higher values of this parameter correspond to steeper slopes which are associated with weak package effects (Duysens 1956, Das 1967) and higher ratios of photoprotective to photosynthetic carotenoids (Eisner et al. 2003). Differences in pigment content, b_{ph}:a_{ph} and a_{ph} slope among species were tested with a Kruskall-Wallis nonparametric analysis of variance (Kruskal & Wallis 1952) and multiple comparisons using the Tukey-Kramer method (Tukey 1953, Kramer 1956). Differences in b_{ph}:a_{ph} and a_{ph} slope between cultures in exponential growth phase and after settling were tested with a Wilcoxon rank sum test (Wilcoxon 1945). Statistical tests were performed with the MATLAB statistics toolbox (version 7.14.0.739, the MathWorks, Inc.).

RESULTS

Cultured species differed considerably in their morphological characteristics (Table 1, Fig. 1). The mean projected area of cells or colonies of different species ranged over three orders of magnitude from 26.9±5.1 μm^2 for *T. amphioxeia* to 36073±9368 μm^2 for *C. eibenii* (Table 1). Flagellates (*T. amphioxeia* and *A. sanguinea*) had relatively simple shapes, *Haslea* sp. was fusiform and highly elongate, and colonial diatoms had more complicated structures with numerous siliceous setae (Fig. 1). *C. socialis* formed hollow, spherical super colonies composed of multiple chains of cells. The thick, hollow setae of *C. eibenii* (subgenus *Phaeoceros*) contained numerous chloroplasts while the thin, hair-like setae of *C. socialis* (subgenus *Hyalochaete*) did not. Portions of diatom cells that did not contain pigments were not

detected by image analysis due to their low contrast in FlowCAM images. The thin ends of *Haslea* sp. cells, the setae of *C. socialis*, and some setae of *C. eibenii* in particular did not exceed threshold levels used to segment images (Fig. 1). As a result, measurements of projected area for these species accurately represent the photosynthetically active portions of cells but slightly underestimate their total area.

Measurements made during exponential growth were used to compute mean Q_a and Q_b spectra for each species (Fig. 2). Q_a was highest for *A. sanguinea* followed by *T. amphioxeia*, *C. socialis*, *C. eibenii*, and *Haslea sp*. Values for *A. sanguinea* were likely overestimated and were larger than 1 at wavelengths shorter than ~500 nm due to the presence of non-algal particles not accurately accounted for by automated image analysis. The Q_a spectrum for *T. amphioxeia* shows enhanced absorption at ~560 nm due to the photosynthetic accessory pigment phycoerythrin. The absorption efficiency of diatoms was lower than that of flagellates throughout most of the spectrum, except for *C. socialis* which was similar to *T. amphioxeia* at the long wavelength chlorophyll absorption peak (~676 nm). The Q_b spectrum was highest for *T. amphioxeia* followed by *A. sanguinea*, *C. socialis*, *C. eibenii*, and *Haslea sp*. The shape of Q_b spectra for *Haslea* sp. and *C. eibenii* was flatter than for other species. As for Q_a, the Q_b spectrum for *A. sanguinea* was likely overestimated due to the presence of non-algal particles not detected in FlowCAM images.

The b_{ph}:a_{ph} ratio varied significantly among species (Kruskal-Wallis test, p = 0.00017, H = 19.98, df = 3) during exponential growth but was not correlated with particle area or C_i (Fig. 3, Table 1). Values of b_{ph}:a_{ph} were highest for *T. amphioxeia* (6.73±0.34), the species with the smallest projected area per particle. This value was

significantly higher than b_{ph}:a_{ph} for *Haslea* sp., *A. sanguinea*, and *C. socialis* ($p < 0.05$). Values of b_{ph}:a_{ph} were also relatively high for *C. eibenii* (5.38±0.18), the species that formed colonies with the largest projected area per particle. The b_{ph}:a_{ph} ratio for *C. eibenii* was significantly higher than that of *A. sanguinea* ($p < 0.05$) but not significantly different from other species. Variation of the b_{ph}:a_{ph} ratio among *Haslea* sp., *A. sanguinea*, and *C. socialis* was noticeable but not significant ($p > 0.05$).

The normalized slope of a_{ph} between 488 and 532 nm varied significantly among species (Kruskal-Wallis test, $p = 0.011$, H = 11.13, df = 3) and was not correlated with particle size or C_i (Table 1, Fig. 3). *A. sanguinea* had the highest a_{ph} slopes (0.0146±0.002). Values were significantly higher than the a_{ph} slopes for *T. amphioxeia*, *C. socialis* and *C. eibenii* ($p < 0.05$, Fig. 3, Table 1). *Haslea* sp. also had a relatively high a_{ph} slope (0.0108±0.0014) although values were not significantly different from other species ($p > 0.05$, Fig. 3, Table 1). Values of a_{ph} slope for *T. amphioxeia*, *C. socialis*, and *C. eibenii* during exponential growth were all similar (~0.008) and not significantly different (Fig. 3, Table 1).

The mean relative chlorophyll content of cells or colonies (C_i) also varied significantly among species during exponential growth (Kruskal-Wallis test, $p = 0.001$, H = 16.23, df = 3) but was not correlated with cell or colony area (Table 1, Fig. 3). *Haslea* sp. had the lowest C_i values while *A. sanguinea* had the highest (Fig. 3). C_i for *Haslea* sp. was significantly lower than values measured for *T. amphioxeia* and *A. sanguinea* ($p < 0.05$). C_i values for *C. eibenii* were also significantly lower than values for *A. sanguinea* ($p < 0.05$). Values of C_i for *C. socialis* were not significantly different from other species.

During exponential growth, Q_a at 676 nm increased with the intracellular pigment concentration of cells (Fig. 4). Estimates of Q_a for *A. sanguinea* are not shown due to interference from non-algal particles. These values were similar to modeled Q_a values for 10 µm spheres with imaginary parts of the complex refractive index ranging from 0.0001 to ~0.003. Q_b at 555 nm was highest for *T. amphioxeia* and lowest for *Haslea* sp. (Fig. 4). Values are shown for projected areas converted to an area equivalent spherical diameter. Measured values of Q_b for *T. amphioxeia*, *C. socialis*, and *C. eibenii* were similar to modeled values for spheres ranging in diameter from 1 to 250 µm. Measured Q_b values for *Haslea* sp. were much lower than modeled Q_b for spheres with equivalent spherical diameter (see Discussion section). As for Q_a, Q_b for *A. sanguinea* could not be reliably calculated due to the presence of non-algal particles and is not shown.

After 8 to 45 days of growth, depending on species, most cells and colonies had settled to the bottom of tanks and visibly changed in appearance and color. These changes were generally associated with increases in b_{ph}:a_{ph} ratios and a_{ph} slopes (Table 1, Fig. 5). *T. amphioxeia* had the largest increase and the highest values of b_{ph}:a_{ph} after settling (23.8). The b_{ph}:a_{ph} ratio for *Haslea* sp., *A. sanguinea*, and *C. socialis* also increased while b_{ph}:a_{ph} for *C. eibenii* decreased. Changes in b_{ph}:a_{ph} were significant for *T. amphioxeia* (p = 0.0095, rank sum = 34), *Haslea* sp. (p = 0.035, rank sum = 32), *C. socialis* (p = 0.019, rank sum = 33), and *C. eibenii* (p = 0.0095, rank sum = 10). *T amphioxeia* also had the largest increase in a_{ph} slope. The a_{ph} slopes for *A. sanguinea* changed little over time while a_{ph} slopes for *Haslea* sp., *C. socialis* and *C. eibenii* increased. Increases in a_{ph} slope were significant for *T. amphioxeia* (p = 0.0095, rank

sum = 34), *C. socialis* (0.0095, rank sum = 34), and *C. eibenii* (p = 0.019, rank sum = 33). For *T. amphioxeia*, changes in optical properties were likely influenced by very small non-algal particles (e.g. bacteria and detritus) that could not be separated from cells by filtration.

Scanning flow cytometry was used to determine the particulate composition of cultures based on the relative contribution of algal and non-algal particles to total light scatter (Figs. 6 & 7). For *T. amphioxeia* cultures during exponential growth, light scatter measured for all particles larger than the detection limit (~2.5 µm) was dominated by cells (Fig. 6). For *Haslea* sp. and *C. socialis* cultures, light scatter by particles larger than 20 µm was dominated by cells or colonies (Fig. 6). For *C. eibenii* cultures, light scatter by particles larger than 20 µm was dominated by colonies and detached setae (Fig. 6). The projected area of detached setae measured by the FlowCAM was included in calculations of Q_a and Q_b. During exponential growth, non-algal particles generally accounted for less than 5% of the total light scattered by particulate material in all cultures except *A. sanguinea*. In *A. sanguinea* cultures, both cells and non-algal particulate material made substantial contributions to total light scattered by particles larger than the nitex mesh screen size (10 µm). This large non-algal particulate material appeared to consist of aggregated transparent exopolymeric compounds excreted by cells (Passow 2002).

After settling, large non-algal particles were abundant in all cultures except *C. socialis*. These particles made significant contributions to total light scatter as measured by the flow cytometer (Fig. 7). Light microscopy suggested that large non-algal particles were primarily composed of dead cells or colony fragments, aggregates

of cell debris, and excreted exopolymeric compounds. For *T. amphioxeia*, very small non-algal particles less than ~10 µm were responsible for the majority of light scatter. These small particles likely included heterotrophic bacteria. For *Haslea* sp. and *A. sanguinea*, many non-algal particles were larger than healthy cells (Fig. 7). After settling, light scatter by particles larger than 20 µm in *C. socialis* cultures continued to be dominated by algal particles. However, colonies were reduced in size and smaller colony fragments with low chlorophyll fluorescence were abundant.

DISCUSSION

The species examined in this study varied considerably in their morphological (Fig. 1), physiological and, consequently, their optical properties (Table 1, Figs. 2 & 3). Flow cytometry showed that the composition of the large size fraction for all cultures except *A. sanguinea* was overwhelmingly dominated by algal cells or colonies (Fig. 6). For *T. amphioxeia*, *Haslea* sp., *C. socialis*, and *C. eibenii* cultures, therefore, size fractionated optical measurements of a_{ph}, b_{ph}, Q_a, and Q_b can be reliably attributed to algal particles. Absorption and scattering efficiency factors (Q_a and Q_b) represent optical characteristics of species dependent on the morphology and physiology of cells and colonies. Unlike most previous studies (Bricaud et al. 1988, Agusti 1991, Green et al. 2003, Zhou et al. 2012), automated image analysis was used to measure the projected area of cells or colonies and determine Q_a and Q_b. Using this method, particles were not assumed to be spherical and the optical properties of large phytoplankton with complex shape were more accurately determined.

Differences in Q_a among cells and colonies may influence photosynthesis, growth rates, and competition for light within natural phytoplankton communities. Q_a for

species tested here did not follow simple relationships with respect to cell or colony size. Rather, absorption efficiency was primarily a function of intracellular pigment concentrations (Fig. 4). While high C_i and Q_a ensure most of the light intercepted by cells is absorbed, this also results in a strong pigment packaging effect and a reduction in light absorbed per unit pigment (Duysens 1956, Das et al. 1967, Kirk 1975). This package effect alters the allometric scaling of metabolic rates and can result in lower growth rates for large cells when intracellular pigment concentrations are high (Finkel & Irwin 2000, Finkel 2001). Small cell size or low C_i, therefore, is advantageous in low light environments such as deep chlorophyll maxima or in turbid coastal waters.

C_i and Q_a were highest for the dinoflagellate *A. sanguinea* (Fig. 2). This is consistent with microscopic observations of large cells containing many chloroplasts. However, the presence of large non-algal particles in cultures interfered with measurements of a_{ph} for this species and Q_a and Q_b are, therefore, overestimated by an unknown amount. Since absorption by non-algal particulate material generally decreases exponentially with increasing wavelength (Kishino et al. 1984, Roesler et al. 1989), Q_a values should be more accurate at long wavelengths (e.g. 676 nm). Non-algal material was most likely aggregated exopolymeric compounds excreted by cells (Passow 2002). Interestingly, these results demonstrate that excreted exopolymeric compounds may be an optically important component of *A. sanguinea* blooms in the ocean. In Monterey Bay, CA these blooms have been associated with copious excreted material (Rines et al. 2010) and have been implicated in the death of sea birds through production of proteinaceous surfactants that damage feather waterproofing (Jessup et al. 2009). Despite problems with measurement of a_{ph} and Q_a, estimates of C_i suggest a

strong package effect for this species. As a motile cell, however, *A. sanguinea* may be able to reduce package effects by continually changing its orientation relative to incident light and by swimming to surface waters where light intensities are higher (Kamykowski et al. 1998). In fact, diurnal vertical migratory behavior that may mitigate package effects is commonly observed for this species (Kiefer & Lasker, 1975, Cullen & Horrigan 1981, Rines et al. 2010).

In contrast to *A. sanguinea*, C_i for *T. amphioxeia*, *Haslea* sp., *C. socialis*, and *C. eibenii* were considerably lower (Fig. 3). Q_a for these species increased with increasing C_i regardless of cell or colony projected area (Fig. 4). Although the diatoms *C. socialis* and *C. eibenii* formed large colonies, lower C_i for these species also resulted in low Q_a which should minimize pigment package effects that could limit growth rates. The long thin morphology of *Haslea* sp. cells and the colony structure of *C. socialis* and *C. eibenii* may also have contributed to low absorption efficiency by minimizing optical path lengths through cells and reducing self-shading of pigments. For *Haslea* sp., path length would depend on cellular orientation relative to incident light, but in many cases would be similar to cell width (~10 μm). For *C. socialis*, although the total colony area is large, the path length through which light passed over this area was generally only 10 – 30 μm, or the depth of one or two cells, due to the arrangement of cells in the colony (Fig. 1). For *C. eibenii*, optical path length through colonies depended on orientation relative to incident light for the central chain of cells, but for many orientations nearly perpendicular to incident light, optical path lengths were the depth of a single cell (~30 – 40 μm). In addition, a substantial amount of photosynthetic pigment was located within thin, hollow setae (Fig. 1). Setae were less

than ~5 μm thick and extended several hundred micrometers from cell corners. These morphological features should greatly reduce self-shading for chloroplasts within setae and decrease the overall Q_a of colonies leading to more efficient light absorption and photosynthesis. As a result, *C. eibenii* in particular seems well adapted to low light environments despite its exceptionally large size. For similar species in the sub-genus *Phaeoceros*, all of which have setae containing chloroplasts, the amount of light necessary to saturate photosynthesis is several times lower than for most other coastal diatoms (Harrison et al. 1993). *Phaeoceros* can also move chloroplasts within setae and has been observed to move chloroplasts towards the base of setae under high light intensities (Pickett-Heaps et al. 1994). In doing so, a colony may change its effective projected area, C_i, Q_a, and ultimately its capacity for photosynthesis and growth in order to adapt to different light environments. The low C_i and Q_a values found for large colonial forms in the present study suggest that the complex morphology of these species helps minimize pigment package effects and may increase fitness with respect to light acquisition.

Despite very different particle morphologies, scattering efficiencies at 555 nm for *T. amphioxeia*, *C. socialis*, and *C. eibenii* decreased with increasing cell or colony projected area similar to modeled values for spheres with a complex refractive index of 1.045-0.001i (Fig. 4). Particle shape or structure, therefore, seems to have little impact on scattering efficiencies for these species. Alternatively, the various components of colonies (e.g. valve, organelles, setae) combine to produce a mean particle Q_b that is closely approximated by Mie theory. Q_b values for *C. socialis* may be slightly overestimated since setae were not resolved in FlowCAM images and were,

therefore, not included in measurements of projected area. Setae for this species, however, are <1 μm thick (thinner than *C. eibenii* setae) and should, therefore, be very inefficient at scattering light as evidenced by their low contrast in acquired images. *Haslea* sp. had much lower values of Q_b than would be expected from Mie theory based on their projected area. This discrepancy could be the result of measurement error caused by alignment of cells within the ac-9 or FlowCAM flow cells. Despite efforts to agitate cells during optical measurements, alignment of cells parallel to the incident irradiance during optical measurements could have resulted in the minimum possible projected areas and underestimation of b_{ph} and Q_b. Perhaps more likely, due to flow induced shear fields, alignment of cells perpendicular to the camera within the FlowCAM flow cell could have resulted in overestimation of projected areas and underestimation of Q_b. If deviations from Mie theory are in fact the result of cell alignment, our results suggest that cellular orientation of elongate species may have a significant impact on scattering by natural populations in ocean waters. Orientation of phytoplankton cells and colonies has been observed for natural populations through the use of in situ holographic imaging techniques (Malkiel et al. 1999, Talapatra et al. 2013). Measurements of Q_a and Q_b in the present study are within the range of other published values, which generally report Q_a at ~676 nm between 0.1 and 0.5, and Q_b at ~555 nm between 1.2 and 2.8 for nano- and microphytoplankton size cells (Bricaud et al. 1988, Iturriaga & Siegel 1989, Agusti 1991, Stramski & Reynolds 1993, Zhou et al. 2012). Much of the variation of Q_a and Q_b within species observed here (Fig. 4) may be attributable to physiological variation among replicate tanks analyzed at different times. Measurements were generally conducted during the day over the

course of ~8 hours, and changes in cellular composition within this time period could account for much of the observed variation within species (Stramski & Reynolds 1993). However, there was no indication in flow cytometry data or by microscopy that cell division was synchronous or in phase with light:dark cycles for any of our cultures.

Within the context of optical theory, the capacity of a particle to absorb light is described by the imaginary part of its complex refractive index. This parameter in combination with the real part of the refractive index and particle size determine Q_a, which can be exactly calculated for a sphere by applying Mie theory (Bohren & Huffman 1998). Modeled Q_a values for 20 μm diameter spheres that were similar to measured values had imaginary refractive indexes (*n'*) generally below 0.002, and an *n'* of 0.001 produced a rate of decrease in Q_b with increasing size that closely matched measured values. This suggests lower *n'* for species studied here compared to other published values in the range of 0.003 to 0.01 (Stramski & Reynolds 1993, Green et al. 2003, Zhou et al. 2012) and is further evidence that large phytoplankton minimize package effects by maintaining low C_i.

Scattering to absorption ratios (b_{ph}:a_{ph}) for each species appeared to be determined by both projected area and C_i. In the case of *T. amphioxeia*, b_{ph}:a_{ph} was likely high due to the high Q_b for this species. Alternatively, the relatively high b_{ph}:a_{ph} for *C. eibenii* was most likely due to the low C_i for this species. *A. sanguinea* had the lowest b_{ph}:a_{ph} ratios as would be expected from its high C_i, although overestimation of a_{ph} due to non-algal particles may have influenced values for this species. Stramski & Reynolds (1993) showed carbon and chlorophyll content of *Thalassiosira pseudonana*

influence b_{ph}:a_{ph} ratios over a similar range as measured here. This ratio, therefore is an indicator of both morphological and physiological characteristics of phytoplankton. The difference in b_{ph}:a_{ph} ratios among species during exponential growth determined here can account for ~25 – 30% of the variability measured in the coastal ocean where values have been measured up to ~20, although at different wavelengths in some cases (Sosik et al. 2001, McFarland et al. in prep. a & b).

The normalized a_{ph} slope can be determined by ratios of photoprotective to photosynthetic carotenoids (PPC:PSC) within cells or by pigment package effects that can flatten absorption spectra (Eisner et al. 2003). PPC:PSC ratios reflect the adaptation of cells to different light levels. In this study, a_{ph} slope was highest for *A. sanguinea* most likely due to absorption by non-algal particulate material. Only *Haslea* sp. showed elevated a_{ph} slopes that could be attributed to pigment ratios, although differences could not be considered significant by multiple comparison tests. Differences were significant ($p < 0.05$), however, if *A. sanguinea* was omitted from the analysis. *T. amphioxeia*, *C.socialis*, and *C. eibenii* all had similar a_{ph} slopes indicative of PPC:PSC ratios less than 0.25 (Eisner et al. 2003). These values are low compared to in situ measurements of a_{ph} slope for natural phytoplankton communities (Eisner & Cowles 2005, McFarland et al. in prep. a & b) possibly due to the relatively low light intensities under which cultures were grown. However, a_{ph} slopes for *Haslea* sp. suggests that species-specific differences may be important and a_{ph} slopes measured for natural communities may vary with species composition as well as light adaptation. The low a_{ph} slope of *T. amphioxeia* is somewhat surprising given its unique pigment composition, including sufficient phycoerythrin to visibly affect the

color of cultures. For this species, weak package effects which might increase a_{ph} slope may be counteracted by enhanced phycoerythrin absorption at 532 nm which would decrease a_{ph} slope.

Increases in b_{ph}:a_{ph} and a_{ph} slope for *T. amphioxeia*, *Haslea* sp., *A. sanguinea*, and *C. eibenii* after cultures settled (Fig. 5) were likely due to the increase in abundance of non-algal particles (Fig. 7). Non-algal particles generally have decreasing absorption with increasing wavelength (Kishino et al. 1984, Roesler 1989) and an increase in their relative abundance would increase b_{ph}:a_{ph} and a_{ph} slopes. However, b_{ph}:a_{ph} and a_{ph} slope also increased for *C. socialis* despite a negligible contribution of non-algal particulate material to total light scatter in settled cultures (Fig. 7). This suggests physiological changes in phytoplankton particle characteristics, possibly associated with abundant colony fragments in the case of *C. socialis*, can also be important in determining b_{ph}:a_{ph} and a_{ph} slope. Increases were greatest for *T. amphioxeia* and values for settled cultures exceeded maximum values measured for natural communities (Sosik 2001, Eisner & Cowles 2005, McFarland et al. in prep. a & b). Increases for other species were more modest and covered only a portion of the range seen for in situ measurements. Since *T. amphioxeia* cultures were not size fractionated, this suggests much of the variation in b_{ph}:a_{ph} and a_{ph} slope in natural communities may be associated with the relative abundance of small non-algal particulate material. Unlike other species, the b_{ph}:a_{ph} ratio for *C. eibenii* increased after cultures settled. This incongruous result may reflect changes in the contribution of setae to b_{ph}. Setae appeared to lose much of their chlorophyll after cultures settled and, devoid of

chloroplasts, their refractive index and scattering efficiency may have been greatly reduced.

As a whole, results demonstrate that differences among species and changes associated with senescence are both important to the optical properties of phytoplankton and the IOPs of ocean waters. The distribution of chlorophyll within colonies and low C_i of large colonial forms suggest that these species are morphologically and physiologically adapted to minimize pigment package effects that would otherwise limit light absorption, photosynthesis and growth (Raven 1984, 1986, 1998). Although disadvantageous for efficient light absorption due to the package effect, large size can protect species from grazers (Tillman 2004 and references therein) and facilitate interaction with small scale turbulence to promote nutrient uptake (Margalef 1978, Karp-Boss et al. 1996). In the natural environment, the bio-optical characteristics of phytoplankton are one of many factors that determine growth rates of species and community structure. Variation in light intensity or spectral distribution in combination with turbulent mixing can create optical niches which favor certain forms over others and provide opportunities for differentiation and coexistence of functionally distinct species (Margalef 1978). This variable optical niche structure coupled with the distinct bio-optical properties of species represents a possible solution to Hutchinson's classic "paradox of the plankton" (Hutchinson 1961, Huisman & Weissing 1999, Huisman et al. 2001).

In natural phytoplankton communities, measurements of particulate absorption and scattering will reflect the combined characteristics of all suspended particulate material. Results of this study, however, indicate that cell or colony size and

physiology can be important factors that determine ocean water IOPs. Particulate absorption and scattering can be measured in the ocean with centimeter scale spatial resolution and second scale temporal resolution (Cowles et al. 1998, Rines et al. 2002, McManus et al. 2003, Holliday et al. 2003, Babin et al. 2005). Optical measurements therefore can resolve patterns of variability in natural phytoplankton communities at scales critical to population dynamics and ecosystem structure. Although the FlowCAM instrument used here is limited to analysis of discrete samples, determination of cell and colony projected areas in situ are possible with techniques such as digital in-line holography (Talapatra et al. 2013). Future field work, therefore, could determine the detailed bio-optical characteristics of natural communities in the ocean to better understand the processes that control marine pelagic ecosystem structure and function. Such a bio-optical trait based approach could provide an improved mechanistic understanding of phytoplankton diversity, distribution, and abundance in the ocean (Litchman & Klausmeier 2008, Edwards et al. 2013).

Acknowledgements

We would like to thank Chris Lane for assistance in identifying *T. amphioxeia*, Susanne Menden-Deuer and Amanda Montalbano for providing the culture of *Akashiwo sanguinea*, and Glen Davis for assistance in building tanks. We thank ONR for their commitment to our research program. This work was supported by ONR grants N000140410275 (JR) and N000140910492 (PD, JR and JS).

REFERENCES

Aas E (1996) Refractive index of phytoplankton derived from its metabolite composition. J Plankton Res 18:2223–2249

Ackleson SG, Spinrad RW (1988) Size and refractive index of individual marine participates: a flow cytometric approach. Appl Opt 27:1270–1277

Agustí S (1991) Allometric scaling of light absorption and scattering by phytoplankton cells. Can J Fish Aquat Sci 48:763–767

Astoreca R, Doxaran D, Ruddick K, Rousseau V, Lancelot C (2012) Influence of suspended particle concentration, composition and size on the variability of inherent optical properties of the Southern North Sea. Cont Shelf Res 35:117–128

Babin M, Cullen JJ, Roesler CS, Donaghay PL, Doucette GJ, Kahru M, Lewis MR, Scholin CA, Sieracki ME, Sosik HM (2005) New approaches and technologies for observing harmful algal blooms. Oceanography 18:210–227

Babin M, Stramski D, Ferrari GM, Claustre H, Bricaud A, Obolensky G, Hoepffner N (2003) Variations in the light absorption coefficients of phytoplankton, nonalgal particles, and dissolved organic matter in coastal waters around Europe. J Geophys Res 108

Bohren CF, Huffman DR (1998) Absorption and Scattering of Light by Small Particles. John Wiley & Sons

Bricaud A, Bédhomme AL, Morel A (1988) Optical properties of diverse phytoplanktonic species: experimental results and theoretical interpretation. J Plankton Res 10:851–873

Bricaud A, Stramski D (1990) Spectral absorption coefficients of living phytoplankton and nonalgal biogenous matter: A comparison between the Peru upwelling area and the Sargasso Sea. Limnol Oceanogr 35:562–582

Churnside JH, Donaghay PL (2009) Thin scattering layers observed by airborne lidar. ICES J Mar Sci 66:778–789

Ciotti AM, Lewis MR, Cullen JJ (2002) Assessment of the relationships between dominant cell size in natural phytoplankton communities and the spectral shape of the absorption coefficient. Limnol Oceanogr 47:404–417

Cowles TJ, Desiderio RA, Carr ME (1998) Small-scale planktonic structure: persistence and trophic consequences. Oceanography 11:4–9

Cullen JJ, Horrigan SG (1981) Effects of nitrate on the diurnal vertical migration, carbon to nitrogen ratio, and the photosynthetic capacity of the dinoflagellate *Gymnodinium splendens*. Mar Biol 62:81–89

Das M, Rabinowitch E, Szalay L, Papageorgiou G (1967) “Sieve-effect” in *Chlorella* suspensions. J Phys Chem 71:3543–3549

Dubelaar GBJ, Geerders PJF, Jonker RR (2004) High frequency monitoring reveals phytoplankton dynamics. J Environ Monitor 6:946

Duysens LNM (1956) The flattening of the absorption spectrum of suspensions, as compared to that of solutions. Biochim Biophys Acta 19:1–12

Edwards KF, Litchman E, Klausmeier CA (2013) Functional traits explain phytoplankton community structure and seasonal dynamics in a marine ecosystem. Ecol Lett 16:56–63

Eisner LB, Cowles TJ (2005) Spatial variations in phytoplankton pigment ratios, optical properties, and environmental gradients in Oregon coast surface waters. J Geophys Res 110

Eisner LB, Twardowski MS, Cowles TJ, Perry MJ (2003) Resolving phytoplankton photoprotective: photosynthetic carotenoid ratios on fine scales using in situ spectral absorption measurements. Limnol Oceanogr 48:632–646

Ferreira A, Stramski D, Garcia CAE, Garcia VMT, Ciotti ÁM, Mendes CRB (2013) Variability in light absorption and scattering of phytoplankton in Patagonian waters: Role of community size structure and pigment composition. J Geophys Res 118:698–714

Finkel ZV (2001) Light absorption and size scaling of light-limited metabolism in marine diatoms. Limnol Oceanogr 46:86–94

Finkel ZV, Irwin AJ (2000) Modeling size-dependent photosynthesis: light absorption and the allometric rule. J Theor Biol 204:61–369

Fogg GE (1991) Tansley review No. 30. The phytoplanktonic ways of life. New Phytol 118:191–232

Gran HH (1912) Pelagic plant life. In: Murray J, Hjort J (eds) The Depths of the Ocean. Macmillan and Co., Limited, p 307–386

Green RE, Sosik HM, Olson RJ, DuRand MD (2003) Flow cytometric determination of size and complex refractive index for marine particles: comparison with independent and bulk estimates. Appl Opt 42:526–541

Guillard RRL, Hargraves PE (1993) *Stichochrysis immobilis* is a diatom, not a chrysophyte. Phycologia 32:234–236

Harrison P, Thompson P, Guo M, Taylor F (1993) Effects of light, temperature and salinity on the growth rate of harmful marine diatoms, *Chaetoceros convolutus* and *C. concavicornis* that kill netpen salmon. J Appl Phycol 5:259–265

Hoepffner N, Sathyendranath S (1991) Effect of pigment composition on absorption properties of phytoplankton. Mar Ecol Prog Ser 73:l–23

Hoepffner N, Sathyendranath S (1992) Bio-optical characteristics of coastal waters: absorption spectra of phytoplankton and pigment distribution in the western North Atlantic. Limnol Oceanogr:1660–1679

Holliday DV, Donaghay PL, Greenlaw CF, McGehee DE, McManus MM, Sullivan JM, Miksis JL (2003) Advances in defining fine- and micro-scale pattern in marine plankton. Aquat Living Resour 16:131–136

Huisman J, Johansson AM, Folmer EO, Weissing FJ (2001) Towards a solution of the plankton paradox: the importance of physiology and life history. Ecol Lett 4:408–411

Huisman J, Jonker RR, Zonneveld C, Weissing FJ (1999) Competition for light between phytoplankton species: experimental tests of mechanistic theory. Ecology 80:211–222

Huisman J, Oostveen P van, Weissing FJ (1999) Species dynamics in phytoplankton blooms: incomplete mixing and competition for light. Am Nat 154:46–68

Huisman J, Sharples J, Stroom JM, Visser PM, Kardinaal WEA, Verspagen JMH, Sommeijer B (2004) Changes in turbulent mixing shift competition for light between phytoplankton species. Ecology 85:2960–2970

Huisman J, Weissing FJ (1999) Biodiversity of plankton by species oscillations and chaos. Nature 402:407–410

Hutchinson GE (1961) The paradox of the plankton. Am Nat 95:137

Iturriaga R, Siegel DA (1989) Microphotometric characterization of phytoplankton and detrital absorption properties in the Sargasso Sea. Limnol Oceanogr:1706–1726

Jessup DA, Miller MA, Ryan JP, Nevins HM, Kerkering HA, Mekebri A, Crane DB, Johnson TA, Kudela RM (2009) Mass stranding of marine birds caused by a surfactant-producing red tide. PLoS ONE 4:e4550

Johnsen G, Samset O, Granskog L, Sakshaug E (1994) In vivo absorption characteristics in 10 classes of bloom-forming phytoplankton: taxonomic characteristics and responses to photoadaptation by means of discriminant and HPLC analysis. Mar Ecol Prog Ser 105:149–157

Karp-Boss L, Boss E, Jumars PA (1996) Nutrient fluxes to planktonic osmotrophs in the presence of fluid motion. Oceanogr Mar Biol 34:71–107

Katz ME, Finkel ZV, Grzebyk D, Knoll A, Falkowski PG (2004) Evolutionary trajectories and biogeochemical impacts of marine eukaryotic phytoplankton. Ann Rev Ecol Evol Syst 35:523–556

Kiefer DA, Lasker R (1975) Two blooms of *Gymnodinium splendens* (Lebour), a large naked dinoflagellate. Fish Bull 73

Kirk JTO (1975) A theoretical analysis of the contribution of algal cells to the attenuation of light within natural waters. I. General treatment of suspensions of pigmented cells. New Phytol 75:11–20

Kirk JTO (1994)Light and Photosynthesis in Aquatic Ecosystems, 2nd ed. Cambridge University Press

Kitchen JC, Zaneveld JRV, Pak H (1982) Effect of particle size distribution and chlorophyll content on beam attenuation spectra. Appl Opt 21:3913–3918

Kramer CY (1956) Extension of multiple range tests to group means with unequal numbers of replications. Biometrics 12:307–310

Kruskal WH, Wallis WA (1952) Use of ranks in one-criterion variance analysis. J Am Stat Assoc 47:583–621

Litchman E (2003) Competition and coexistence of phytoplankton under fluctuating light: Experiments with two cyanobacteria. Aquat Microb Ecol 31:241–248

Litchman E, Klausmeier CA (2008) Trait-based community ecology of phytoplankton. Ann Rev Ecol Evol Syst 39:615–639

Litchman E, Klausmeier CA, Bossard P (2004) Phytoplankton nutrient competition under dynamic light regimes. Limnol Oceanogr 49:1457–1462

Lohrenz SE, Weidemann AD, Tuel M (2003) Phytoplankton spectral absorption as influenced by community size structure and pigment composition. J Plankton Res 25:35–61

Lorenzen CJ (1972) Extinction of light in the ocean by phytoplankton. J Cons Int Explor Mer 34:262–267

Mahalanobis PC (1936) On the generalized distance in statistics. P Natl Inst Sci India 12:49–55

Malkiel E, Alquaddoomi O, Katz J (1999) Measurements of plankton distribution in the ocean using submersible holography. Meas Sci Technol 10:1142–1152

Mann HB, Whitney DR (1947) On a test of whether one of two random variables is stochastically larger than the other. Ann Math Statist 18:50–60

Margalef R (1978) Life-forms of phytoplankton as survival alternatives in an unstable environment. Oceanol Acta 1:493–509

McFarland M, Rines J, Donaghay P, Sullivan J (in prep. a) Optical signatures of marine phytoplankton communities over small scales.

McFarland M, Rines J, Donaghay P, Sullivan J (in prep. b) Variation of marine phytoplankton community size structure and physiology over small scales determined with in situ optical measurements.

McManus MA, Alldredge AL, Barnard AH, Boss E, Case JF, Cowles TJ, Donaghay PL, Eisner LB, Gifford DJ, Greenlaw CF (2003) Characteristics, distribution and persistence of thin layers over a 48 hour period. Mar Ecol Prog Ser 261:1–19

Morel A, Bricaud A (1986) Inherent optical properties of algal cells including picoplankton: Theoretical and experimental results. In: Platt T, Li WKW (eds) Photosynthetic Picoplankton. Department of Fisheries and Oceans, p 521–559

Passow U (2002) Transparent exopolymer particles (TEP) in aquatic environments. Prog Oceanogr 55:287–333

Pickett-Heaps JD, Carpenter J, Koutoulis A (1994) Valve and seta (spine) morphogenesis in the centric diatom *Chaetoceros peruvianus* Brightwell. Protoplasma 181:269–282

Raven JA (1984) A cost-benefit analysis of photon absorption by photosynthetic unicells. New Phytol 98:593–625

Raven JA (1986) Physiological consequences of extremely small size for autotrophic organisms in the sea. In: Platt, T, Li, W K W (eds) Photosynthetic Picoplankton. Department of Fisheries and Oceans, Ottawa, Ontario, Canada, p 1–70

Raven JA, Finkel ZV, Irwin AJ (2005) Picophytoplankton: bottom-up and top-down controls on ecology and evolution. Vie Milieu 55:209–215

Rines JEB, Donaghay PL, Dekshenieks MM, Sullivan JM, Twardowski MS (2002) Thin layers and camouflage: hidden *Pseudo-nitzschia* spp. (Bacillariophyceae) populations in a fjord in the San Juan Islands, Washington, USA. Mar Ecol Prog Ser 225:123–137

Rines JEB, McFarland MN, Donaghay PL, Sullivan JM (2010) Thin layers and species-specific characterization of the phytoplankton community in Monterey Bay, California, USA. Cont Shelf Res 30:66–80

Roesler CS, Perry MJ, Carder KL (1989) Modeling in situ phytoplankton absorption from total absorption spectra in productive inland marine waters. Limnol Oceanogr:1510–1523

Roy S, Blouin F, Jacques A, Therriault J-C (2008) Absorption properties of phytoplankton in the Lower Estuary and Gulf of St. Lawrence (Canada). Can J Fish Aquat Sci 65:1721–1737

Sathyendranath S, Lazzara L, Prieur L (1987) Variations in the spectral values of specific absorption of phytoplankton. Limnol Oceanogr 32:403–415

Sosik HM, Green RE, Pegau WS, Roesler CS (2001) Temporal and vertical variability in optical properties of New England shelf waters during late summer and spring. J Geophys Res 106:9455–9472

Sournia A (1982) Form and function in marine phytoplankton. Biol Rev 57:347–394

Stomp M, Huisman J, Stal LJ, Matthijs HCP (2007) Colorful niches of phototrophic microorganisms shaped by vibrations of the water molecule. The ISME Journal 1:271–282

Stramski D, Bricaud A, Morel A (2001) Modeling the inherent optical properties of the ocean based on the detailed composition of the planktonic community. Appl Opt 40:2929–2945

Stramski D, Reynolds RA (1993) Diel variations in the optical properties of a marine diatom. Limnol Oceanogr 38:1347–1364

Sullivan JM, Twardowski MS, Donaghay PL, Freeman SA (2005) Use of optical scattering to discriminate particle types in coastal waters. Appl Opt 44:1667–1680

Sullivan JM, Twardowski MS, Zaneveld JRV, Moore CM, Barnard AH, Donaghay PL, Rhoades B (2006) Hyperspectral temperature and salt dependencies of absorption by water and heavy water in the 400-750 nm spectral range. Appl Opt 45:5294–5309

Talapatra S, Hong J, McFarland M, Nayak AR, Zhang C, Katz J, Sullivan J, Twardowski M, Rines J, Donaghay P (2013) Characterization of biophysical interactions in the water column using in situ digital holography. Mar Ecol Prog Ser 473:29–51

Tillmann U (2004) Interactions between planktonic microalgae and protozoan grazers 1. J Eukaryot Microbiol 51:156–168

Tukey JW (1953) The Problem of Multiple Comparisons: Introduction and Parts A, B, and C. Princeton University

Twardowski MS, Sullivan JM, Donaghay PL, Zaneveld JRV (1999) Microscale quantification of the absorption by dissolved and particulate material in coastal waters with an ac-9. J Atmos Ocean Tech 16:691–707

Zaneveld JRV, Kitchen JC, Moore CC (1994) Scattering error correction of reflecting-tube absorption meters. In: p 44–55

Zhou W, Wang G, Sun Z, Cao W, Xu Z, Hu S, Zhao J (2012) Variations in the optical scattering properties of phytoplankton cultures. Opt Express 20:11189–11206

TABLES

Table 1. Mean and standard deviation (s.d.) of morphological and optical properties for each species during exponential growth phase and senescence (settled). Mean areas were determined with the FlowCam. Mean lengths were determined with the CytoSense scanning flow cytometer.

		Teleaulax amphioxeia		*Haslea* sp.		*Akashiwo sanguinea*		*Chaetoceros socialis*		*Chaetoceros eibenii*	
		mean	s.d.	mean	s.d.	mean	s.d.	mean	s.d.	mean	s.d.
exponential	area (μm^2)	26.9	5.1	973.5	125.6	1072.4	52.6	4831.5	1674.2	36074	9368
	length (μm)	10.28	1.05	177.2	1.31	48.73	0.898	158.8	14.02	634.2	58.4
	Q_a 676 nm	0.39	0.04	0.12	0.01	0.79	0.11	0.39	0.04	0.21	0.03
	Q_b 555 nm	2.63	0.16	0.47	0.14	2.54	0.94	1.37	0.20	1.14	0.14
	b_{ph}:a_{ph}	6.73	0.34	4.04	0.92	3.14	0.80	3.52	0.41	5.38	0.18
	a_{ph} slope	0.0079	0.0012	0.0108	0.0014	0.0154	0.0010	0.0080	0.0004	0.0083	0.0008
	C_i	44.5	6.9	20.7	6.3	116.6	8.1	36.0	5.8	29.6	3.6
settled	b_{ph}:a_{ph}	23.80	9.58	8.03	3.24	5.01	1.18	6.71	2.27	3.41	0.07
	a_{ph} slope	0.0566	0.0228	0.0154	0.0046	0.0160	0.0031	0.0133	0.0033	0.0102	0.0009

FIGURES

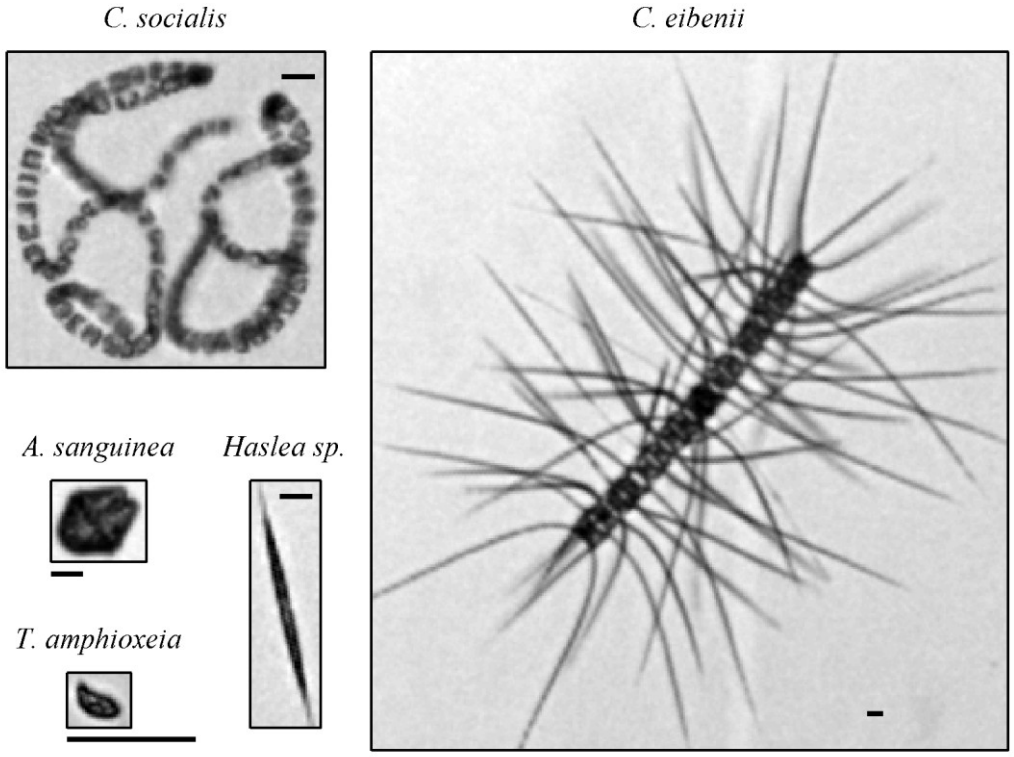

Figure 1. Example images acquired by the FlowCAM particle analyzer for each phytoplankton species. Black scale bars represent 20 µm. *A. sanguinea*, *Haslea* sp. and *C. socialis* are shown at the same scale. Scales for *T. amphioxeia* and *C. eibenii* are different. Note that setae were not resolved for *C. socialis*.

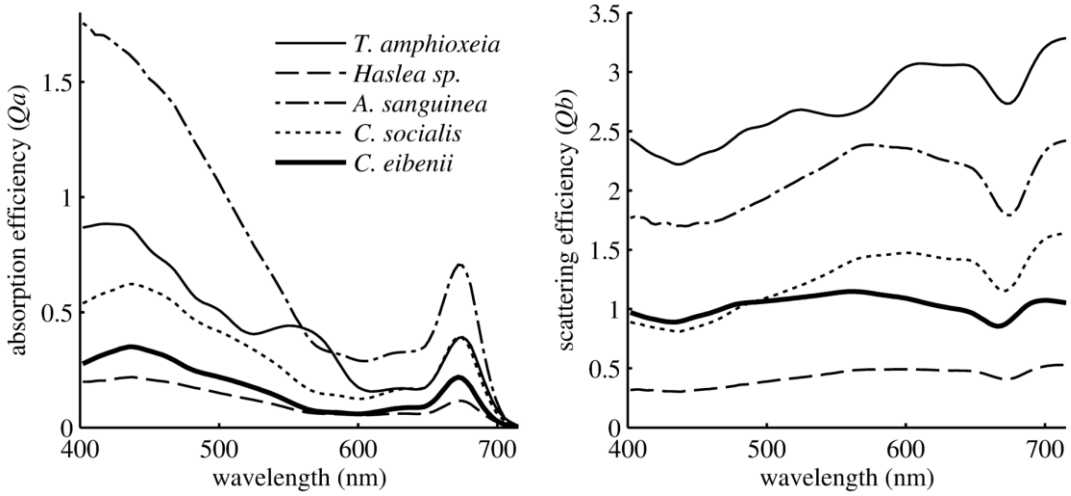

Figure 2. Mean absorption and scattering efficiency for each culture during exponential growth.

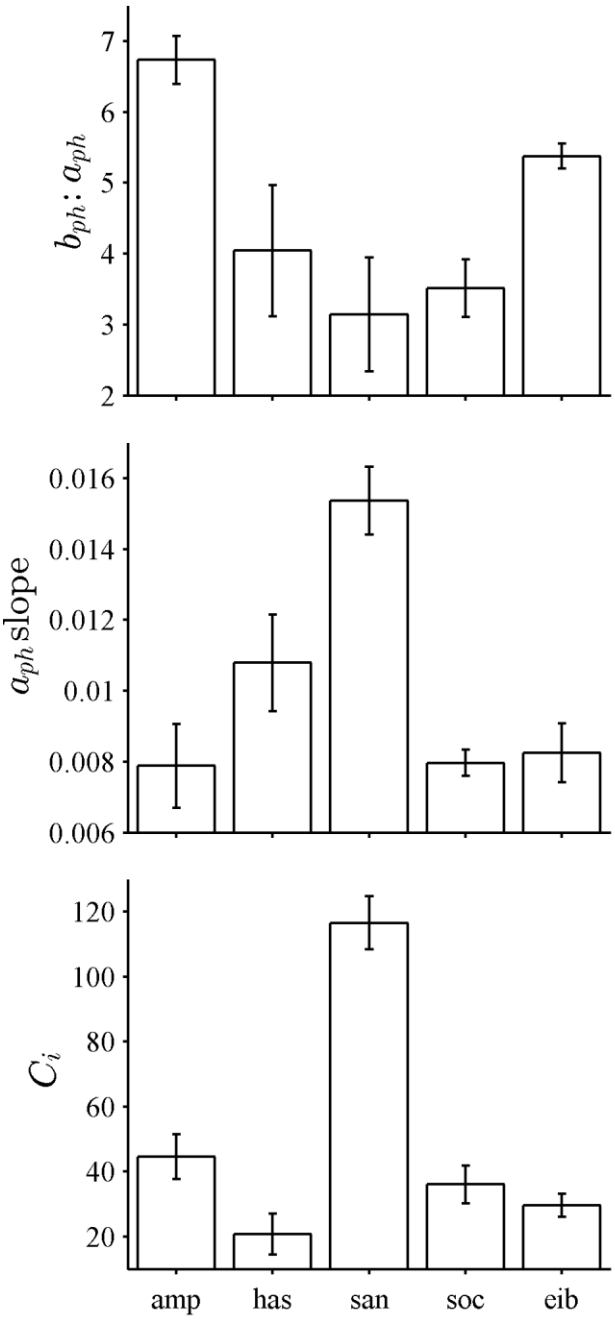

Figure 3. Mean b_{ph}:a_{ph} ratios, a_{ph} slopes, and chlorophyll fluorescence per cell or colony during exponential growth for *T. amphioxeia* (amp), *Haslea* sp. (has), *A. sanguinea* (san), *C. socialis* (soc), and *C. eibenii* (eib). Species are ordered from left to right by increasing projected area (see Table 1).

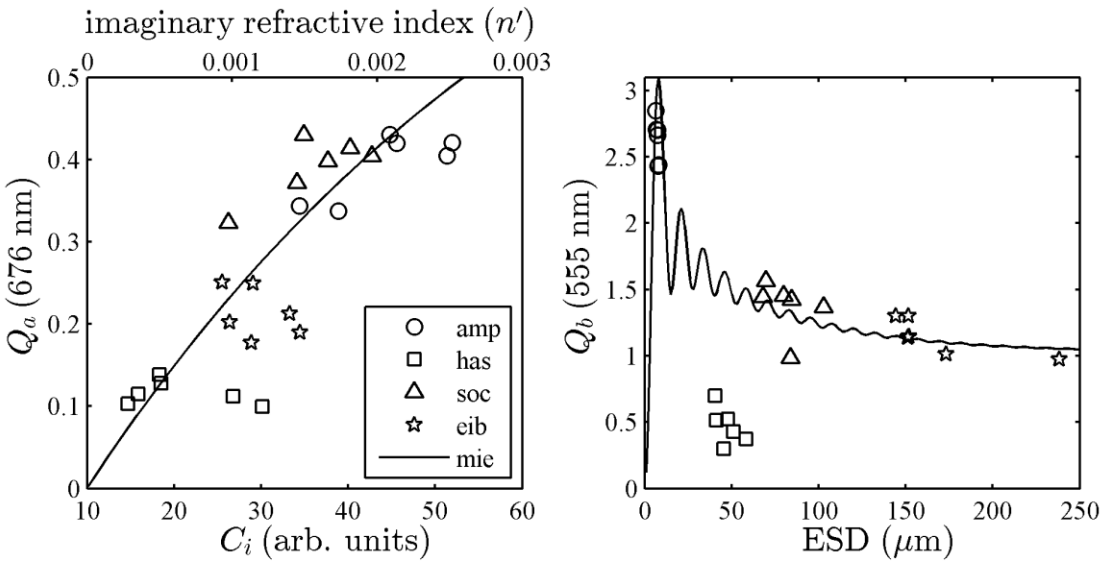

Figure 4. Absorption efficiency at 676 nm of species as a function of intracellular chlorophyll concentrations (C_i) and scattering efficiency at 555 nm of species as a function of area equivalent spherical diameter (ESD). Lines indicate efficiency factors modeled using Mie theory. Modeled Q_a values were computed by varying the imaginary part of the refractive index (n'). Modeled Q_b values were computed by varying the diameter.

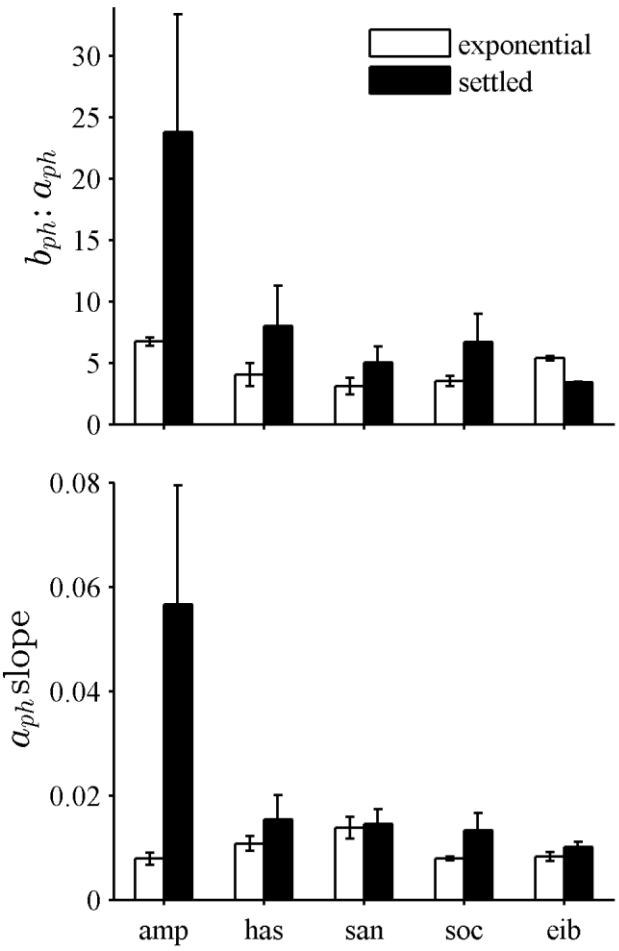

Figure 5. Mean b_{ph}:a_{ph} ratio and a_{ph} slopes during exponential growth and after settling for *T. amphioxeia* (amp), *Haslea* sp. (has), *A. sanguinea* (san), *C. socialis* (soc), and *C. eibenii* (eib).

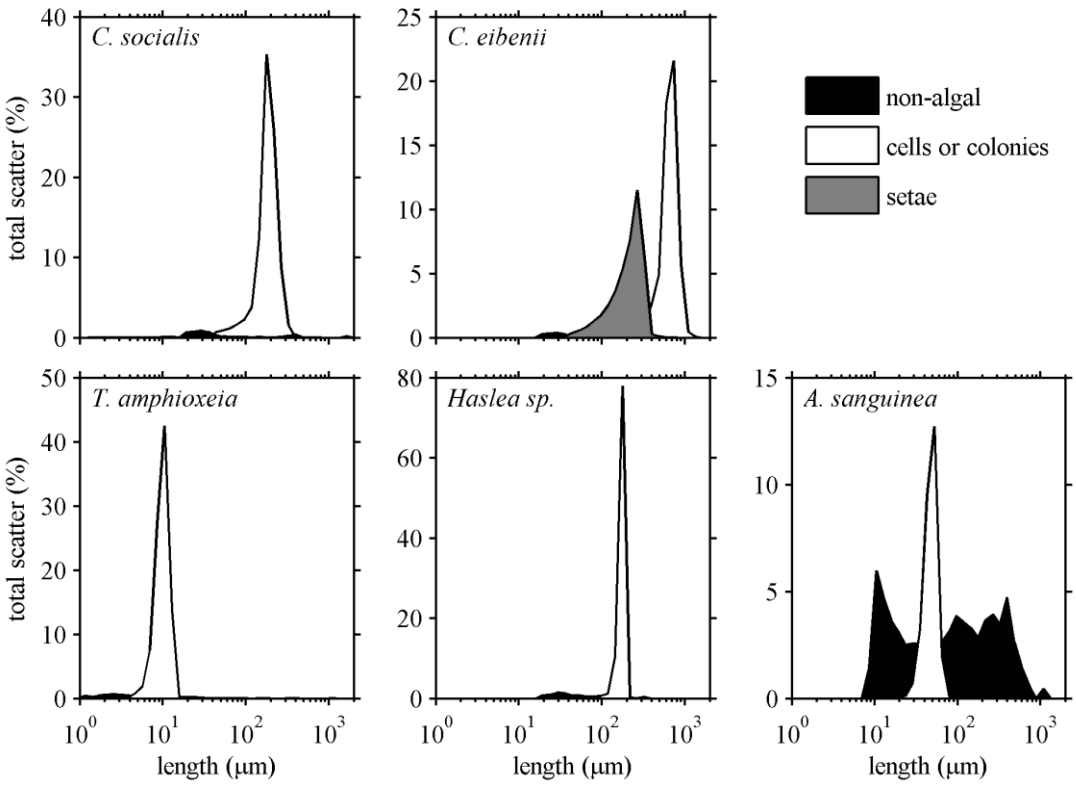

Figure 6. Mean particulate composition of cultures during exponential growth determined by the relative contribution of particle types to total light scatter measured with the scanning flow cytometer. Only particles larger than the Nitex mesh screen size are shown for all species except *T. amphioxeia*.

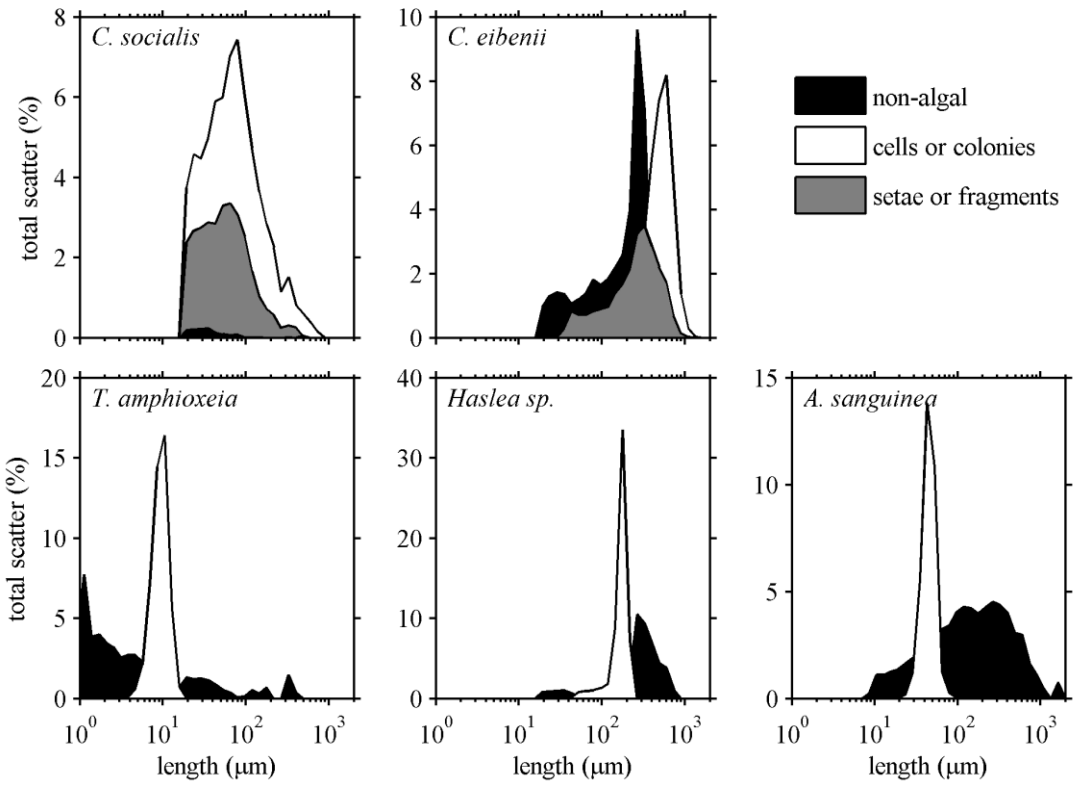

Figure 7. Mean particulate composition of settled cultures determined by the relative contribution of particle types to total light scatter measured with the scanning flow cytometer. Only particles larger than the Nitex mesh screen size are shown for all species except *T. amphioxeia*.

CONCLUSIONS

The fundamental goal of this dissertation was to improve observations of natural phytoplankton communities in the ocean. To achieve this goal, optical methods to determine community structure and bio-optical characteristics of cells and colonies over small spatial and temporal scales were developed and tested. Results show optical parameters that can be measured in situ with high resolution such as the c_p slope, a_p slope, and b_p:a_p ratio can be indicative of phytoplankton cell or colony size and pigment content, characteristics that vary with species composition, physiology, and bio-optical fitness. Non-algal particles such as bacteria, sediments, and exopolymers which may also influence optical properties, varied predominantly with b_b:b ratios. The combination of these optical parameters, which reflect the shape and relative magnitude of particulate absorption and scattering spectra, facilitate analysis of phytoplankton composition and characteristics with high resolution over small scales in the ocean.

The studies conducted here advance techniques necessary to achieve a better understanding of phytoplankton population dynamics, responses to environmental conditions, interactions among species, and impacts on biogeochemical cycles. Optical methods revealed detailed information about the distribution, abundance, morphology and physiology of phytoplankton that can lead to a better understanding of their ecology and the function of diverse forms in the ocean. Such methods provide a dramatic improvement in resolution over discrete sampling techniques and offer a new perspective on the ecology of planktonic organisms. The major findings of the three components of this research are summarized below.

Manuscript 1

The primary goal of this study was to determine the extent to which phytoplankton species composition is correlated with inherent optical properties (IOPs) over small scales in hydrographically complex coastal ocean waters. Although such a correlation does not necessarily imply phytoplankton are responsible for measured optical values, the lack of any correlation would indicate in situ optical data, as measured here, cannot be used to determine community characteristics over small scales. This first study, therefore, established whether further development of optical methods as ecological tools was warranted.

Results show a strong association between distinct phytoplankton communities and the shape and relative magnitude of the particulate absorption (a_p), scattering (b_p), and attenuation (c_p) coefficient spectra. Furthermore, optical properties varied with the morphological and physiological characteristics of species within different communities in agreement with previous theoretical and empirical work. Specifically, the c_p slope decreased with increasing mean cell size and the a_p slope decreased with intracellular pigment concentrations. The b_p:a_p ratio also increased with decreasing cell size or pigment content, although to a lesser degree.

These results confirmed that in situ optical data can relate information about the distribution and composition of phytoplankton communities over small scales in the coastal ocean. Cell size and pigment content appeared to be important cellular characteristics responsible for the bio-optical differentiation of species assemblages. However, this study did not directly measure these cellular characteristics and did not account for suspended non-algal particulate material. The next study, therefore, was

designed to quantify the size and pigment content of cells, colonies, and non-algal particulate material.

Manuscript 2

Based on results of the first study, the primary goal of the second field study was to determine the effects of phytoplankton cell or colony size, pigment content, and non-algal particles on IOPs over small scales in coastal waters. Scanning flow cytometry was used to measure the size distribution and pigment content of phytoplankton and non-algal particles. These data provided a more robust and quantitative method of relating optical properties to the diverse characteristics of phytoplankton species and populations by directly measuring optically important particle features.

Results indicate large (>20 μm) and morphologically variable phytoplankton can dominate optical signals in dense bloom conditions or concentrated thin layers of cells that are common in the coastal ocean. As observed in previous studies, the size and physiological characteristics of phytoplankton varied with the shape and relative magnitude of a_p, b_p, and c_p coefficient spectra. Optical parameters such as the b_p:a_p ratio and a_p slope increased dramatically with the relative abundance of dead and dying cells, identified by their weak chlorophyll fluorescence. The c_p slope increased with the relative abundance of large phytoplankton cells or colonies while the b_b:b ratio increased with the relative abundance of suspended sediment particles. High resolution optical data collected with an autonomous profiler enabled visualization of these phytoplankton community characteristics over centimeter vertical scales and hourly temporal scales.

The strong variation of c_p slope with phytoplankton size distributions demonstrates that optical data can be used to discriminate among communities dominated by species of different size. However, particle morphology and the method of determining particle size may be important since large morphologically complex colonies of *Chaetoceros socialis* had lower than expected c_p slopes. These optically important morphological characteristics may have adaptive significance, and may help certain forms compete for light by increasing light harvesting efficiency. The strong variation of b_p:a_p and a_p slope with the pigment characteristics of phytoplankton demonstrates that optical properties can be used to determine the physiological state of cells and the ecologically important process of mortality in natural communities. The relative abundance and size distribution of non-algal particles such as heterotrophic bacteria and suspended sediments are also important to bulk optical properties and must be taken into account when interpreting in situ measurements. Fortunately, high refractive index non-algal particles such as suspended sediments have a disproportionately strong impact on b_b:b and this parameter, therefore, can serve to indicate when their abundance is optically significant.

High resolution data were effective in visualizing phytoplankton community characteristics and ecological processes over very small scales. This facilitated localization of transitions in phytoplankton community composition and accumulations of senescent cells. In one case, senescent cells were observed to aggregate in a near surface layer while in another case, aggregation of senescent cells was observed along the pycnocline. These observations would not have been possible through the use of discrete sampling techniques.

Results of this study demonstrate the use of in situ optical properties to identify characteristics of natural phytoplankton communities that help explain their function, distribution, abundance and dynamics in the ocean. Measurements were made for whole species assemblages whose natural range of variation is determined by populations of many different particles. To better understand how individual species and their characteristics contribute to this natural variation, a series of laboratory measurements on monospecific cultures were conducted.

Manuscript 3

The goal of this study was to determine variation of optical properties among live and senescent cells of five morphologically distinct species including large complex colonial forms that have not been previously studied yet can dominate optical signals in coastal ocean waters. Results were compared to field measurements to determine the amount of natural variation that could be attributed to either morphological or physiological differences in natural communities. Measured optical properties were also used to better understand the optical function of species specific traits and their effects on bio-optical fitness and adaptation to life in the pelagic environment.

As seen in field studies, variation in the size, shape, and pigment content of species resulted in significant differences in bio-optical properties. The b_p:a_p ratio increased for small cells due to high scattering efficiency (Q_b) and for large colonies due to low absorption efficiencies (Q_a) and intracellular pigment concentrations. Large diatoms had very low Q_a values compared to other published results which may enhance bio-optical fitness by minimizing pigment package effects. Orientation of highly elongate *Haslea* sp. cells appeared to cause underestimation of Q_b values and

suggests that orientation within natural communities may have important implications for the optical properties and light harvesting capabilities of certain taxa. Among cultures in exponential growth phase, the magnitude of variation of b_p:a_p accounted for ~30% of variation observed in natural communities while the magnitude of variation of a_p slope could account for nearly all observed natural variation. However, a_p slope variation could be attributed to exopolymeric material excreted by cells, pigment package effects, or changes in photoprotective:photosynthetic pigment ratios. For all but one species, senescent cultures showed increases in b_p:a_p and a_p slope due to loss of pigment and accumulating cell debris. Loss of chlorophyll from hollow setae in senescent *Chaetoceros eibenii* cultures resulted in a decrease of b_p:a_p demonstrating that species specific characteristics can be optically important, may impact bio-optical fitness, and may have adaptive significance. For large particles, isolated by size fractionation, the changes in b_p:a_p and a_p slope after onset of senescence accounted for ~25% of the variation seen in natural communities.

Results of this laboratory based study demonstrate that the unique morphological and physiological characteristics of different species can account for a substantial proportion of the variation of optical properties measured for natural communities over small scales in the coastal ocean. Therefore, optical properties can be used to visualize community structure and function in the ocean with high resolution over small spatial scales. However, other particle types such as heterotrophic bacteria and cell debris are likely to be optically important for natural suspended particle assemblages but these particles are likely to covary with phytoplankton ecological processes such as mortality. Furthermore, the low intracellular pigment concentrations

and complex morphology of colonial diatom species tested here suggests that these species are adapted to minimize self-shading of chloroplasts which can limit light harvesting efficiency, growth, and fitness.

Implications

The results of this work have important implications for ocean observation techniques upon which our understanding of natural phytoplankton community structure and function is built. In situ observation systems can easily incorporate the types of optical measurements made here to better understand changes in phytoplankton community composition, size structure, and pigment content over longer time scales. Such measurements could provide a continuous record of phytoplankton structure and population dynamics through all types of environmental conditions, data sets that have been impossible to obtain with ship based and discrete sampling methods. Remote observation systems such as airborne LIDAR and satellite based sensors can provide synoptic optical measurements over regional to global scales. For these types of optical data, a better understanding of absorption and scattering by phytoplankton can help improve estimates of biomass and primary production that are often derived from remote measurements. Ultimately, the relationships among phytoplankton cellular characteristics and high resolution optical data revealed by this dissertation can be used to better understand natural phytoplankton community structure and function in the ocean and the selective processes that drive phytoplankton evolution.

Integration of phytoplankton bio-optical dynamics into optical and ecological ocean models could greatly improve their accuracy and their ability to predict

response to changing environmental conditions. Inverse optical models strive to determine characteristics of dissolved and particulate material from optical measurements. Although unique solutions to inverse models may still be unattainable, it should be possible to derive useful biological information with a better understanding of the effects of phytoplankton characteristics on optical variation in the ocean. Results presented here show how optical properties vary with phytoplankton size, shape, and pigment content, and suggest that these characteristics could be derived from optical measurements provided we can account for the influence of non-algal particles. Current ecological models often assume constant biomass specific absorption and reflectance, yet results of this study indicate that such assumptions are not valid for dynamic coastal ecosystems where phytoplankton biomass and rates of primary production are often very high and extremely variable. Better model parameterization that captures the variable bio-optical characteristics of phytoplankton will improve their ability to predict local phenomena such as harmful algal blooms and long term, global scale responses to climate change. Results of this dissertation suggest that ecological models should incorporate phytoplankton size and pigment content as variables that influence their distribution and function.

In the long term, a better understanding of ecological pattern and process in natural phytoplankton communities is only possible with better in situ observational techniques that can resolve the small scale biological features important to population dynamics. Although the function of marine ecosystems is critical to the global biosphere, our ability to measure and model their structure and function at all but the coarsest scales has been severely limited. Improved observational capabilities based

on optical measurements will undoubtedly help explain the distribution of phytoplankton species in space and time, diversification over their 2.6 billion year history, the functioning of earth's biological systems, and may even be applied to the search for life in other parts of the solar system.

Future directions

The results of work conducted in this dissertation suggest several lines of possible future research. A logical next step would be to compare phytoplankton optical properties and their patterns of variation in different ocean ecosystems such as central ocean gyres, upwelling regions, or permanently stratified tropical ocean waters. Optical data may reveal unique community structure and function in these globally important ocean environments that reflect the distinct conditions to which diverse species are adapted. Further investigation with a larger number of morphologically and physiologically diverse uni-algal cultures would also improve our understanding of the effects of species-specific characteristics on the optical properties of cells, colonies and ocean waters.

Different methods of acquiring optical data may also further enhance our understanding of distinct phytoplankton communities. For example, sensor platforms that can follow phytoplankton communities over time could provide a detailed picture of community level processes such as differential growth, mortality, competition, and succession. Linking these patterns and processes to environmental conditions and hydrographic features would provide a new and more detailed understanding of biological organization in the ocean.

In situ observations might be further improved by combining optical data with other existing and emerging technologies. Automated particle imaging and analysis techniques, as used in the laboratory studies presented here, applied to tens of thousands of individual cells, colonies, and non-algal particles could facilitate determination of optical efficiency factors and bio-optical function for natural phytoplankton populations. Techniques such as digital inline holography, capable of imaging particles in an undisturbed volume of sea water, could be used to quantify the effects of orientation of cells or colonies on inherent optical properties and population dynamics. Quantitative imaging techniques could combine absorption or attenuation measurements with morphological measurements into a single sensor. Fast repetition rate fluorometry could provide information on the photophysiology of communities identified by their optical signatures. Molecular and genetic methods adapted for in situ measurements through the development of microfluidic technologies and used in combination with high resolution optical data could address a large number of biological questions ranging from community diversity to gene expression. In fact, the high resolution optical methods developed here can be used to guide any number of in situ measurement techniques or sampling strategies that might target different phytoplankton communities.

In short, there is much work remaining to be done before we fully understand the complex structure and function of planktonic communities or the evolutionary processes that have shaped phytoplankton species. What we currently know is compiled from sparse observations, scattered in space and time. These form an incomplete picture that is incapable of accurately representing the dynamic ecology of

pelagic marine ecosystems. Future research must overcome these limitations by focusing on methods that can quantify community characteristics over the small scales critical to population growth and mortality. This dissertation has provided a step in that direction by improving our ability to infer phytoplankton characteristics from high resolution optical data. By changing how we observe phytoplankton communities we can achieve a deeper understanding of their structure and function.

APPENDICES

A. GLOSSARY

a – absorption coefficient (m^{-1})

a_g – dissolved absorption coefficient (m^{-1})

a_p – particulate absorption coefficient (m^{-1})

a_{pg} – particulate plus dissolved absorption coefficient (m^{-1})

a_{ph} – phytoplankton absorption coefficient (m^{-1})

b – scattering coefficient (m^{-1})

b_b:b – backscatter ratio

b_p – particulate scattering coefficient (m^{-1})

b_p:a_p – particulate scattering to absorption ratio

b_{ph} – phytoplankton scattering coefficient (m^{-1})

c – attenuation coefficient (m^{-1})

CDOM – colored dissolved organic matter

C_i – relative intracellular chlorophyll concentration

c_p – particulate attenuation coefficient (m^{-1})

c_{pg} – particulate plus dissolved attenuation coefficient (m^{-1})

ESD – equivalent spherical diameter (μm)

IOP – inherent optical property

λ – wavelength (nm)

n' – imaginary part of the complex refractive index

PPC:PPS – ratio of photoprotective to photosynthetic carotenoids

Q_a – absorption efficiency factor

Q_b – scattering efficiency factor

σ – particle projected area (m^2)

B. SLIDES PRESENTED AT THE ORAL DEFENSE OF THIS DISSERTATION

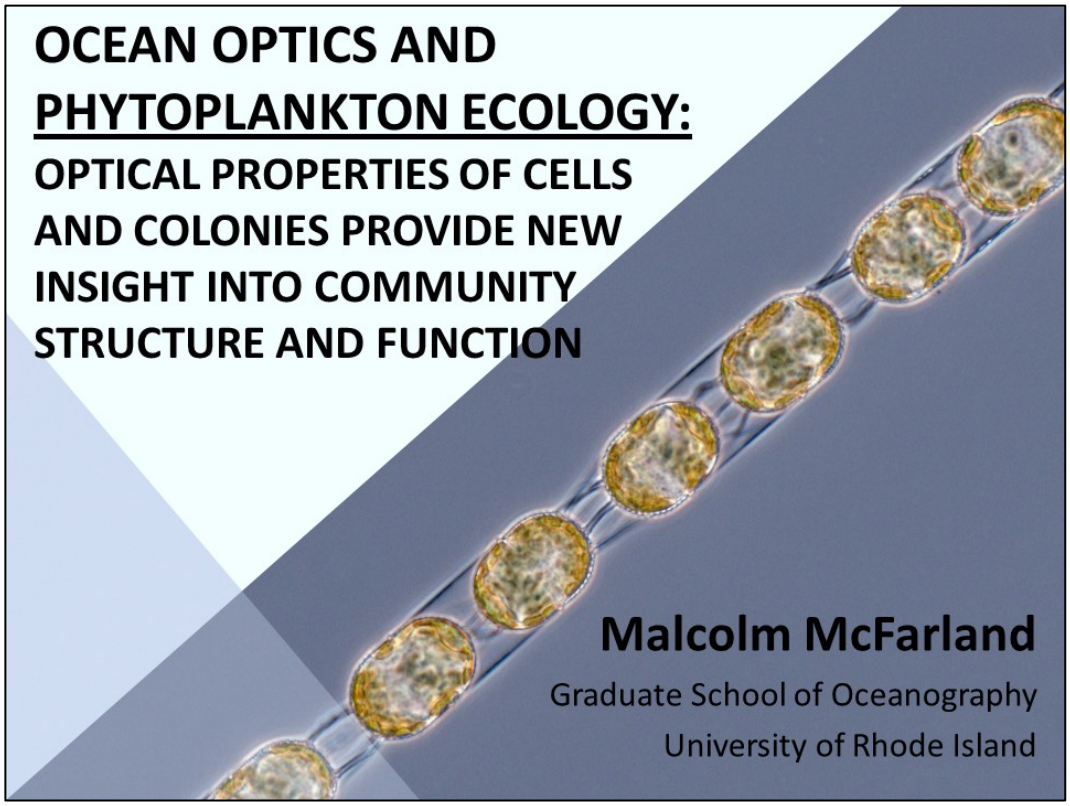

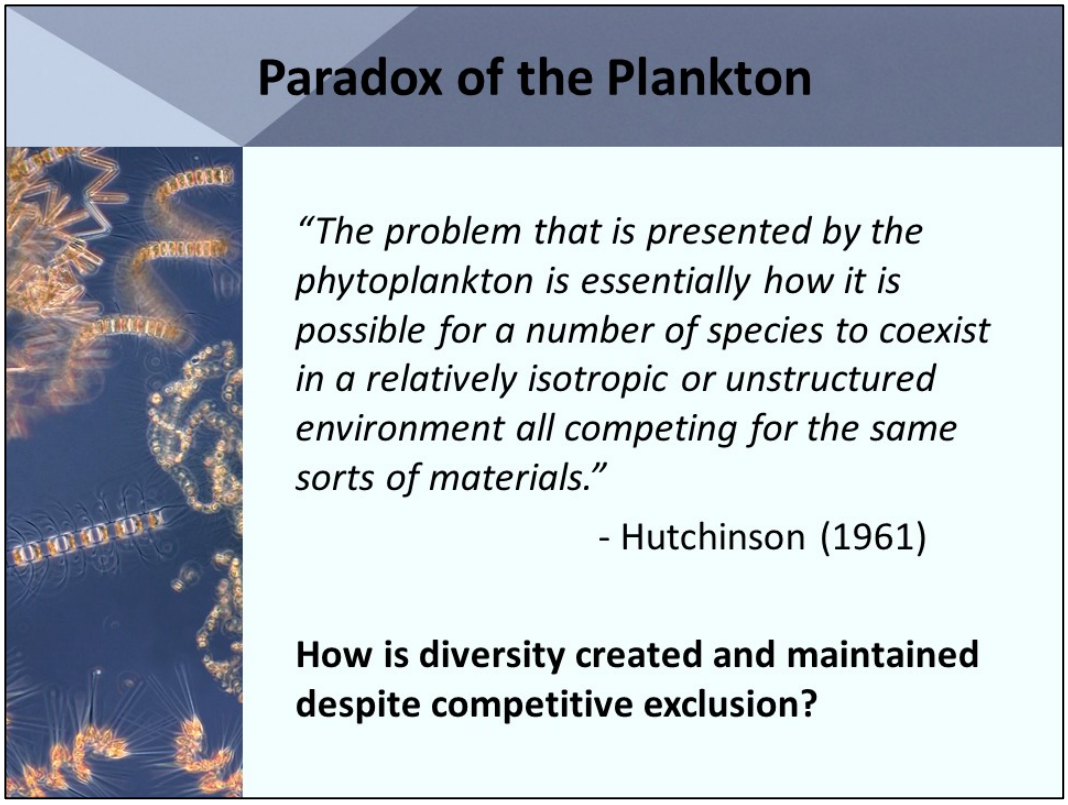

The ocean is NOT isotropic or unstructured!

The problem and a potential solution

Problem: inadequate resolution

– Determination of phytoplankton distribution, abundance and characteristics over small scales is extremely difficult!

Potential solution: optical properties

– High resolution *in situ* measurements
– Sensitive to abundance, size, shape, and pigments
– Direct measure of light harvesting

Can optics resolve phytoplankton composition and characteristics over small scales?

1. **Monterey Bay**
   - Do optical properties vary with species composition?
2. **East Sound**
   - How do cellular characteristics (size and pigment content) affect optical properties?
   - What's the significance of non-algal particles?
3. **Laboratory cultures**
   - Can morphological and physiological differences account for observed variation?

Inherent Optical Properties (IOP)

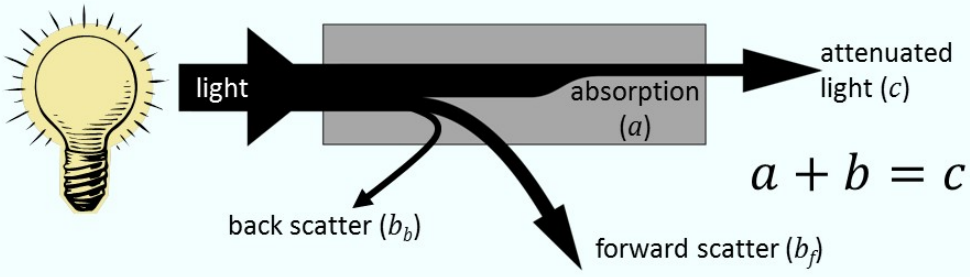

$$a + b = c$$

- Dissolved and particulate components:

$$a_g + a_p = a_{total}$$

- Ratios affected by particle characteristics:

$b_p{:}a_p$ $\qquad$ $b_b{:}b$

Normalized IOP spectra

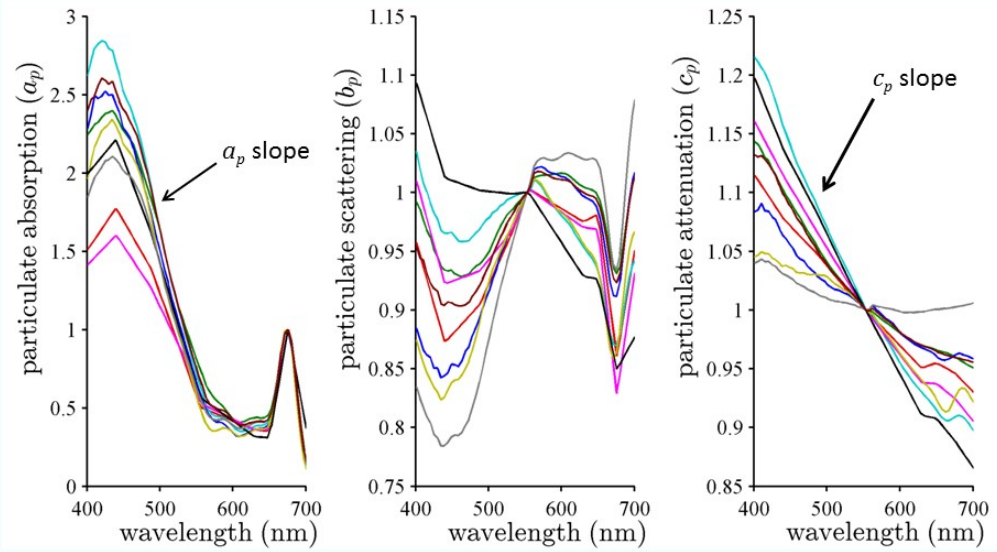

Monterey Bay

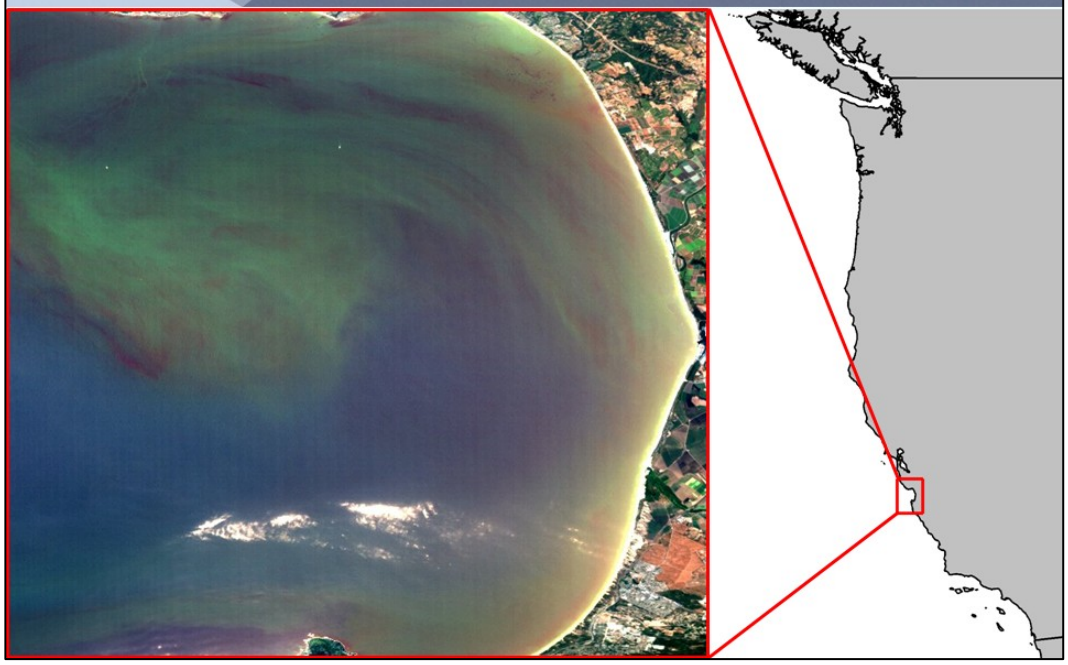

Questions

- Are communities associated with distinct optical signatures?
- How do optical properties vary among communities?

Optical profiles and sample analysis

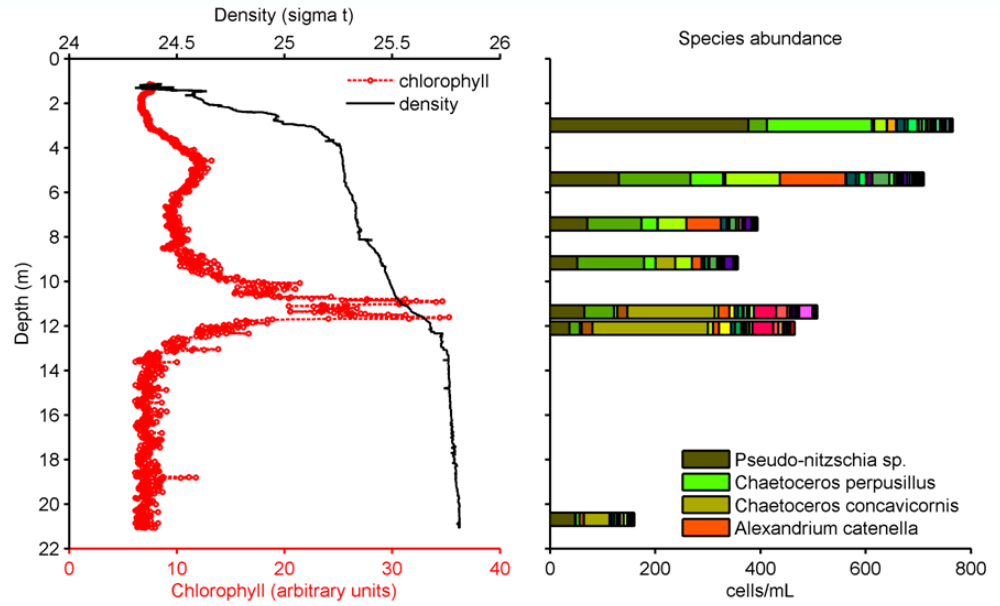

Communities

- Hierarchical cluster analysis
- Based on manual count data
- 9 communities

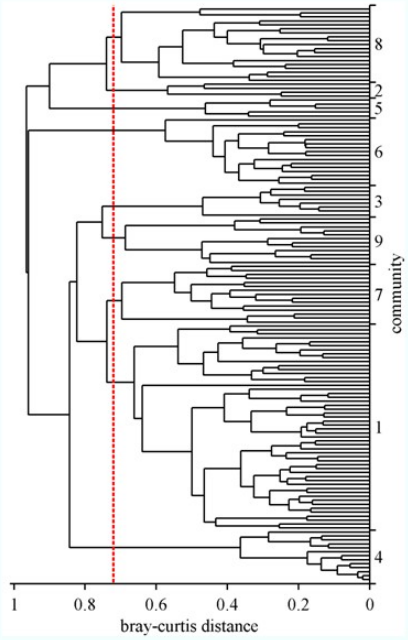

Microphytoplankton (>10µm)

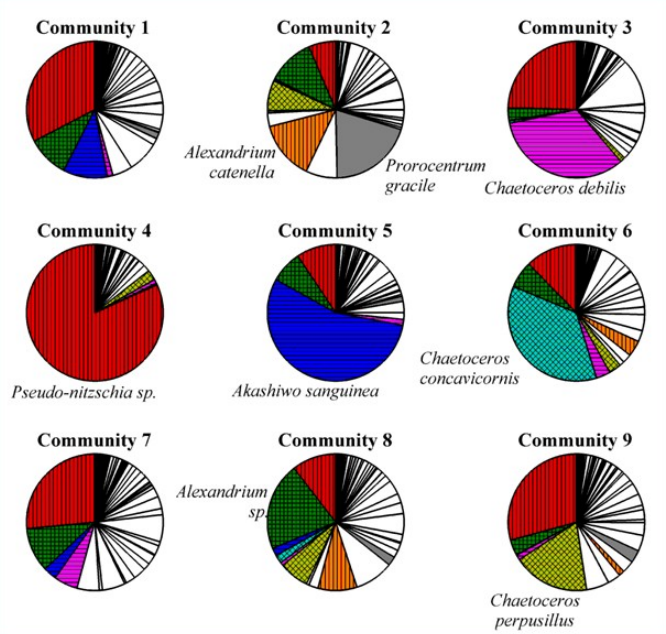

Dominant cell types

Pico & nanophytoplankton

Cells collected on filters, imaged with epifluorescence microscopy

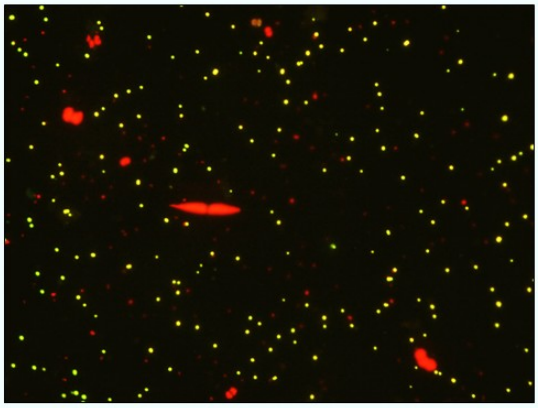

Cells classified, counted and sized using image analysis

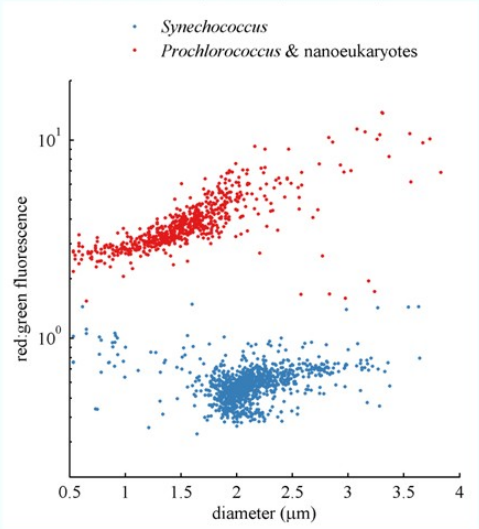

Pico & nanophytoplankton

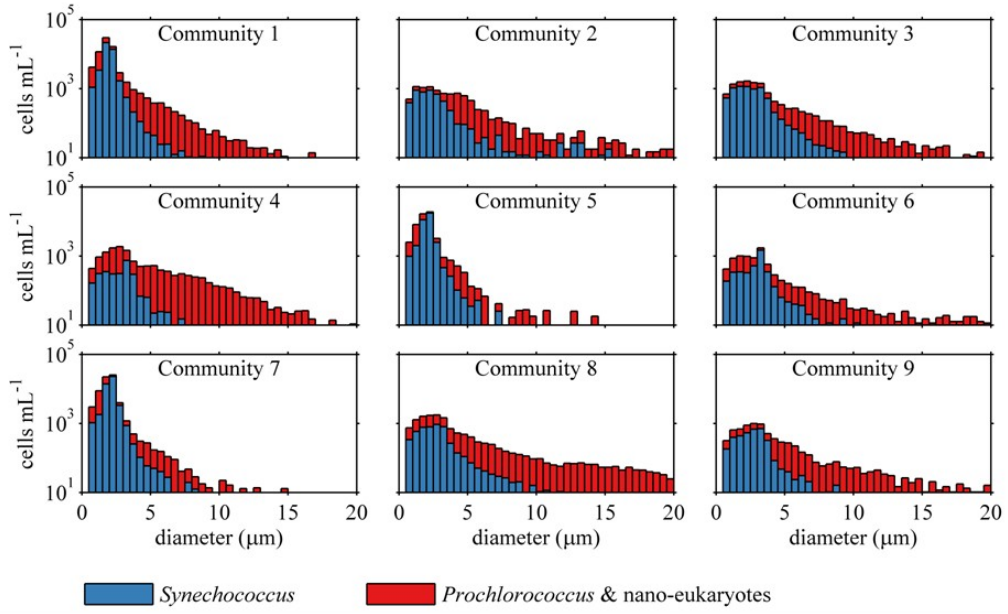

Community Optical Properties

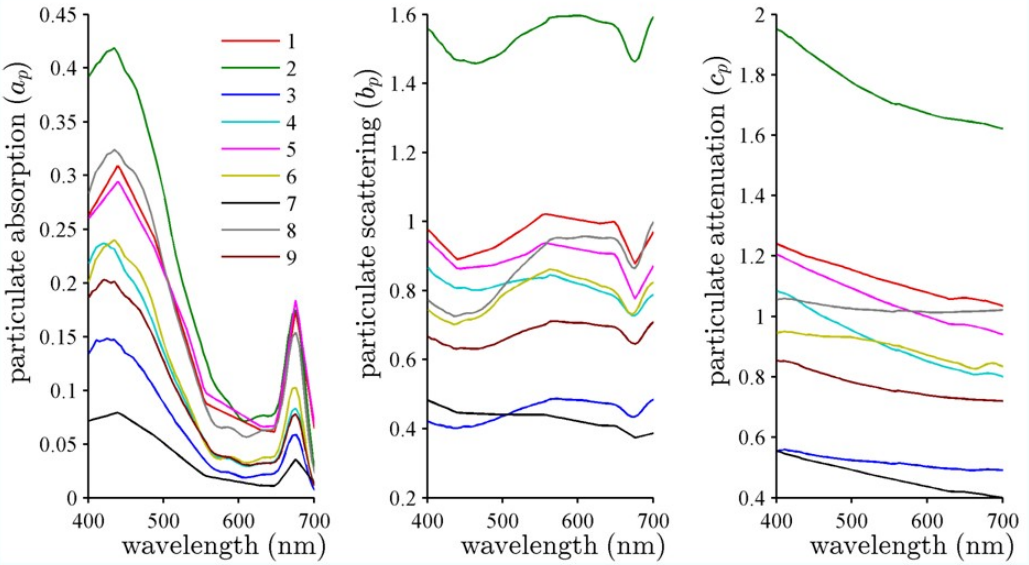

Redundancy Analysis

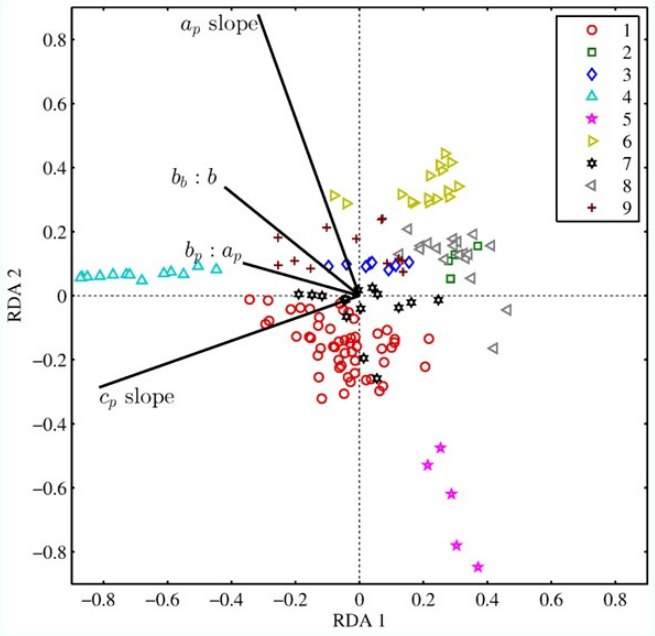

4 – abundant but stressed *Pseudo-nitzschia* and abundant nano-eukaryotes

5 – abundant *Akashiwo sanguinea* and abundant *Synechococcus*

6 – abundant *Chaetoceros concavicornis* and few pico and nanoplankton

Conclusions (Monterey Bay)

- Shape and relative magnitude of a_p and b_p vary among distinct communities
- Cell size and pigment content appear to be optically important characteristics

- Next steps:
  - Measure cellular characteristics
  - Measure non-algal particles

East Sound

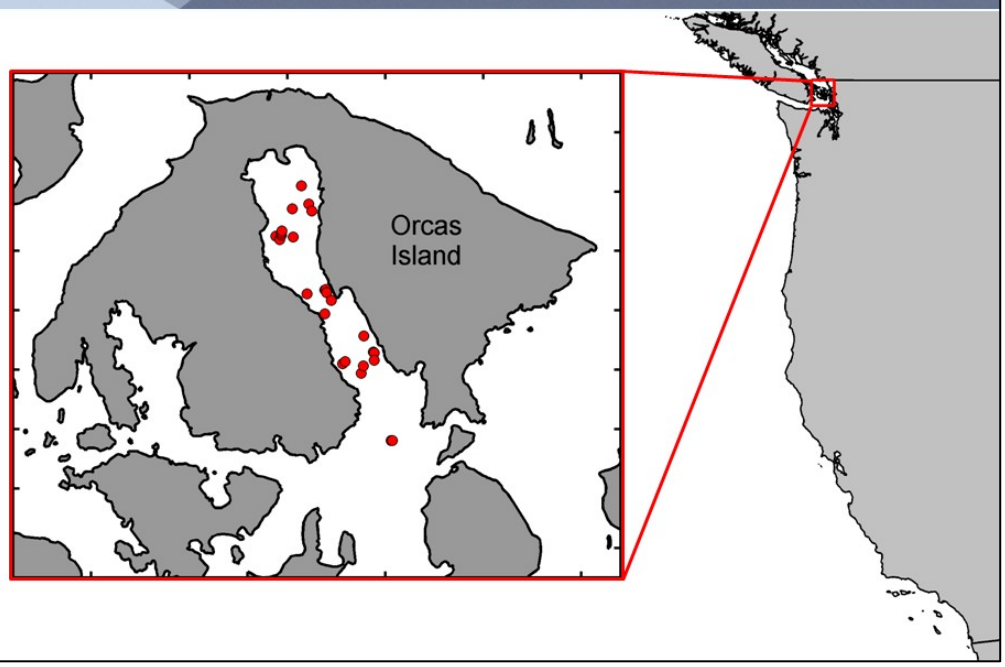

Questions

- Do phytoplankton size and pigment content vary with optical properties?
- What is the influence of non-algal particles?
- Can we visualize phytoplankton characteristics over small scales with high resolution optical data?

Optical profiles and sample collection

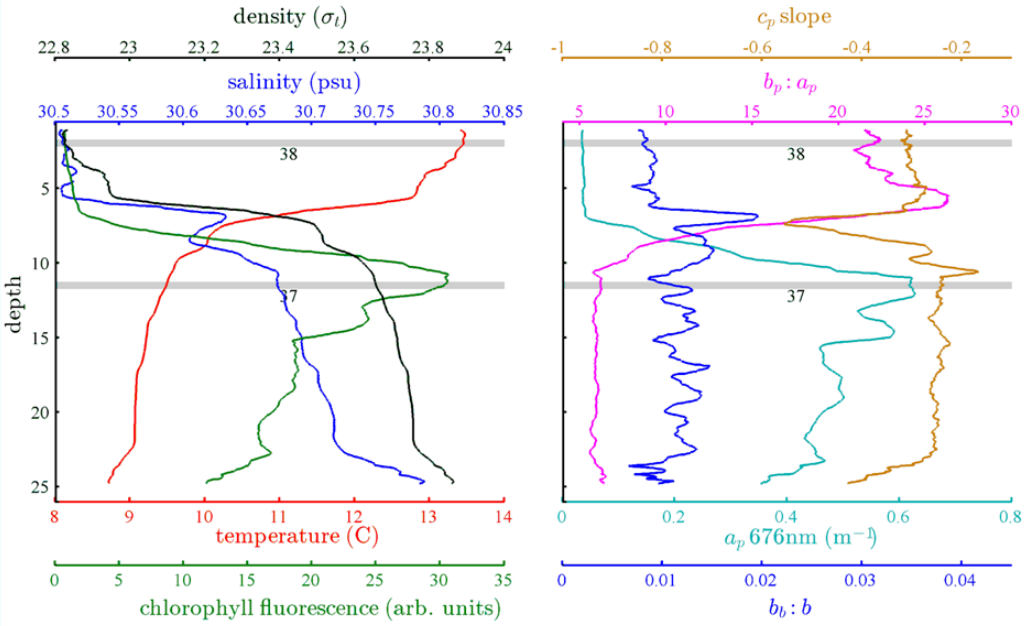

Scanning Flow Cytometry

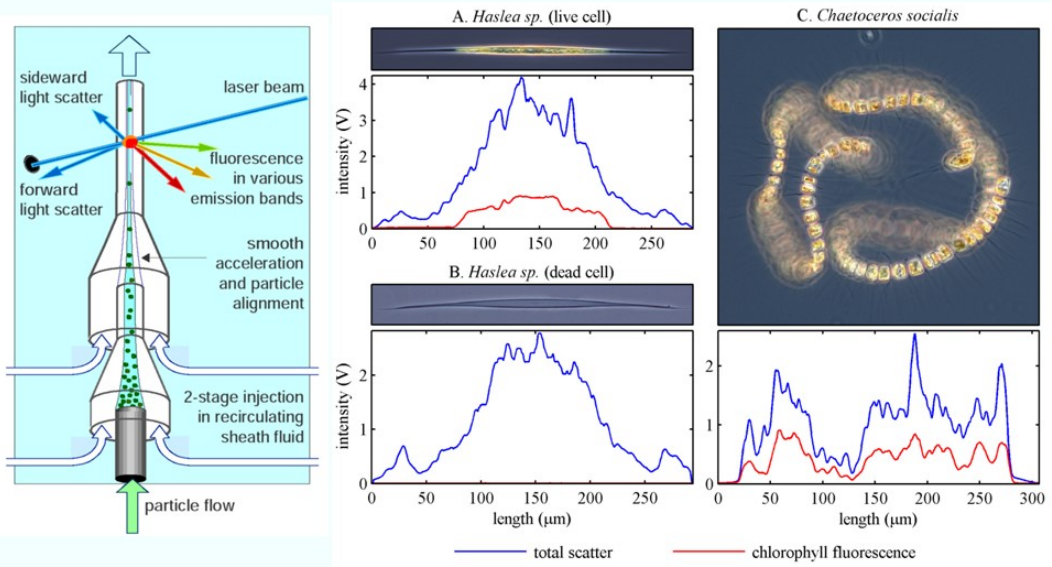

Scanning Flow Cytometry

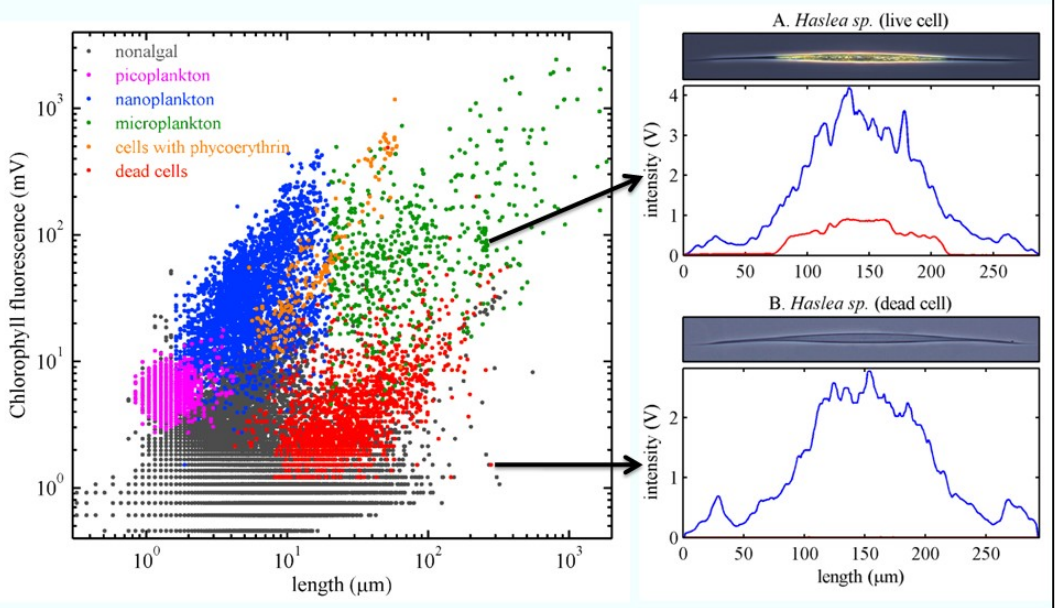

Communities

- Hierarchical cluster analysis
- Based on flow cytometry data
- 4 communities in each year

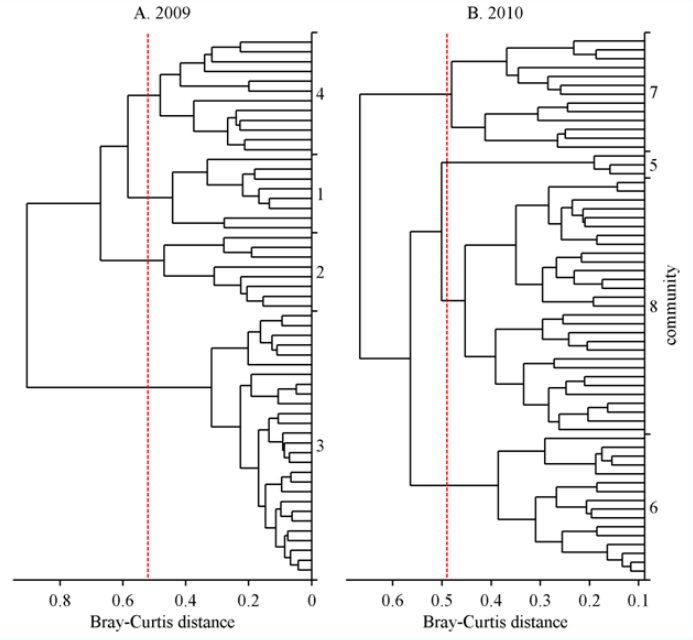

Community composition

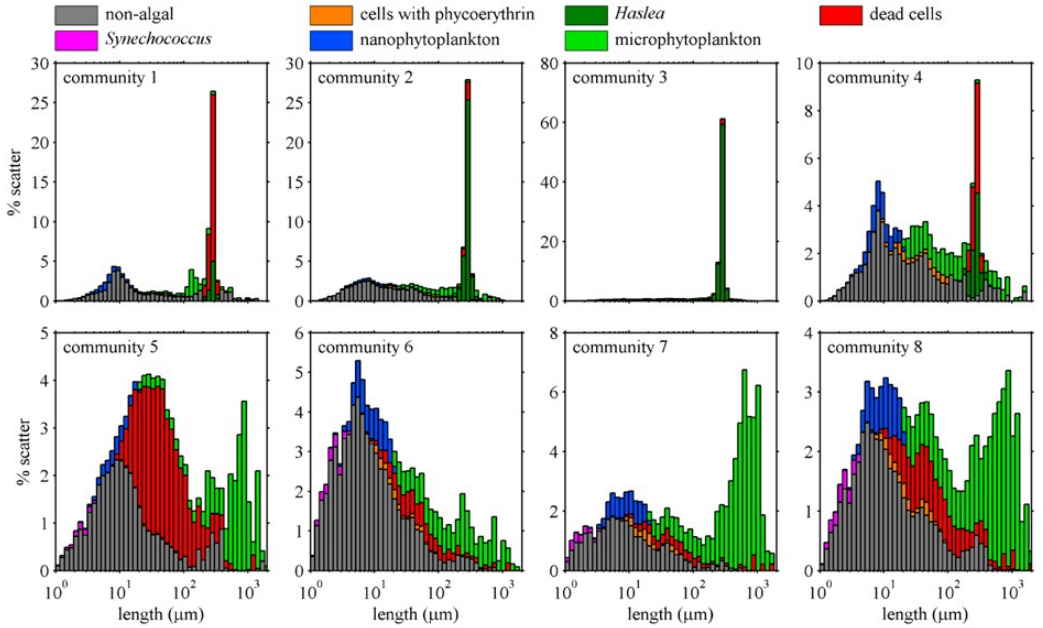

Redundancy analysis 2009

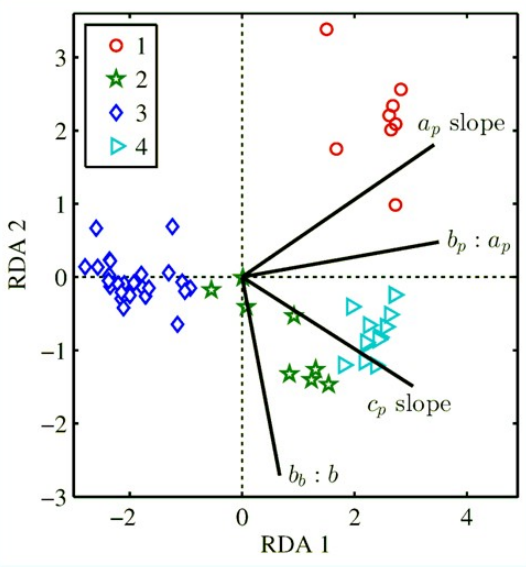

Community 1 – abundant dead *Haslea* cells

Community 3 – dominated by live *Haslea*

Community 4 – abundant non-algal particles and smaller phytoplankton

Redundancy analysis 2010

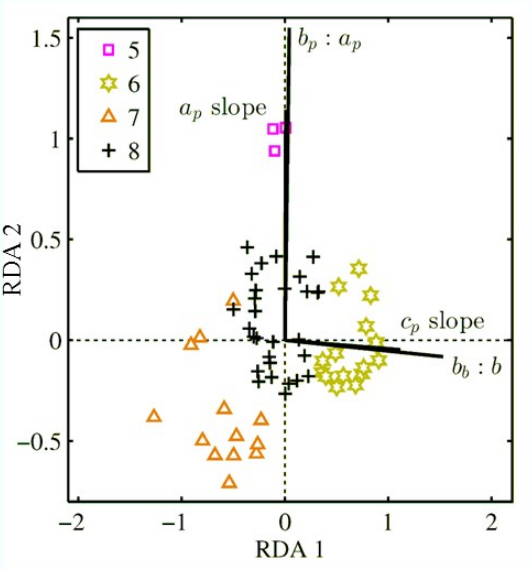

Community 5 – abundant dead cells

Community 6 – abundant non-algal particles

Community 7 – abundant large colonial diatoms

Results of multivariate analyses

- b_p:a_p and a_p slope increase with the relative abundance of dead cells
- c_p slope decreases with the relative abundance of large cells and colonies
- b_b:b and c_p slope increase with the relative abundance of non-algal particles
- Can we apply this to high resolution optical data?

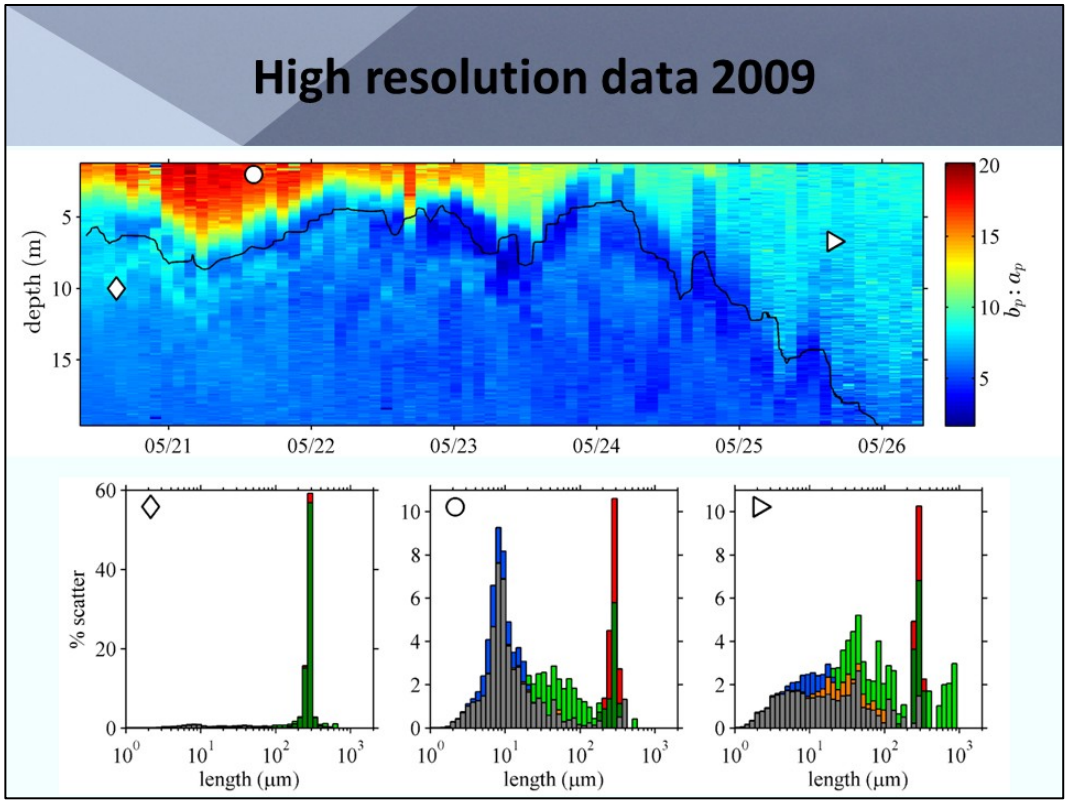
High resolution data 2009
depth (m)
5
10
15
05/21
05/22
05/23
05/24
05/25
05/26
20
15
10
5
$b_p : a_p$
% scatter
60
40
20
0
length (μm)
10
8
6
4
2
0
length (μm)
length (μm)

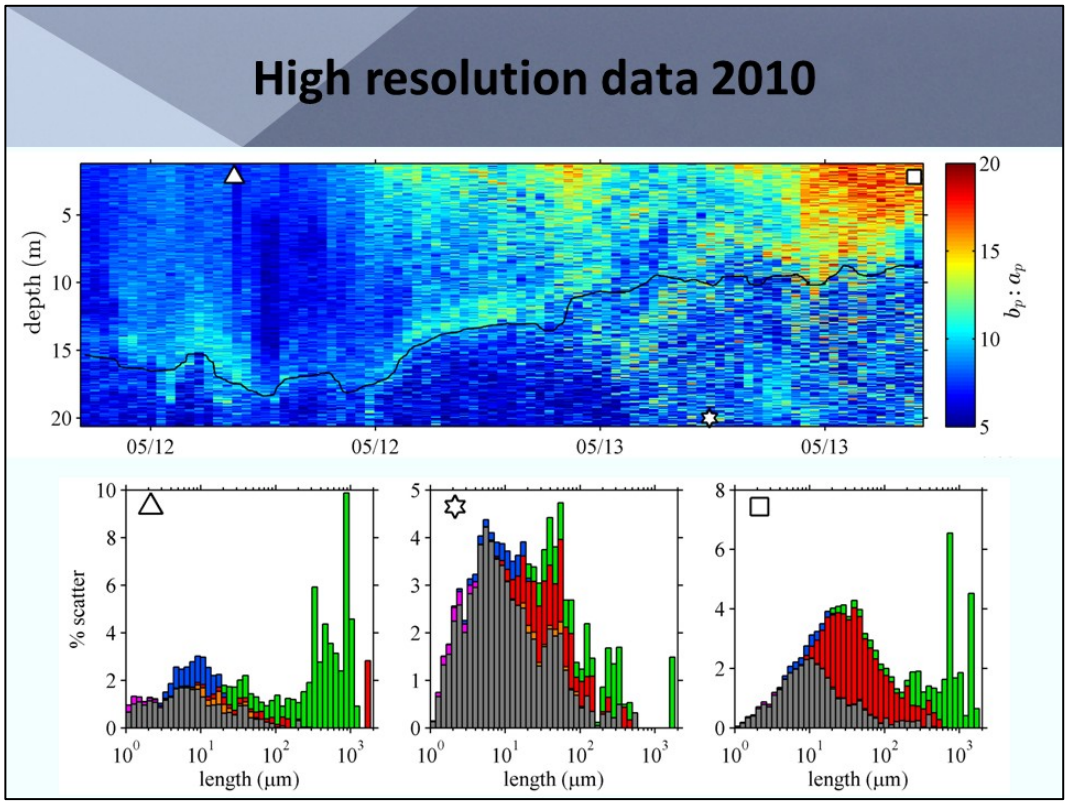
High resolution data 2010
depth (m)
5
10
15
20
05/12
05/12
05/13
05/13
20
15
10
5
$b_p : a_p$
% scatter
10
8
6
4
2
0
length (μm)
5
4
3
2
1
0
length (μm)
8
6
4
2
0
length (μm)

High resolution data 2010

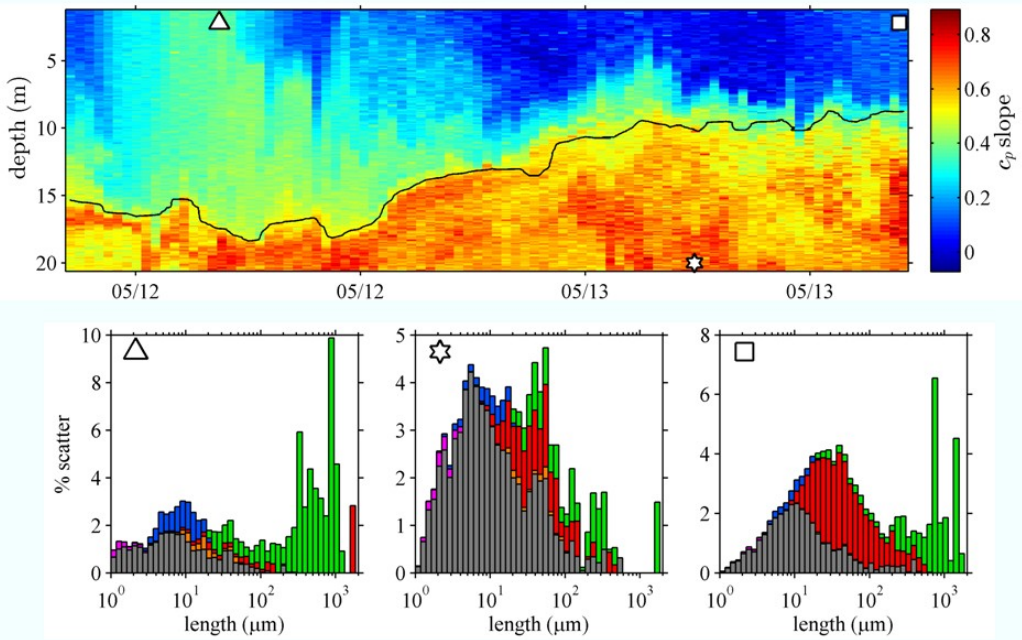

Conclusions (East Sound)

- Phytoplankton size and pigment content influence optical properties
- Non-algal particles are associated with high b_b:b and c_p slope
- Can visualize processes (e.g. mortality) and small scale distributions
- Morphology may be optically important characteristics

Laboratory studies: questions

- Can morphological and physiological variation account for optical variation observed in the field?
- Do morphological and physiological traits have a bio-optical function?

Cultures

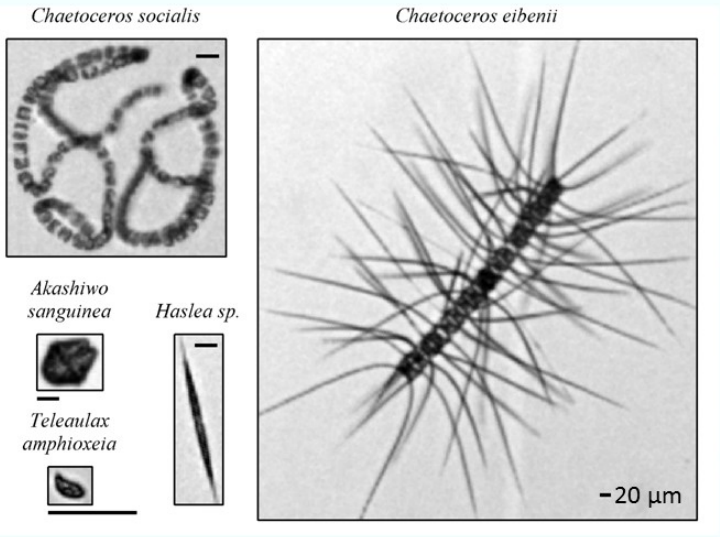

Optical properties: b_p:a_p and a_p slope

FlowCam: projected area of cells and colonies (σ)

Flow Cytometry: intracellular pigment concentrations (C_i)

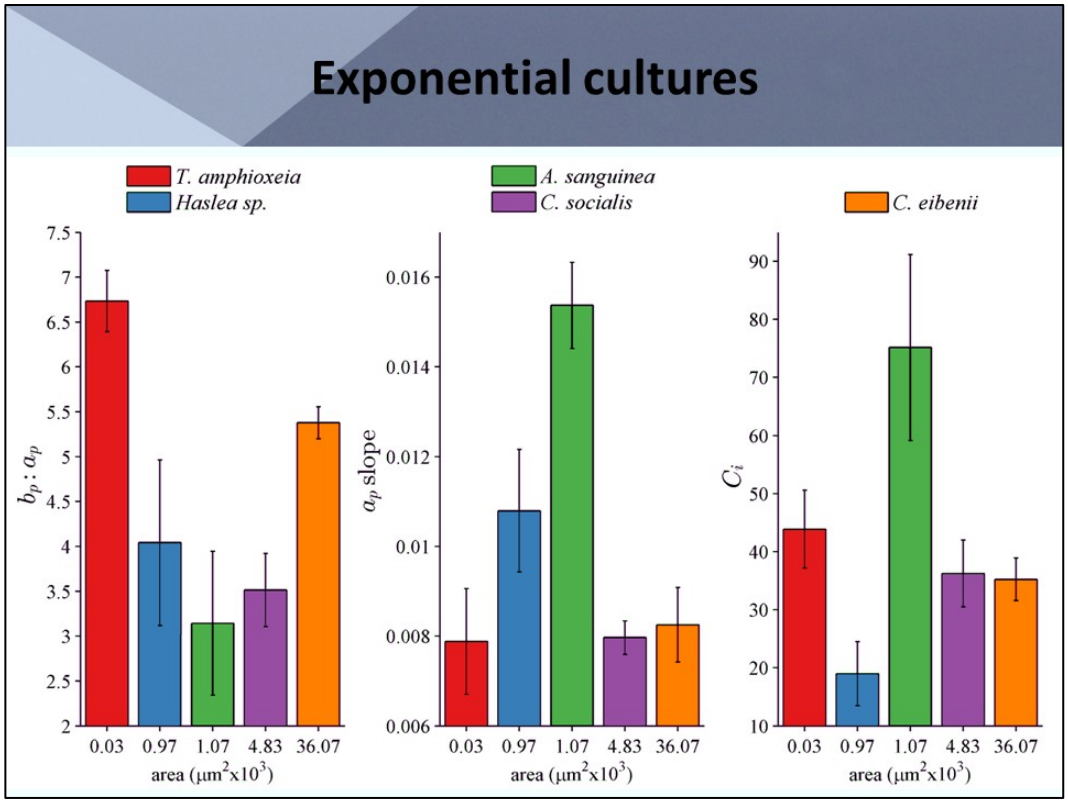
Exponential cultures
T. amphioxeia
Haslea sp.
A. sanguinea
C. socialis
C. eibenii
$b_p : a_p$
a_p slope
C_i
area ($\mu m^2 x10^3$)
0.03 0.97 1.07 4.83 36.07

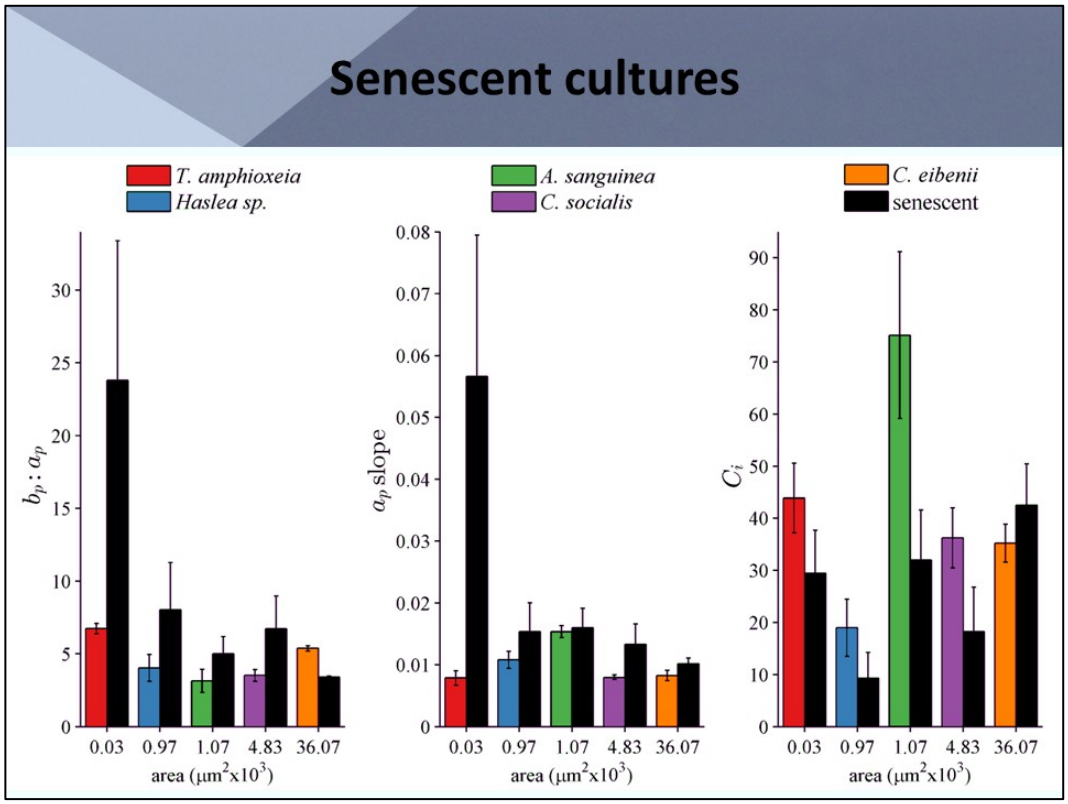
Senescent cultures
T. amphioxeia
Haslea sp.
A. sanguinea
C. socialis
C. eibenii
senescent
$b_p : a_p$
a_p slope
C_i
area ($\mu m^2 x10^3$)
0.03 0.97 1.07 4.83 36.07

Effects on light harvesting

- Absorption efficiency factors:

$$Q_a = \frac{a_p}{\sigma}$$

- σ = total projected area of particles from FlowCam
- Q_a is typically large for large particles
- Measured values are low compared to other published studies

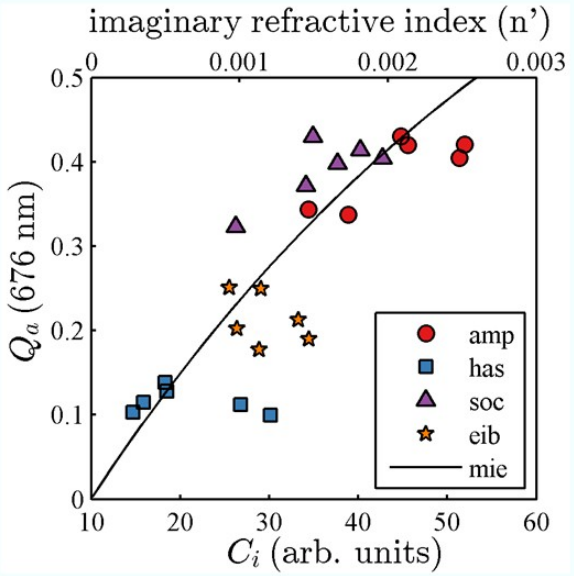

Conclusions (lab studies)

- Morphological or physiological differences account for ~25-30% of observed variability in b_p:a_p and a_p slope
  - Other particles (e.g. bacteria) must also contribute to observed variation
- Morphology is important, not just size
- Low intracellular chlorophyll concentrations and complex morphology of large forms minimize pigment self shading

Overall Conclusions

- Morphological and physiological characteristics of cells and colonies determine the optical properties of phytoplankton communities
- High resolution optical data reveals detailed information about the distribution, composition and characteristics of phytoplankton in the ocean

Future Directions

- Wider application
- Ocean observing systems
- Robust inverse models
- Population tracking
- Complementary observation techniques
  - In situ imaging: FlowCam, holography
  - Molecular approaches: Environmental Sample Processor
  - Satellite, LIDAR

Acknowledgements

- Core committee
  - Jan Rines
  - Percy Donaghay
  - Brian Hiekes
  - Carol Thornber
- Defense committee
  - Rebecca Robinson
  - Marta Gomez-Chiarri

Collaborators:

- Jim Sullivan
- Mike Twardowski
- Jason Graff
- Tatiana Rynearson

Funding agencies:

- Office of Naval Research
- RI EPSCoR
- GSO Alumni Foundation